Electronic Thesis and Dissertation Repository

8-6-2019 1:00 PM

Connectomic Analysis of Substantia Nigra Pars Compacta and Ventral Tegmental Area Projections to the Striatum and Cortex

Nicholas Handfield-Jones, *The University of Western Ontario*

Supervisor: MacDonald, Penny A., *The University of Western Ontario*
Co-Supervisor: Khan, Ali R., *The University of Western Ontario*
Co-Supervisor: Owen, Adrian M., *The University of Western Ontario*
A thesis submitted in partial fulfillment of the requirements for the Master of Science degree in Neuroscience
© Nicholas Handfield-Jones 2019

Recommended Citation

Abstract

We investigated the connectivity of dopamine (DA) neurons emerging from the substantia nigra pars compacta (SNc) and ventral tegmental area (VTA) and targeting the dorsal striatum (DS), ventral striatum (VS), and prefrontal cortex (PFC). We used diffusion magnetic resonance imaging (dMRI) probabilistic tractography on human connectome project MRI data. We found that unlike conventional descriptions of DA pathways (i.e., nigrostriatal, mesolimbic, mesocortical), connectivity from both SNc and VTA each targeted DS, VS, and PFC. We also found that from the DS, VS, and PFC, a greater proportion of connections targeted the SNc as compared to the VTA. These findings suggest that DA pathways are more complex than conventionally described. In a follow-up dMRI experiment, we found reduced connectivity from the SNc/VTA complex to the caudal motor region of the striatum in patients with Parkinson's disease, indicating a potential role of dMRI to measure DA connectivity changes in patients with DA-mediated diseases.

Keywords

Summary for Lay Audience

Dopamine (DA) is a neurotransmitter in the brain that binds to brain cells (neurons) and which is responsible for a plethora of behaviours like movement, decision-making, reward-processing, learning, and memory. When DA transmission goes awry, it can lead to the development of various DA-mediated disorders like Parkinson's disease, schizophrenia, substance use disorder, and obsessive-compulsive disorder.

There are two primary brain regions in which DA is produced: the substantia nigra pars compacta (SNc) and the ventral tegmental area (VTA). DA from these two areas project to the striatum, which itself can be divided into the dorsal striatum (DS) and ventral striatum (VS), and the prefrontal cortex (PFC). Classically, DA connectivity from the SNc and VTA to the DS, VS, and PFC has been described according to three different pathways. In the nigrostriatal pathway, SNc projects DA to the DS. In the mesolimbic pathway, VTA projects DA to the VS. In the mesocortical pathway, VTA projects DA to the PFC. This convention, while providing a convenient model to understand DA function and DA-mediated diseases, does not take into account a body of evidence that suggests that DA projections to the DS, VS, and PFC are far more complex.

To test this in living adults, we obtained magnetic resonance imaging (MRI) data from the Human Connectome Project, a consortium that has amassed high-resolution MRI data. We used an MRI technique called probabilistic tractography to measure SNc and VTA connectivity to the DS, VS, and PFC. At odds with conventional descriptions of DA pathways, we found evidence suggesting a VTA to DS pathway, an SNc to VS pathway, and an SNc to PFC pathway. Our findings add further evidence to suggest that conventional descriptions of DA pathways oversimplify the true underlying complexity.

Finally, as a validation for this method and as a demonstration of probabilistic tractography as a means to measure DA pathway changes in disease, we performed probabilistic tractography on a population of recently-diagnosed patients with Parkinson's disease and on age-matched controls. We found that, as predicted, the connectivity from the SNc/VTA to a certain area of the striatum was reduced.

Co-Authorship Statement

In Experiment 1, Dr. Ali Khan downloaded and pre-processed the Human Connectome Project data. I performed subsequent pre-processing steps using MRI pre-processing pipelines designed by Dr. Ali Khan and performed all statistical analyses, with assistance from Dr. Penny MacDonald.

In Experiment 2, I received assistance in data collection from Erind Alushaj. I performed all pre-processing steps using MRI pre-processing pipelines designed by Dr. Ali Khan. I troubleshot these pipelines with assistance from Dr. Ali Khan. I performed all data analysis with assistance from Dr. Nole Hiebert and Dr. Penny MacDonald.

I wrote the entirety of this thesis manuscript, which was edited by Dr. Penny MacDonald.

Dedication

This thesis is dedicated to my beloved cat Thomas. Rest in peace, Tom Tom.

Acknowledgments

I would like to express my gratitude to the following people, without whom this thesis never would have been written:

- Dr. Penny MacDonald for your unending, unwavering support and for your tireless efforts to make my time in your lab such an enriching experience. Thank you for challenging me to ask tough questions about neuroscience and for supporting me through many hardships along the way. You have gone the extra mile for me on many occasions and have believed in me when I did not believe in myself, and for that I cannot thank you enough. Any student would be lucky to be in your lab.

- Dr. Ali Khan for your guidance through the challenges of dMRI analysis. This project could never have been completed without your help. Thank you for your collaborative philosophy on this project and for your willingness to answer my Slack messages at virtually all hours.

- Dr. Adrian Owen for your support on this project.

- The members of my advisory committee, Dr. Derek Mitchell and Dr. Jody Culham, for supporting my work and suggesting new ideas to broaden my lines of inquiry.

- Erind Alushaj,the other half of the Basal Ganglia Gemini, for braving 7:00AM MRI scans with me and for all the stats help.

- Dr. Nole Hiebert for teaching me everything I needed to know when it comes to being in the MacDonald Lab.

- Students of the MacDonald Lab for providing great company and for always lending an ear when I need to rant: Kasey van Hedger, Abdullah Al Jaja, Maggie Prenger, Dimuthu, Hemachandra, Shiny Yang.

- The WIRBdashians for your fourth floor antics: Sonia Varma, Mark O'Reilly, Chad Buckland, and Matt Bain.

- My mom, dad, and brother for your unwavering support and love. You have been a great source of comfort and peace amidst the chaos of writing.

- Kyle. For everything.

Table of Contents

List of Tables

List of Figures

List of Appendices

List of Abbreviations

3D	3-Dimensional
ANOVA	Analysis of variance
BG	Basal ganglia
BOLD	Blood-oxygen-level-dependent
BW	Bandwidth
CM	Caudal motor
CPu	Caudate-Putamen
DA	Dopamine
DAergic	Dopaminergic
DCC	Deleted in colorectal cancer
dMRI	Diffusion MRI
DS	Dorsal striatum
DWI	Diffusion weighted imaging
EPI	Echo planar imaging
Exec	Executive
FA	Fractional anisotropy
FB	Fast blue
FDR	False discovery rate
FG	Fluoro-gold
fMRI	Functional magnetic resonance imaging
FOV	Field of view
GABA	Gamma-aminobutryic acid
GFP	Green fluorescent protein
Gmax	Maximum gradient strength
GP	Globus pallidus
GPe	Globus pallidus external segment
GPi	Globus pallidus internal segment
HARDI	High angular resolution diffusion imaging
HC	Healthy control

HCP	Human Connectome Project
HRP	Horseradish peroxidase
Ins	Insula
L-dopa	Levodopa
Limb	Limbic
MB	Multiband
MCMC	Markov chain Monte Carlo
MD	Mean diffusivity
MPRAGE	magnetization-prepared rapid acquisition with gradient echo
MRI	Magnetic resonance imaging
MSN	Medium spiny neuron
NAcc	Nucleus accumbens
Occi	Occipital
OCD	Obsessive compulsive disorder
Pari	Parietal
PBP	Parabrachial pigmented area
PD	Parkinson's disease
PFC	Prefrontal cortex
RD	Radial diffusivity
RF	Radiofrequency
RM	Rostral motor
ROI	Region of interest
RSFC	Resting state functional connectivity
SEM	Standard error of the mean
SN	Substantia nigra
SNc	Substantia nigra pars compacta
SNr	Substantia nigra pars reticulata
STN	Subthalamic nucleus
SUD	Substance use disorder
T	Tesla
TE	Time to echo

Temp	Temporal
TH	Tyrosine hydroxylase
TI	Inversion time
TR	Time to repetition
VS	Ventral striatum
VTA	Ventral tegmental area

Chapter 1 – Introduction

1.1 – The Role of Dopamine in Behaviour and Disease

The substantia nigra pars compacta (SNc) and the ventral tegmental area (VTA) are the two primary dopamine (DA) producing nuclei of the midbrain and form a part of the larger basal ganglia (BG) system. Through efferent dopaminergic (DAergic) connections to the striatum and cortex, the SNc/VTA complex has been implicated in a wide range of behavioural outputs.

The SNc, which is located lateral to the VTA and medial to the substantia nigra pars reticulata (SNr) has been classically ascribed a role in voluntary movement (**Figure 1**). Lesions to the SNc of non-human primates result in bradykinesia, and the degeneration of SNc neurons in patients with Parkinson's disease (PD) is known to underlie symptoms of bradykinesia, tremor, and rigidity observed in these patients (Alexander, 2004; Burns et al., 1983; Stern, 1966; Viallet, Trouche, Beaubaton, Nieoullon, & Legallet, 1981). In addition, the SNc has also been demonstrated to have a role in goal-directed behaviour, habit formation, learning, working memory, and potentially in reward processing and/or salience (Da Cunha, Angelucci, Canteras, Wonnacott, & Takahashi, 2002; Faure, Haberland, Condé, & El Massioui, 2005; Frank & Surmeier, 2009; Matsumoto & Hikosaka, 2009; Zaghloul et al., 2009)

The VTA, which is located medial to the SNc, is known to have an important role in the creation of reward associations and in the detection of reward prediction errors, which are discrepancies between a predicted reward and a received reward (Cohen, Haesler, Vong, Lowell, & Uchida, 2012; Matsumoto & Hikosaka, 2009; Schultz, Dayan, & Montague, 1997; Takahashi et al., 2009; **Figure 1**). The VTA has also been implicated in motivation, incentive salience, aversion to noxious stimuli, and memory formation (Adcock, Thangavel, Whitfield-Gabrieli, Knutson, & Gabrieli, 2006; Berridge, 2007; Brischoux, Chakraborty, Brierley, & Ungless, 2009; Bromberg-Martin, Matsumoto, & Hikosaka, 2010; Morales & Margolis, 2017).
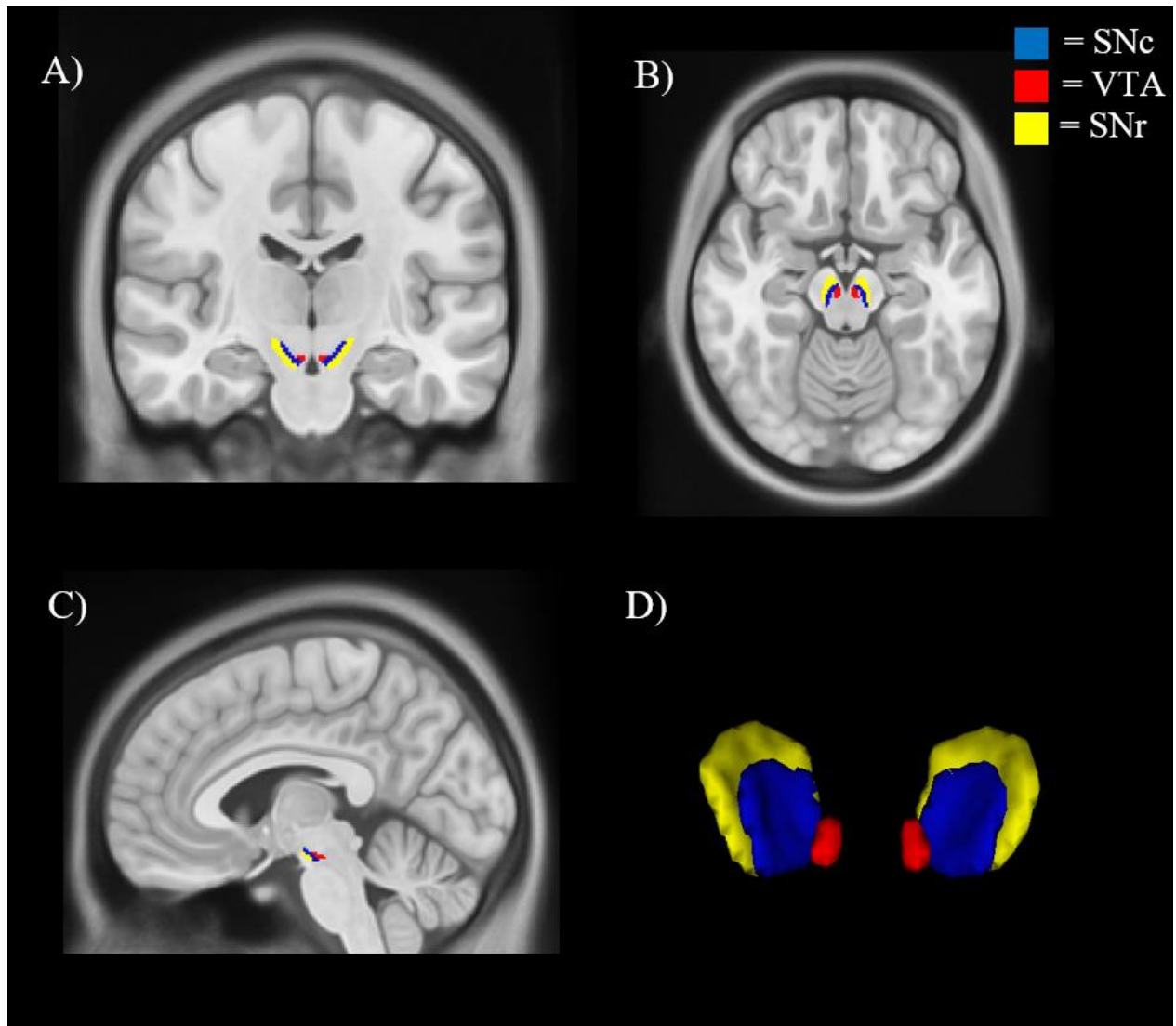
Figure 1. Anatomy of SNc, VTA, and SNr. Brain images are shown in MNI152 T1w space. SNc, VTA, and SNr are derived from the CIT168 atlas. SNc, VTA, and SNr are shown in 1A) coronal, 1B) axial, and 1C) sagittal planes. 1D) shows a 3D view of the SNc, VTA, and SNr, shown in the axial plane. (SNc = Substantia nigra pars compacta, VTA = Ventral tegmental area, SNr = Substantia nigra pars reticulata).

In addition to its neuromodulatory effects on many basic behaviors of normal functioning, the importance of SNc/VTA DA is highlighted by its implication in numerous neurodegenerative and neuropsychiatric disorders. Perhaps the most well-known of these is PD. PD is a progressive disorder in which DA neurons of the SNc and VTA degenerate. This degeneration occurs at different rates, such that up to 80% of SNc degenerate by the time of symptom onset, whereas the VTA remains relatively replete (Kish, Shannak, & Hornykiewicz, 1988). PD is often characterized by its motor symptoms, whereby patients suffer tremor, rigidity, bradykinesia, and

postural impairment, and these symptoms have been attributed to the degeneration of SNc neurons (Morales & Margolis, 2017). PD is also characterized by the co-incidence of non-motor symptoms like cognitive impairment (Goldman et al., 2018; MacDonald & Monchi, 2011). To alleviate motor deficits, patients with PD are typically prescribed levodopa (L-dopa), a DA-precursor that increases DA release from the SNc and VTA (LeWitt, 2015). Although this can ameliorate motor symptoms by returning SNc DA release to normal levels, L-dopa can DA overdose the relatively replete VTA neurons. This overdose of DA has been implicated in a number of cognitive deficits in PD, including deficits in learning (Gotham, Brown, & Marsden, 1986; Kish et al., 1988; Vaillancourt, Schonfeld, Kwak, Bohnen, & Seidler, 2013).

The importance of DA is also highlighted by its potential role in schizophrenia (Howes & Kapur, 2009; Howes, McCutcheon, & Stone, 2015). Schizophrenia is a neuropsychiatric illness characterized by positive symptoms of delusions and hallucinations, as well as by negative symptoms like anhedonia and avolition (Owen, Sawa, & Mortensen, 2016). Subcortical DA hyperactivity is thought to underlie the incidence of psychosis within schizophrenia (Howes & Kapur, 2009). This is highlighted by the fact that in patients with schizophrenia, the level of tyrosine hydroxylase (TH), the rate limiting enzyme in the synthesis of DA, is elevated in the SNc, indicating that there is an increased capacity for DA production (Howes et al., 2013). In addition, Positron Emission Topography studies have demonstrated that antipsychotic medication used to treat schizophrenia symptoms does so by blocking D2-like receptors on the striatum, suggesting that an over-binding of DA to D2-like receptors might contribute to schizophrenia symptoms (Howes et al., 2015). Despite these known characteristics of schizophrenia, the precise role of the SNc/VTA on symptom etiology remains understudied (Rice, Roberts, Melendez-Ferro, & Perez-Costas, 2016).

Finally, DA alterations have been implicated in substance use disorder (SUD), otherwise known as addiction, and in obsessive compulsive disorder (OCD), though the role this plays in symptom etiology remain unclear. In SUD, drug seeking and drug taking are voluntary at first, but these behaviours become compulsive over time. The use of addictive drugs has been found to increase DA signalling to the striatum (Ashok, Mizuno, Volkow, & Howes, 2017). This results in a sensitization of the DA striatal system, including a downregulation of post-synaptic DA receptors on the striatum (Volkow & Morales, 2015). This sensitization, coupled with increased

striatum activation in response to drug cues, is thought to motivate compulsive drug taking (Berridge & Robinson, 2016; Jasinska, Stein, Kaiser, Naumer, & Yalachkov, 2014). Though the VTA has been studied within the context of SUD, the involvement of the SNc, if any, has not received extensive analysis to this end (Oliva & Wanat, 2016; Wise, 2009).

OCD is characterized by frequent, obsessional, and distressing thoughts and the performance of repetitive, compulsive behaviours linked to anxiety. Functional neuroimaging studies have yielded evidence to suggest that abnormalities in the striatum could be linked to deficits in cognitive flexibility (e.g., choosing different thoughts or responses) and inhibition (e.g. withholding more habitual but erroneous responses) in OCD patients (Del Casale et al., 2011; Figee et al., 2011). By virtue of its role in behaviours related to compulsivity like reward processing, the deficit of VTA function has been proposed as a potential factor in the pathogenesis of OCD (Wood & Ahmari, 2015).

1.2 – Basal Ganglia

To elucidate the complex role of the SNc and VTA in healthy behaviours and in the pathogenesis of diseases, it will be critically important for a more detailed understanding of their connections with other regions of the brain (Yetnikoff, Lavezzi, Reichard, & Zahm, 2014). The SNc and VTA form part of the larger BG system, which is a group of sub-cortical nuclei that comprises the striatum, globus pallidus (GP), and subthalamic nucleus (STN) (Meyer & Quenzer, 2012). On a fundamental level, the SNc and VTA project DA to the striatum, which is the input nuclei of the BG. The striatum is comprised primarily by medium spiny neurons (MSNs), which express DA receptors, receive glutamatergic innervation from the cortex, and which propagate gamma-aminobutryic acid (GABA) (Thibault et al., 2016). DA receptors are divided into D1-like receptors and D2-like receptors based the binding to G_s stimulatory G proteins and G_i inhibitory G proteins, respectively (Beaulieu & Gainetdinov, 2011). Binding of DA to D1-like receptors results in the activation of the direct pathway, whereby MSNs release GABA to the GP internal segment (GPi), which itself transmits GABA to the thalamus. Inhibition of the GPi, in effect disinhibiting the thalamus, results in increased thalamic glutamatergic firing to the cortex, which yields cortical activation. Binding of DA to D2-like receptors results in the activation of the

4

indirect pathway, which opposes the actions of the direct pathway through an indirect loop through the GP external segment (GPe) and the STN. The STN releases glutamate to the GPi, resulting in increased inhibition to the thalamus and by extension decreased thalamic glutamatergic firing to the cortex and decreasing cortical excitation (Calabresi, Picconi, Tozzi, Ghiglieri, & Di Filippo, 2014). In this sense, neurons of the SNc and VTA can modulate behaviour, and through reciprocal connections from the striatum and cortex, they can receive information from the environment and adjust firing rates to alter behaviour in response to external cues (Deperrois & Gutkin, 2018; Joel & Weiner, 2000; Lee & Tepper, 2009; Yetnikoff et al., 2014)

Importantly, different regions of the striatum are known to modulate different behaviours. Anatomically, the striatum comprises of the caudate nucleus and putamen (CPu) and the nucleus accumbens (NAcc). Functionally and histologically, however, the striatum is divided into the dorsal striatum (DS), which comprises the bulk of the dorsal CPu, and the ventral striatum (VS), which comprises of the most ventral aspects of the CPu and the entire NAcc (Humphries & Prescott, 2010; Voorn, Vanderschuren, Groenewegen, Robbins, & Pennartz, 2004; Wickens, Budd, Hyland, & Arbuthnott, 2007). Compared to the VS, the DS is rich in DA input and projects to cortical regions associated with movement such as the primary, premotor, and supplementary motor cortices as well as cortical regions that mediate executive functions such as the prefrontal, somatosensory, and parietal cortices. This is supported by observations of patients with DS lesions with impairments to movement, set shifting, planning, memory retrieval, and decision-making. Conversely, the VS, when compared to the DS, receives less DAergic input and projects to anterior cingulate, orbitofrontal, and anterior temporal cortices. Lesions to the VS have been associated with impairments to learning, motivation, and salience processing (MacDonald & Monchi, 2011 for full review).

1.3 - SNc/VTA Efferent Projections

One aspect of the SNc/VTA and its relation to the BG that has been underappreciated, especially in the context of humans *in vivo*, is the complexity of the efferent neural pathways to the striatum and to the cortex. By convention, SNc/VTA projections to these regions have often been described as three distinct pathways, referred to here as the *conventional pathway heuristic*. In

the *nigrostriatal pathway*, DA neurons from the SNc project to the DS, which has a role in motor induction and control (Meyer & Quenzer, 2012). In the *mesolimbic pathway*, VTA DAergic neurons project to the VS, hippocampus, and limbic cortices. In the *mesocortical pathway*, VTA DAergic neurons project to the prefrontal cortex. Together, these latter two pathways play a role in reward processing and motivation (Meyer & Quenzer, 2012; **Figure 2**). Typically, the DAergic pathways are essentially summarized by these three pathways. As examples, recent as well as prominent reviews of DA circuitry, function, and influence on disease etiology have used this heuristic to describe SNc/VTA targets (Arias-Carrión, Stamelou, Murillo-Rodríguez, Menéndez-González, & Pöppel, 2010; Bressan & Crippa, 2005; Caminiti et al., 2017; Cools, Ivry, & D'Esposito, 2006; Klein et al., 2019)

Although providing a convenient explanation for DA-mediated behaviours, this convention is now known to be an oversimplification of SNc/VTA DAergic circuits (Bissonette & Roesch, 2016; Björklund & Dunnett, 2007; Düzel et al., 2009; Yetnikoff et al., 2014). A closer examination of the literature reveals evidence that SNc/VTA DA projections do not strictly adhere to this conventional pathway heuristic (Joel & Weiner, 2000).
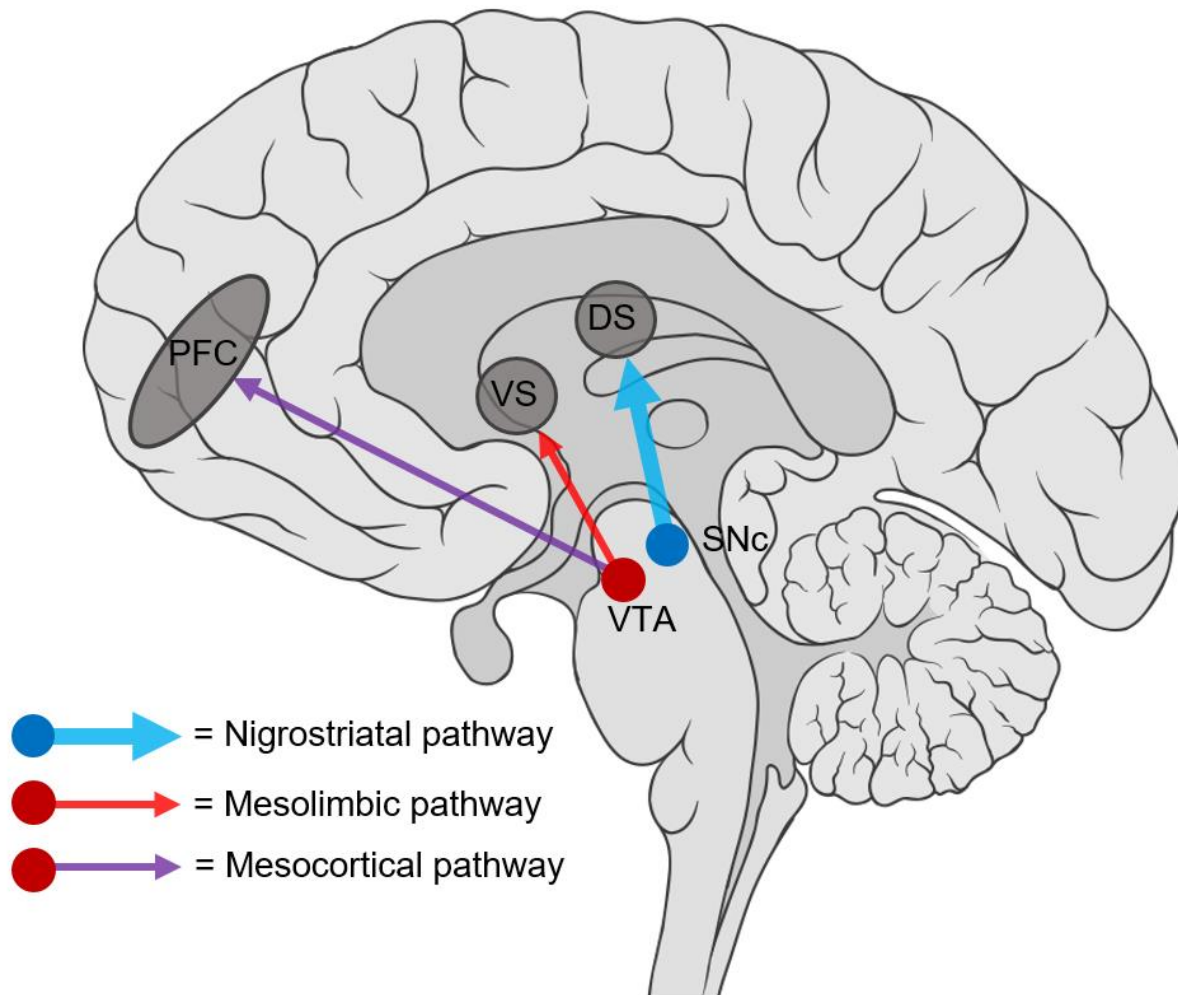
Figure 2: Visualization of the Conventional Pathway Heuristic. In the nigrostriatal pathway (blue), SNc projects to the DS; in the mesolimbic pathway (red), VTA projects to the VS; in the mesocortical pathway (purple), VTA projects to the PFC. Figure was adapted from Klein et al. (2019). Brain illustration used with permission from Patrick J. Lynch.

1.4 – The Conventional SNc/VTA Pathway Heuristic

The conventional pathway heuristic has been adopted as it provides convenient explanations for DA-mediated diseases (Alcaro, Huber, & Panksepp, 2007). In the case of the nigrostriatal pathway, the 1960 discovery that SNc produces DA coupled with previous knowledge that a) SNc cells are lost in PD patients and b) that DS projects prominently to motor regions in the brain, resulted in the inference that the DA projections from the SNc to the DS mediate motor function and dysfunction in the case of PD (Ehringer & Hornykiewicz, 1960; Haber & Fudge,

1997; Ungerstedt, 1971). During this period, the non-motor symptoms of PD patients were largely unrecognized, and thus projections of SNc were thought to be limited to the DS (Lidsky, 1995; Pfeiffer, 2016; Ungerstedt, 1971). Subsequent lesion studies of SNc and DS seemed to confirm this function (Andén, Dahlström, Fuxe, & Larsson, 1966). The establishment of the mesolimbic and mesocortical pathways was spurred by interest in DA's role in symptoms in schizophrenia patients (Brisch et al., 2014; Lidsky, 1995). Given observations that DA receptor agonists alleviated schizophrenic symptoms, it was hypothesized that DA hyperactivity resulted in schizophrenic symptoms (Baumeister, 2013; Carlsson & Lindqvist, 1963). The link between DA and schizophrenic symptoms was unresolved at first given the contemporaneous concept that the nigrostriatal DA pathway mediated motor function (Lidsky, 1995). The 1966 description of a DA bundle from the VTA to the NAcc (i.e., the VS) and of DA neurons to limbic brain regions like the hippocampus and amygdala allowed for a conceptualization of how DA hyperactivity could result in the psychiatric symptoms of schizophrenia, given that these brain regions were known to affect emotion, attention, and memory (Andén et al., 1966; Lidsky, 1995; Stevens, 1973). The efficacy of medications that had impacts on DA (i.e., DA replacement therapy in PD and DA antagonists in schizophrenia), in addition to an account for how different DAergic pathways mediate disparate functions and symptoms (i.e., deficiency in the nigrostriatal pathway producing movement symptoms in PD, and hyperactivity in the mesolimbic pathways producing psychotic symptoms in PD) solidified this paradigm (Iversen & Iversen, 2007; Lidsky, 1995; Moore & Bloom, 1978; Ungerstedt, 1971). The establishment of a direct mesocortical pathway occurred following the discovery of DA in the PFC areas with cell bodies clustered in the VTA (Koslow, Cattabeni, Costa, Stinus, & Glowinski, 1972; Lindvall, Björklund, Moore, & Stenevi, 1974).

1.5 – Counterevidence of the Conventional Pathway Heuristic

Histochemical, tracer, and molecular studies in rodent and non-human primate models seem to indicate that the SNc targets the VS as well as the DS and that the VTA projects to the DS in addition to the VS. This has been demonstrated in both rodent and non-human primate models.

1.5.1 - Evidence in Rodent Models

1.5.1.1 - SNc Projections to the VS

Numerous retrograde studies examining the afferent connections to the NAcc have reported non-insignificant numbers of labelled cells in the SNc, suggesting a connection from the SNc to the VS. In Nauta et al. (1978), injections of horseradish peroxidase (HRP) into the ventral aspect of the NAcc resulted in labelled cells clustered in the SNc, but it was also reported that there was labelling of the SNc increasing in a rostral-caudal orientation (Nauta, Smith, Faull, & Domesick, 1978). This was replicated by Brog and colleagues, who reported the presence of labelled cells in the SNc following the injection of Fluoro-Gold (FG) radiotracer into the core and lateral shell of the NAcc (Brog, Salyapongse, Deutch, & Zahm, 1993). In a more recent retrograde tracer study, it was demonstrated that following injection of Fast Blue (FB) an FG into the NAcc core and NAcc shell, up to 7% of cells labelled in the SNc/VTA were found in the SNc (Rodríguez-López, Clascá, & Prensa, 2017). These retrograde tracer studies provide evidence that the SNc projects to the VS; in fact, given that the VS is composed of the dorsal aspects of the caudate nucleus and putamen in addition to the NAcc, it might be that the extent of connections from the SNc to the VS are underreported in these studies. A more conclusive finding to suggest the existence of these connections was reported by Matsude and colleagues (2009), who injected a recombinant Sindbis viral vector with a membrane-targeting green fluorescent protein (GFP) into the SNc to allow for the tracking of individual SNc DA neurons (Matsuda et al., 2009). Of eight neurons examined, five were found to innervate the DS, whereas the remaining three were found to innervate the middle and ventral portions of the striatum, including the border of the ventral CPu *and* the NAcc (Matsuda et al., 2009).

1.5.1.2 - VTA Projections to the DS

Rodent studies have also demonstrated the possibility of VTA efferent neurons that target the DS. In a set of experiments by Fallon et al. (1978), anterograde radioactive proline/leucine tracer injected in the VTA resulted in limited labelling in the medial and anterior sectors of the DS, whereas retrograde HRP tracer injection into the DS resulted in HRP labels in the lateral VTA in

addition to the SNc (Fallon & Moore, 1978). The former result was replicated a year later, in which injections of anterograde proline/leucine tracer into the VTA resulted in the labelling of a wide distribution of cells in the striatum (Beckstead, Domesick, & Nauta, 1979). Many of these cells were located in the VS as expected, but labelled cells were also found extending in the dorsal direction into much of the CPu in a graded fashion (Beckstead et al., 1979). This was also demonstrated in a study in which retrograde fluorescent beads were injected into various sites of the DS, which resulted in labels in the VTA (in 29/33 injection sites) in addition to the SNc (in 31/33 injection sites), although the VTA projections seemed less dense than those of the SNc (Pan, Mao, & Dudman, 2010).

In more direct observations of individual neurons following the injection of VTA cells with the anterograde tracer biotinylated dextran amine, it was noted that certain classes of VTA neurons projected to regions in the ventral aspect of the DS, whereas others projected to the VS (Prensa & Parent, 2001). In a combined anterograde tracer-GFP viral vector approach, Aransay et al. (2015) described intense labelling in the NAcc and the CPu following injection into the VTA, though they did not specific to what regions of the CPu (Aransay, Rodríguez-López, García-Amado, Clascá, & Prensa, 2015) Using the GFP-viral vector, they also described a cluster of "mesostriatal" neurons that targeted the central and dorsal sections of the striatum (Aransay et al., 2015). These neurons were interpreted to potentially emerge from an overlap between the VTA and SNc, but similar direct VTA-DS connections were also described by Brier et al. (2019) (Aransay et al., 2015; Beier et al., 2019). In their study, a cacine advenovirus expressive cre-dependent Flp recombinase was injected into the medial PFC and into the amygdala of a DAT-cre mouse line (Beier et al., 2019). Subsequently, an Flp-dependent adeno-associated virus expressing GFP was injected into the VTA such that projections from the VTA that received projections from the PFC and amygdala could be measured. The researchers found that efferent projections tended to exit the VTA in clusters, and that one cluster class contained axon collaterals that targeted the dorsomedial and dorsolateral striatum in addition to the NAcc (Beier et al., 2019).

1.5.2 – Evidence in Non-Human Primate Models

Investigations into SNc/VTA projections in non-human primates have perhaps been even more illustrative of the potential pitfalls of a nigrostriatal/mesolimbic dichotomy. It has been demonstrated that the organization of SNc and VTA neurons is more complex in non-human primates compared to rodents (Düzel et al., 2009; Haber & Knutson, 2010; Joel & Weiner, 2000). Based on cellular characteristics, the DA neurons of the midbrain can be divided into a dorsal tier comprised of the dorsal aspects of the SNc and the VTA versus a ventral tier comprised of the medial and ventral aspects of the SNc (Haber & Knutson, 2010; Lynd-Balta & Haber, 1994). On the basis that certain regions of the SNc overlap with the VTA, it has been argued that the nigrostriatal/mesolimbic heuristic might be inaccurate in humans (Düzel et al., 2009; Wise, 2009). Indeed, following the injection of anterograde tracers into the dorsal tier, labelled cells were found in the VS, indicating that certain neurons of the SNc projected to the VS (Haber, Fudge, & McFarland, 2000). Conversely, in a number of studies, following retrograde tracer into the DS, it has been shown that though the majority of neurons projecting to the DS were from the SNc, there were also labels found in the VTA (Parent, Mackey, & De Bellefeuille, 1983; Szabo, 1980).

1.6 – Evidence of SNc-PFC Projections

Finally, though the discovery of VTA innervation to the PFC prompted the proposal of the mesocortical pathway, it was subsequently discovered that the SNc also projects to the PFC (Fallon, 1988; Lindvall et al., 1974; Wise, 2009). Evidence in support of this finding has been elucidated by numerous studies. In one study of rodents, for example, retrograde HRP was injected into various regions of the cortex; following injection into the PFC, retrograde labels were found in the medial SNc in addition to the VTA (Loughlin & Fallon, 1984). This has been demonstrated in non-human primates as well. For instance, the injection of retrograde tracer cells into the PFC resulted in retrograde labelling in the dorsal aspects of the SNc and the VTA (Gaspar, Stepniewska, & Kaas, 1992). In a similar study, retrograde labels were also found in the dorsal aspects of the SNc and VTA following injection into the dorsolateral PFC (Williams & Goldman-Rakic, 1998).

1.7 – SNc/VTA Projections in Humans *in Vivo*

Few investigations have been undertaken to investigate SNc/VTA connectivity of humans *in vivo,* and this has largely been due to technological limitations. Magnetic resonance imaging (MRI) has been a promising tool to accomplish this due to its non-invasiveness and because of its multiple modalities that can measure brain anatomy, function, and connectivity.

A full description of MRI physics and principles can be found elsewhere (Huettel, Song, & McCarthy, 2008). Briefly, MRI uses a powerful magnet that generates a primary magnetic field (B_0). This magnetic field aligns the hydrogen atoms of water in brain tissue in a parallel fashion in the low-energy state and in an antiparallel fashion in the high-energy state. Gradient coils can add additional magnetic fields across different orientations. Radiofrequency (RF) pulses (B_1) reorient some parallel atoms into a high-energy antiparallel state, in which they are in phase. Subsequent relaxation of high-energy antiparallel atoms into the low-energy parallel state emits RF energy that is converted to a digital signal and into an image on a computer screen. White and gray matter return to relaxation at different rates, and thus they can be distinguished anatomically (Huettel et al., 2008). The resolution of MRI images is largely dependent on the strength of the magnet, with higher magnetic strength, measured in Tesla (T), yielding greater resolution (Ladd et al., 2018).

Thus far, attempts to measure SNc/VTA connectivity using MRI have employed diffusion MRI (dMRI) and functional MRI (fMRI) to measure structural and functional connectivity, respectively.

1.7.1 – Structural Connectivity Measured with Diffusion MRI

Structural neural connectivity can be measured using dMRI imaging. dMRI is an imaging technique that allows for the inference of white matter location and orientation based on the 3D anisotropic diffusion of water molecules in brain tissue (Baser, 1995; Peter J. Basser & Jones, 2002; Soares, Marques, Alves, & Sousa, 2013). dMRI is reliant on the acquisition of diffusion weighted imaging (DWI) scans. DWI is an MRI modality that measures the level of water

diffusion within each voxel (Soares et al., 2013). Briefly, DWI scans are acquired with the use of gradient pulses of equal strength applied along the same orthogonal plane but in different directions (Bammer, 2003). Following the excitatory RF pulse, two gradient pulses are applied in opposite directions. The first is a dephasing gradient pulse which places the hydrogen protons out of phase. The second is a rephasing gradient pulse that puts the hydrogen protons back in phase by applying a gradient of equal magnitude in the opposite direction. However, if the hydrogen protons move via diffusion in the time between these two opposing gradients, the protons will not return in phase in the same location and there will be a signal loss. Thus, regions without diffusion restriction (i.e., within brain ventricles) will have a signal loss, whereas regions with diffusion restriction (i.e., within the cell membrane-confined axon) will have no signal loss (Bammer, 2003).

Notaby, dMRI allows for the reconstruction of white matter tracts throughout the brain using fiber tractography methods, which can calculate the connectivity density between brain regions (Basser, Pajevic, Pierpaoli, Duda, & Aldroubi, 2000). Using mathematical models, sampled streamlines are calculated that traverse continuous pathways of anisotropic diffusion by connecting each voxel to its adjacent voxel with respect to corresponding anisotropic fields (Alexander, Lee, Lazar, & Field, 2007).

Probabilistic tractography, as opposed to deterministic tractography, calculates thousands of seeded streamlines from a seed brain region to target brain regions (A. L. Alexander et al., 2007; Behrens, Woolrich, et al., 2003; Parker & Alexander, 2003; **Figure 3**). These probability density functions are estimated using Markov Chain Monte Carlo (MCMC) sampling, which calculates a probability index between the seed region and the target regions. It should be noted that these maps cannot determine the polarity of axon fibers (Behrens, Woolrich, et al., 2003). Probabilistic tractography has been used to create connectomic maps amongst brain regions based off the extent to which sampled streamlines connect between brain regions, offering insight into the extent that regions structurally connect with one another (Cacciola et al., 2016, 2017; Chung et al., 2017; Kwon & Jang, 2014; Lenglet et al., 2012; Shi & Toga, 2017; Skudlarski et al., 2008; Theisen et al., 2017; Vosberg et al., 2018; Yu Zhang, Larcher, Misic, & Dagher, 2017). In addition, it can be used to sub-divide, or parcellate brain regions based on each of its voxel's connectivity patterns. This can be accomplished using various clustering methods

as well as sampled streamline voting (Behrens, Johansen-Berg, et al., 2003; Eickhoff, Thirion, Varoquaux, & Bzdok, 2015). These methods have been used extensively to parcellate the cortex but have also shown promise in parcellating the BG and midbrain DAergic structures. (Chowdhury, Lambert, Dolan, & Düzel, 2013a; Ganepola, Nagy, Ghosh, Papadopoulo, & Sereno, 2018; Gao et al., 2018; Gong et al., 2009; Lambert et al., 2012; Liu et al., 2013; Menke, Jbabdi, Miller, Matthews, & Zarei, 2010; Schiffler, Tenberge, Wiendl, & Meuth, 2017; Tziortzi et al., 2014; Wiegell, Tuch, Larsson, & Wedeen, 2003; Y. Zhang et al., 2014; Yu Zhang et al., 2017).
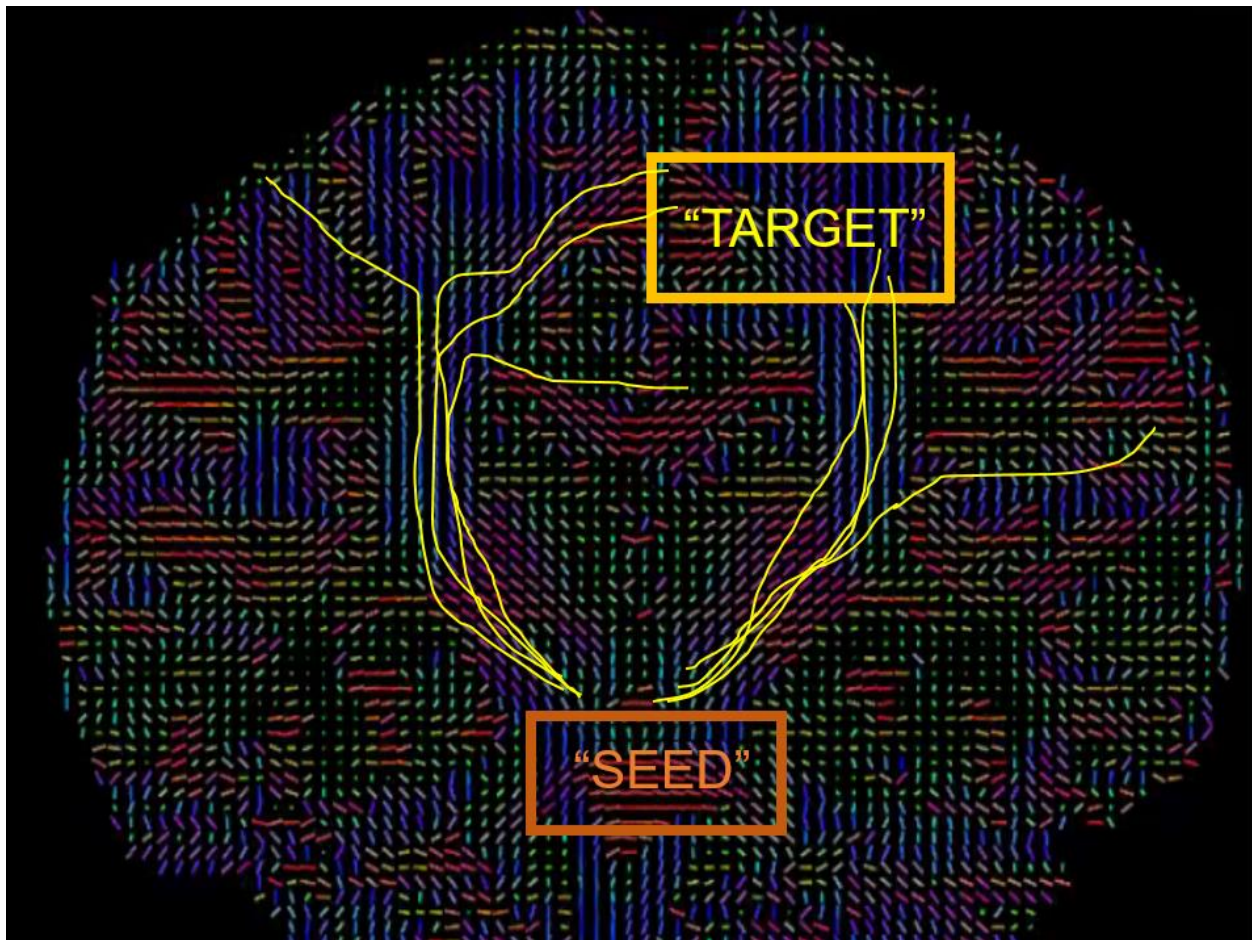
Figure 3: Representative Example of Probabilistic Tractography. In this example, the brain of a sample participant is shown in the coronal plane. Probabilistic tractography is performed from a seed region ("SEED"). Seeded streamlines (yellow) follow paths according to adjacent voxel's anisotropic character (shown in red, green, and blue). The number of streamlines that contact a target region ("TARGET") are retained to calculate connectivity density. Adapted from Behrens et al. (2003).

Though many studies have utilized dMRI to measure FA, MD, and RD within the SNc and the VTA, very few have taken advantage of dMRI to measure the connectivity density of the SNc/VTA to other brain regions (Atkinson-Clement, Pinto, Eusebio, & Coulon, 2017; Deng, Wang, Yang, Li, & Yu, 2018; Langley et al., 2016). This is in part due to challenges with this form of MRI imaging. The SNc and VTA can be prone to image distortions and artifacts due to their small sizes, and their projections to the striatum and cortex pass through the internal capsule, where fibers from very disparate areas of the brain converge, risking erroneous claims about connectivity between SNc/VTA and cortical areas because of inaccurate tracking, especially at lower magnetic field strengths (Jbabdi, Sotiropoulos, Haber, Van Essen, & Behrens, 2015; Meola, Yeh, Fellows-Mayle, Weed, & Fernandez-Miranda, 2016; Yu Zhang et al., 2017). Furthermore, the lack of an accurate, publicly-available subcortical atlas has made it difficult to define the SNc and VTA or delineate between them in MRI space (Pauli, Nili, & Tyszka, 2018).

To our knowledge, only one study has used dMRI to measure the connectivity of the SNc/VTA to the striatum and cortex in which the SNc and VTA were measured as separate regions of interest (ROIs; Kwon & Jang, 2014). In this study by Kwon et al. (2014), anatomical and DWI images measured at 1.5T were acquired from 63 participants. Probabilistic tractography was performed on the DWI scans to assess the connectivity of the SNc and the VTA to various regions in the striatum and cortex. The authors defined connectivity between either the SNc or the VTA to a target as the percentage of participant hemispheres in which sampled streamlines reached the target region at a threshold of 0.1%. They found that both the SNc and the VTA connected with the CPu, though the SNc had a significantly higher connectivity than the VTA (SNc to CPu = 99.21%, VTA to CPu = 68.25%, $p < 0.001$). They also found that both the SNc and the VTA connected with the NAcc; intriguingly, the connectivity of the SNc to the NAcc was also significantly higher than that of the VTA (SNc to NAcc = 97.62%, VTA to NAcc = 65.87%, $p < 0.001$). SNc and VTA connectivity were also measured with respect to the PFC, wherein the SNc connectivity was 95.24% and VTA connectivity was 65.87%, with SNc being significantly higher than VTA ($p = 0.001$; Kwon & Jang, 2014). Their results are intriguing because they are at odds with the conventional SNc/VTA pathway heuristic. However, their study was limited by the facts that a) MRI scans were performed at 1.5T, risking the generation of less accurate connectivity profiles due to erroneous mapping, especially in the internal capsule, and b) the ROIs for the VTA were hand-drawn. Further, their definition of connectivity

to a target as the *incidence* of connectivity was measured as the percent of participant hemispheres in which that target was innervated. For instance, if 0.1% connectivity occurred from SNc to the DS in 90 participant hemispheres out of 100, they would have reported 90% connectivity from SNc to DS. This definition does not reveal information about the connectivity densities among the structures themselves, however. For these reasons, their results, which challenge the conventional DA pathway heuristic have been largely discounted, with reviews and theories of disease continuing to implement the conventional pathway heuristic without qualification. An analysis of relative SNc and VTA connectivity density, as defined by streamline density, measured with ultra-high field MRI, using SNc/VTA atlases derived from high resolution imaging investigations, and employing sampled streamline counts, remains to be performed *in vivo* in humans to fully address this issue.

Other investigations into the connectivity patterns of the DAergic midbrain have either used only an SNc ROI, only a VTA ROI, or a combined, undifferentiated SNc/VTA ROI, though these studies have offered insight into DAergic pathways to the striatum and cortex as well. In a study by Chowdhury et al. (2013), dMRI measured at 3T was used to parcellate a combined SNc/VTA ROI into ventrolateral and dorsomedial subregions based upon connectivity to the DS or VS, respectively (Chowdhury, Lambert, Dolan, & Düzel, 2013). That both subregions contained aspects of the SNc and the VTA lends evidence to a more complex DAergic projection pattern than the conventional pathway heuristic contends. Potential evidence to this end was also reported by Vosberg et al. (2018). They performed dMRI probabilistic tractography on MRI data of healthy controls and of DCC (Deleted in Colorectal Cancer)-haploinsufficient participants (Vosberg et al., 2018). The DCC gene produces DCC protein, which is an axon guidance molecule receptor thought to play a role in axon guidance and known to increase DA innervation to the NAcc (Manitt et al., 2011; Vosberg et al., 2018). They employed a seed ROI that contained voxels primarily of the SNc but potentially overlapped with part of the VTA. They found that connectivity density from the SNc/VTA to the NAcc was reduced in carriers of the DCC mutation, indicating potential connectivity between the SNc and the NAcc. Finally, evidence for connectivity between the SNc and the PFC was also demonstrated in a study by Menke et al. (2010), in which a substantia nigra (SN) ROI that included both SNc and SNr was parcellated into two subregions based off the location of fibre connections through each voxel within the ROI. It was noted that one of these regions corresponded with the SNc, and that using

probabilistic tractography, it mostly connected with the posterior striatum, GP, anterior thalamus, and PFC (Menke et al., 2010).

1.7.2 – Functional Connectivity Measured with Functional Magnetic Resonance Imaging

ROI-based functional connectivity, quantified via fMRI, has also been posited as an indirect measure of connectivity (Damoiseaux et al., 2006; Lv et al., 2010). fMRI measures the blood-oxygen-level-dependent (BOLD) contrast of different brain regions that activate temporally either in response to a task or at rest. BOLD is a proxy measurement for neural activity that relies on the fact that neurons consume a massive amount of energy following activation (Attwell & Laughlin, 2001). The activation of neurons within a brain region results in increased vascular supply of oxygen, which is transported on the hemoglobin molecule in red blood cells (Attwell et al., 2010). Rather conveniently, the magnetic properties of hemoglobin are different when oxygenated and when deoxygenated: when oxygenated, hemoglobin is diamagnetic, but when deoxygenated, it is paramagnetic which disrupts the local magnetic field (Ogawa, Lee, Kay, & Tank, 1990). The relative decrease of paramagnetic deoxygenated hemoglobin following the flux of oxygenated hemoglobin to active brain region has been exploited with MRI sequences to measure BOLD (Kirilina, Lutti, Poser, Blankenburg, & Weiskopf, 2016). Functional connectivity is the organization and inter-relationship of BOLD response of different brain regions; regions whose BOLD responses correlate overtime are considered functionally connected (Rogers, Morgan, Newton, & Gore, 2007).

Potential evidence to suggest that the conventional pathway heuristic is an oversimplification has also been demonstrated in functional connectivity studies. In ROI-based functional connectivity studies in which ROIs have been defined for both the SNc and the VTA, it has been shown, for example, that both the SNc and the VTA demonstrated highly significant resting state functional connectivity (RSFC) with both the DS and the VS (Bär et al., 2016; Tomasi & Volkow, 2014). Furthermore, Peterson et al. (2017) found that the SNc and the VTA had positively correlated RSFC with the VS, and that there was no significant difference in these RSFC levels. These studies have also demonstrated that the SNc and the VTA have positively correlated RSFC with

broad cortical regions, including the PFC (Bär et al., 2016; Peterson, Zhang, Hu, Chao, & Li, 2017; Tomasi & Volkow, 2014).

These findings are, however, inconsistent with that of Murty et al. (2014), who found that only the VTA was positively correlated with VS; oddly, they found that neither the SNc nor the VTA functional activity was positively correlated with that in the DS (Murty et al., 2014). This could be reflective of the potential limitations of functional connectivity as a measure of structural connectivity. Indeed, the extent to which functional connectivity is correlated to structural connectivity remains a matter of debate (Honey et al., 2009; Huang & Ding, 2016; Lv et al., 2010; Tsang et al., 2017). As a matter of principle, a pair of ROIs with correlated BOLD activity could reflect a) a direct connection between the two, but also b) a common input from a separate region or regions, or c) an interaction that is mediated by a separate region or regions (Huang & Ding, 2016). Furthermore, it has been suggested, given the small volume of the SNc and VTA, that only high resolution fMRI with voxel sizes of 1.5 mm x 1.5 mm x 1.5 mm isotropic and smaller be used to assess differences among SNc and VTA BOLD signals (Düzel et al., 2009). Studies examining SNc and VTA functional connectivity have all been performed at 3T, which can typically perform fMRI at a resolution of 3 mm x 3 mm x 3 mm, potentially limiting the accuracy of their findings (Bär et al., 2016; Goense, Bohraus, & Logothetis, 2016; Murty et al., 2014; Peterson et al., 2017; Tomasi & Volkow, 2014) In fact, some studies examining SNc/VTA functional connectivity at 3T have opted not to compare the difference in SNc and VTA connectivity for this reason (Di Martino et al., 2008).

1.8 – Aims of the Present Study

Given that there remains uncertainty regarding even the most commonly-held notions of the DAergic pathways from the SNc/VTA to the striatum and cortex, it follows that investigations into these circuits will offer insight into how DA regulates a wide range of essential behaviours and how DA-mediated disease symptomology occurs. This is especially important for humans *in vivo*, in which neuroimaging can potentially be used to uncover biomarkers of disease (Khan et al., 2019). In addition, though post-mortem dissections are often held as the gold-standard to measure human anatomical mapping, significant changes are known to occur to the central

nervous system immediately following death, potentially limiting understanding as to how SNc/VTA neural tracts are structured *in vivo* (Weickenmeier et al., 2018). Thus, a connectomic analysis of human SNc/VTA tracts to the striatum and cortex using high resolution neuroimaging remains an important but unfulfilled goal.

The goal of Experiment 1 of the present study was to investigate the pathways of the SNc and the VTA in the context of the conventional heuristic of SNc/VTA pathways to DS, VS, and the PFC. Specifically, we measured and compared the connectivity density of the SNc and VTA to and from the DS, VS, and PFC, which might inform about the extent to which the SNc and VTA project to each of these regions. We have also measured the connectivity density of the DS, VS, and PFC to and the SNc and VTA. We compared each region's connectivity to SNc versus VTA, which might inform about the extent to which each region's total innervation arose from the SNc and the VTA.

To overcome some of the limitations of the few others studies that have employed dMRI on the SNc and VTA, we have used data acquired from the Human Connectome Project (HCP) (Van Essen et al., 2012; Van Essen et al., 2013). This data has been acquired from human participants scanned on a 3T scanner with added customizations to improve DWI acquisitions to even higher resolution than conventional 7T scanners (Uğurbil et al., 2013). We have also employed the use of the CIT168 SNc/VTA atlas, which was delineated on the same scanner as the HCP data (Pauli et al., 2018). Finally, we have used a probabilistic tractography modality called ball & stick (BEDPOSTX) which attempts to overcome the dMRI limitation of crossing fibers by using MCMC within each voxel to estimate the anisotropic measurements across many orientations (Behrens, Berg, Jbabdi, Rushworth, & Woolrich, 2007).

However, given the knowledge that there is a potential overlap between SNc and VTA, with some arguing that these are not accurate with respect to underlying anatomy, we have extended a model by Tziortzi et al. (2014) to assess connectivity from the VTA/SNc to the striatum without relying on defined borders between subregions (Tziortzi et al., 2014). Tziortzi et al. (2014) described a method to parcellate the striatum into limbic, executive, caudal motor (CM), rostral motor (RM), parietal, occipital, and temporal subregions based on connectivity to cortical lobes (Tziortzi et al., 2014). They accomplished this by using a winner-take-all approach, where each

voxel in the striatum was labelled based on whichever cortical subregion the majority of its streamlines targeted (Johansen-Berg et al., 2005; Tziortzi et al., 2014).

We have previously shown that the CM region of the striatum, which is connected primarily to CM cortex, is significantly smaller in PD patients as compared to controls (Khan et al., 2019). We conjectured that this was because of its connectivity to the CM subregion of the SNc, which is known to degenerate first and most in PD (Fearnley & Lees, 1991; Kish et al., 1988) Furthermore, the CM striatum connects to the CM cortex, made up of the premotor and motor cortices accounting for the motor symptoms that characterize PD. These include slowed movements (i.e., bradykinesia), tremor, and muscular rigidity.

In Experiment 2 of this study, we extend this line of reasoning to the SNc/VTA by at first parcellating the striatum with respect to the cortex and then assessing independent connectivity of the SNc/VTA to each striatal subregion. Independent connectivity measures the seeded streamline count from all voxels in the SNc/VTA to each striatal subregion. Connectivity to each striatal subregion is calculated one by one, allowing for connectivity measures across potentially overlapping SNc/VTA subregions. This avoids potential limitations of parcellating the SNc/VTA under winner-take-all voting before probabilistic tractography. Voting, although beneficial for creating subregions, discards some potential information about voxel targets. For example, if a voxel in the SNc sends 1000 streamlines to the limbic striatal subregion and 500 to the executive striatal subregion, it will be labelled as a limbic voxel under winner-take-all voting, essentially disregarding its streamlines to the executive subregion. In this example, independent connectivity would account for these 500 streamlines to the executive striatum because it does not create the SNc/VTA parcellations in the first place.

To explore this connectivity scheme, we have at applied it to a population of recently diagnosed PD patients who, by virtue of the progressive nature of SNc degeneration in PD, might not have progressed enough in the disease to see changes in the striatum. The purpose of this experiment is to a) offer validation that probabilistic tractography can more or less accurately measure DAergic tracts emerging from the SNc and the VTA, and to b) demonstrate that dMRI can be used to explore changes to DAergic tracts in patients with DA-mediated diseases.

1.9 – Hypotheses

In Experiment 1, we predicted that the connectivity of the SNc and VTA to and from the DS, VS, and cortex would be more complicated than the conventional pathway heuristic. In other words, we predicted that there would be significant connectivity density of the SNc to and from the VS, of the VTA to and from the DS, and of the SNc to and from the PFC. Similarly, we predicted that the percentage of connections in the DS, VS, and PFC that target the SNc and VTA would not follow conventional pathway heuristic, such that the DS would target the VTA, that the VS would target the SNc, and that the PFC would target the SNc.

In Experiment 2, we predicted that there would be lower independent connectivity from the SNc/VTA to the CM striatum in PD patients as compared to controls. We also predicted that connectivity from the whole SNc to the whole striatum would not be significantly different between groups.

Chapter 2 – Methods

2.1 – Experiment 1: Human Connectome Project

      3T MRI Data from the WU-Minn 1200 subjects Release (S1200) of March 01, 2017 were utilized in this study (Van Essen et al., 2012; Van Essen et al., 2013). The dataset is available in the Human Connectome Project repository (https://www.humanconnectome.org/study/hcp-young-adult).

2.1.1 - Participants

      In this study, we analyzed the 100 unrelated (U100) subjects sub-dataset, which consisted of 54 females and 45 males with an age range of 22 to 35 years of age (Hodge et al., 2016). Healthy participants between the ages of 22 and 25 were eligible for the study and were screened for the inclusion/absence of inclusion/exclusion criteria (Van Essen et al., 2012). Participants who smoked, were overweight, or who had a history of alcohol/recreational substance use were eligible as long as they had not experienced severe symptoms. Participants were excluded if they had a diagnosis of or familial history of a neurodevelopmental, neuropsychiatric, or neurological disorder. The Semi-Structured Assessment for the Genetics of Alcoholism was provided to each participant to ensure the absence of significant psychiatric illness (Bucholz et al., 1994). As per HCP protocol, all participants had provided informed consent to the Human Connectome Project Consortium (Van Essen et al., 2013).

2.1.2 - MRI Acquisition

      The U100 participants were asked to complete 3T MRI sessions according to the HCP protocol, which included structural, fMRI (resting state and task-evoked), and DWI acquisitions over the span of two days. Scans took place within a customized Siemens 3T "Connectome Skyra" scanner at Washington University in St. Louis, which contained a number of customizations to improve resolution, the full details of which can be found elsewhere (Van

Essen et al., 2013). Relevant to the present study, a customized SC72 gradient insert typically used in 7T field strength was used to improve the resolution of DWI images (Uğurbil et al., 2013). This, along with gradient coil and gradient power amplifiers, allows for a maximum gradient strength (G_{max}) of 100 mT/m, which is higher than typical 40-60 mT/m G_{max} scanners (S. Y. Huang et al., 2015). The increased G_{max} as a result of these customizations is especially beneficial to DWI scans because it reduces the signal loss that occurs during the delay between proton signal excitation and image acquisition during which diffusion encoding occurs, therefore increasing DWI resolution (Setsompop et al., 2013; Uğurbil et al., 2013).

The present study utilized the U100 pre-processed structural data (T1w and T2w) and pre-processed DWI data. For the T1w anatomical scan, 3D magnetization-prepared rapid acquisition with gradient echo (MPRAGE) sequence was performed with the following parameters: TR = 2400ms, TE = 2.14 ms, TI = 1000 ms, flip angle = 8º, FOV = 224x224 mm, voxel size = 0.7 mm x 0.7 mm x 0.7 mm, BW = 210 HZ/Px, and acquisition time = 7 min, 40s.

A multi-slice echo-planar imaging (EPI) with multiband (MB) excitation sequence was used to collect DWI data (Sotiropoulos et al., 2013). The following parameters were used: TR = 5520 ms, TE = 89.5 ms, flip angle = 78º, FOV = 210x180 pixels, acquisition matrix = 168x144 pixels, and with one whole brain image consisting of 111 slices with slice thickness = 1.25 mm and with voxel size = 1.25 mm x 1.25 mm x 1.25 mm. The DWI images were collected using gradient tables with R/L and L/R phase encoding polarities for a total of six runs. Each run had 95-97 directions and six b=0 acquisitions. Diffusion weighting had three shells of b = 1000, 2000, 3000 s/mm^2 which were interspersed with an approximately equal number of acquisitions/shell within each run.

2.1.3 - T1 and DWI Pre-processing

2.1.3.1 - Anatomical pre-processing

A full description of the HCP anatomical pre-processing pipeline can be found elsewhere (Fischl, 2012; Glasser et al., 2013; Jenkinson, Bannister, Brady, & Smith, 2002; Jenkinson, Beckmann, Behrens, Woolrich, & Smith, 2012).

In brief, Gradient distortion correction is applied to each participant's T1w and T2w image using the HCP pipeline gradunwrap (https://github.com/Washington-University/gradunwarp/). T1w and T2w images were aligned and averaged using FSL FLIRT and an HCP in-house script and then registered to Anterior Commissure-Posterior Commissure coordinates using FLIRT such that each image was in participant's native space (Jenkinson et al., 2002). Brain extraction was accomplished with FSL FNIRT (J. L. R. Andersson et al., 2007; Jenkinson et al., 2012). Then, all images underwent field map distortion correction and B1 field bias correction using a customized FSL FLIRT Boundary-Based registration pipeline and sqrt (t1w X t2w), respectively. The t1w and t2w images were then non-linearly registered to MNI152 space using FSL FNIRT.

2.1.3.2 - DWI pre-processing

The DWI pre-processing pipeline is described in full elsewhere (Andersson, Skare, & Ashburner, 2003; Andersson & Sotiropoulos, 2015, 2016).

Briefly, pre-processing is initialized with intensity normalization across the six runs. Following this, FSL TOPUP was used to correct for EPI distortions and FSL EDDY was used to correct for eddy currents and motions. The pipeline used FSL EDDY v5.0.10, which detects slice outliers which have been distorted due to participant movement and is replaced by non-parametric Gaussian Process Modelling predictions. Subsequently, gradient b-value and b-vector deviations were corrected with gradient nonlinearity correction. Following these steps, registration of each participant's average B0 image was registered to the T1w image using FLIRT BBR-bbregister, which also transformed the dMRI into 1.25 mm x 1.25 mm x 1.25 mm T1w-space.

Finally, FSL Bayesian Estimation of Diffusion Parameters Obtained using Sampling Technique (BEDPOSTX) was used to model the estimate the probability of dMRI diffusion parameters (Behrens, Woolrich, et al., 2003; Behrens et al., 2007). This pre-processing pipeline used MCMC sampling to establish probability estimates of diffusion at each voxel by modelling diffusion as sticks (anisotropic tensors) and a ball (isotropic background). This step is a prerequisite to run probabilistic tractography.

2.1.4 – Mask Segmentation

To analyze the connectivity of the SNc/VTA to the striatum and cortex, we used a variety of publicly available atlases.

2.1.4.1 – Segmentations of the SNc/VTA and Cortex

Left and right SNc and VTA labels of the CIT168 atlas were used to form the segmentation of the SNc and VTA (Pauli, Nili, & Tyszka, 2018; https://neurovault.org/collections/3145/). The CIT168 is optimal for this analysis due to its clear demarcation of the SNc and the VTA. It was also derived with respect to HCP data collected on the same machine as the U100 set, reducing the risk of high inter-machine variability, which is an important consideration for dMRI data, and because of its high inter-rater and intra-rater reliability (Bonilha et al., 2015; Pauli et al., 2018). The SNc and VTA ROIs were generated by at first creating eight validation templates by merging 84 T1w and 84 T2w image pairs that had been randomly selected from 168 image pairs. Then, subcortical ROIs were delineated by three observers in the left hemisphere of each validation template; the ROIs were then averaged across observer and template and projected to the right hemisphere (Pauli et al., 2018). The subcortical ROIs were delineated with reference to the Allen Institute Adult 34 year old human atlas (Hawrylycz et al., 2012). The SNc was defined as the hyperintense band between the parabrachial pigmented area (PBP) and SNr with the rostral limit coinciding with the caudal limit of the hypothalamus (Pauli et al., 2018). The VTA was delineated ventral to the red nucleus (RN) at the ventromedial limit of the PBP and extending rostrocaudally from the rostrocaudal midpoint of the RN to slightly beyond the caudal limit of the RN (Pauli et al., 2018).

Cortical regions were adapted from the Harvard-Oxford FSL atlas, which features 48 anatomically-derived subregions, lateralized by side (Fischl et al., 2004; Rademacher, Galaburda, Kennedy, Filipek, & Caviness, 1992). We also added an additional rostral-motor subregion within the frontal lobe, located posterior to the superior and middle frontral gyri, anterior to the precentral gyrus, and extending from the midline to the superior border of the inferior frontal gyrus pars opercularis. This region was added to be more in line the frontal

cortical sub-divisions described by Tziortzi et al. (Tziortzi et al., 2014). As a result, 98 cortical subregions were used in the analysis. (See Appendix A for list of regions and abbreviations).

The designation of the PFC is ambiguous in the literature; here, we considered the PFC to include frontal pole, superior frontal gyrus, middle frontal gyrus, paracingulate gyrus, anterior cingulate gyrus, and subcallosal cortex, according to Tziortzi et al. (2014) and Santos et al. (2011) (Santos, Seixas, Brandão, & Moutinho, 2011; Tziortzi et al., 2014).

2.1.4.2 – Segmentation of the Striatum

To measure connectivity density from the SNc/VTA to the DS/VS, we used the striatumstruc striatum atlas supplied by FSL (https://fsl.fmrib.ox.ac.uk/fsl/fslwiki/Atlases/striatumstruc). The striatumstruc atlas is divided into the VS and DS, lateralized by side (Tziortzi et al., 2011). VS is defined as the NAcc, medial caudate nucleus, and rostral-ventral putamen. The remaining portions of the caudate nucleus and the putamen were defined as the DS. Though the CIT168 atlas has defined a version of the striatum with more accurately external boundaries than that of striatumstruc, striatumstruc has been parcellated into the DS and VS, whereas CIT168 has not (Pauli et al., 2018).

2.1.4.3 – Atlas Registration

All cortical, striatal, and VTA/SNc labels were registered to each participant using NiftyReg linear and deformable b-spline registration tools. The probabilistic labels of the entire cortex, striatum, and VTA/SNc were then transformed back into MNI space with non-linear transformations.

2.1.5 - Probabilistic Tractography

2.1.5.1 – SNc and VTA Connectivity to DS, VS, and PFC

FSL PROBTRACKX was used to calculate connectivity density from seed voxels in the SNc and VTA to striatal and cortical targets. 1500 streamlines were seeded from each seed voxel to proximal probability density functions previously established by FSL BEDPOST. Default step length of 0.5 mm and curvature of 0.2 (80°) were used. Streamlines that made contact with a striatal or cortical subregion were tallied. Within each seed structure (left and right SNc and VTA), a streamline count map was generated for every striatal or cortical target, whereby each voxel was labelled with an intensity value representing the number of seeded streamlines that emerged from the seed structure and made contact with a particular striatal or cortical subregion. Each streamline count map was normalized by the largest intensity value within each map so that each map contained values ranging from 0-1. These values were then averaged across all seed voxels within each streamline count map to generate an aggregate connectivity value from 0-1 within each seed structure. The aggregate value was multiplied by 100% to generate connectivity density.

2.1.5.2 – Relative Connectivity of DS, VS, and PFC from SNc and VTA

To assess the relative percentages of DS, VS, and PFC connections that arose from the SNc and the VTA, FSL PROBTRACKX was used to calculate connectivity from seed voxels from the DS, VS, and PFC to SNc and VTA targets. 1500 streamlines emerged from each seed voxel using the parameters and methods described above. Within each seed structure (left and right DS, VS, and PFC), a streamline count map was generated for every SNc and VTA target, whereby each voxel was labelled with an intensity value representing the number of seeded streamlines that emerged from the seed structure and made contact with a particular SNc and VTA subregion. Each streamline count map was normalized by the largest intensity value within each map so that each map contained values ranging from 0-1. These values were then averaged across all seed voxels within each streamline count map to generate an aggregate connectivity

27

value from 0-1 within each seed structure. The aggregate value was multiplied by 100% to generate connectivity density.

2.1.6 – Connectogram Construction

To visualize the connectivity densities among subregions, we used Circos software to create connectograms, as described by Irimia et al. (2012) (Irimia, Chambers, Torgerson, & Van Horn, 2012; Krzywinski et al., 2009). SNc/VTA, striatal, and cortical subregions were modelled in a circle to represent a coronal section of the brain, with lobes clustered together. Connectivity densities between subregions were modelled as connecting links. Connectivity densities were weighted against an arbitrary link width of 50 pixels, such that the highest connectivity density would be modelled as 50 pixels. A connectivity density at half the highest value would be modelled as 25 pixels. Thus, all connections were relatively weighted.

2.1.7 – Statistical Analysis

Typically, studies of connectomic data threshold against a minimum connectivity %, considering the limitations of probabilistic tractography (van Wijk, Stam, & Daffertshofer, 2010), with some suggesting that only connectivity densities >1% should be considered (Cacciola et al., 2017). However, given that there are clear predictions about SNc and VTA connectivity to the DS, VS, and PFC in conventional theories, we have considered connectivity density below 1% if it had been computed between one of these areas. However, any connections with a connectivity density below 1% should be interpreted with caution (Cacciola et al., 2017). Connections with connectivity strength < 1% from the SNc and VTA to non-PFC cortical regions have not been considered.

Given the known differences between ipsilateral connectivity and contralateral connectivity, with ipsilateral connections estimated to have 95% greater innervation than contralateral connections, statistical analyses among ipsilateral and contralateral connections were performed separately (Parent et al., 1983).

Statistical analyses are described as follows:

2.1.7.1 – Ipsilateral Connectivity to and from the DS

Connectivity density of the SNc and VTA to and from the ipsilateral DS was used as the dependent measure in a 2 x 2 repeated-measures ANOVA with SNc/VTA Structure (SNc vs. VTA) and Ipsilateral DS Target (Left DS vs. Right DS) as within-subject variables.

Connectivity density of the Left and Right DS to and from the Ipsilateral SNc/VTA was used as the dependent measure in a 2 x 2 repeated-measures ANOVA with DS Side (Left DS vs. Right DS) and Ipsilateral SNc/VTA Target (SNc vs. VTA) as within-subject variables

2.1.7.2 – Ipsilateral Connectivity to and from the VS

Connectivity density of the SNc and VTA to and from the ipsilateral VS was used as the dependent measure in a 2 x 2 repeated-measures ANOVA with SNc/VTA Structure (SNc vs. VTA) and Ipsilateral VS Target (Left VS vs. Right VS) as within-subject variables.

Connectivity density of the Left and Right VS to and from the Ipsilateral SNc/VTA was used as the dependent measure in a 2 x 2 repeated-measures ANOVA with VS Side (Left VS vs. Right VS) and Ipsilateral SNc/VTA Target (SNc vs. VTA) as within-subject variables

2.1.7.3 – Ipsilateral Connectivity to and from the PFC

Connectivity density of the SNc and VTA to and from the ipsilateral PFC was used as the dependent measure in a 2 x 6 x 2 repeated-measures ANOVA with SNc/VTA Structure (SNc vs. VTA), PFC Subregion (Frontal Pole vs. Superior Frontal Gyrus vs. Middle Frontal Gyrus vs. Paracingulate Gyrus vs. Anterior Cingulate Gyrus vs. Subcallosal Cortex), and Ipsilateral PFC Side (Left PFC vs. Right PFC) as within-subject variables.

Connectivity density of Left and Right PFC regions to and from the Ipsilateral SNc/VTA was used as the dependent measure in a 6 x 2 x 2 repeated-measures ANOVA with PFC Subregion (Frontal Pole vs. Superior Frontal Gyrus vs. Middle Frontal Gyrus vs. Paracingulate Gyrus vs. Anterior Cingulate Gyrus vs. Subcallosal Cortex), PFC Side (Left PFC vs. Right PFC), and SNc/VTA Structure (SNc vs. VTA) as within-subject variables.

2.1.7.4 – Comparisons of Connectivity to and from Ipsilateral DS, VS, and PFC

To compare between ipsilateral connectivity to DS and VS, connectivity of the SNc to and from the ipsilateral DS and ipsilateral VS was used as the dependent measure in a 2 x 2 repeated-measures ANOVA with Ipsilateral Target (DS vs. VS) and SNc Side (Left SNc vs Right) as within-subject variables.

To allow for comparisons to the PFC regions, we first averaged the connectivity of the left SNc to and from the six left PFC regions (left frontal pole, superior frontal gyrus, middle frontal gyrus, paracingulate gyrus, anterior cingulate gyrus, subcallosal cortex) to generate one left SNc connectivity to ipsilateral PFC value. We then averaged the connectivity of the right SNc to and from the six right PFC regions right frontal pole, superior frontal gyrus, middle frontal gyrus, paracingulate gyrus, anterior cingulate gyrus, subcallosal cortex) to generate one right SNc connectivity to ipsilateral PFC value

To compare between SNc ipsilateral connectivity to and from the DS and PFC, connectivity of the SNc and from ipsilateral DS and ipsilateral PFC was used as the dependent measure in a 2 x 2 repeated-measures ANOVA with Ipsilateral Target (DS vs. PFC) and SNc Side (Left SNc vs Right) as within-subject variables.

To compare between SNc ipsilateral connectivity to and from the DS and PFC, connectivity of the SNc to and from the ipsilateral VS and ipsilateral PFC was used as the dependent measure in a 2 x 2 repeated-measures ANOVA with Ipsilateral Target (VS vs. PFC) and SNc Side (Left SNc vs Right) as within-subject variables.

These analyses will also be performed with VTA ispilateral connectivity using the same procedures.

2.1.7.5 – Contralateral Connectivity to and from the DS

Connectivity density of the SNc and VTA to and from the contralateral DS was used as the dependent measure in a 2 x 2 repeated-measures ANOVA with SNc/VTA Structure (SNc vs. VTA) and Contralateral DS Target (Left DS vs. Right DS) as within-subject variables.

Connectivity density of the Left and Right DS to and from the Contralateral SNc/VTA was used as the dependent measure in a 2 x 2 repeated-measures ANOVA with DS Side (Left DS vs. Right DS) and Contralateral SNc/VTA Target (SNc vs. VTA) as within-subject variables.

2.1.7.6 – Contralateral Connectivity to and from the VS

Connectivity density of the SNc and VTA to and from the contralateral VS was used as the dependent measure in a 2 x 2 repeated-measures ANOVA with SNc/VTA Structure (SNc vs. VTA) and Contralateral VS Target (Left VS vs. Right VS) as within-subject variables.

Connectivity density of the Left and Right VS to and from the Contralateral SNc/VTA was used as the dependent measure in a 2 x 2 repeated-measures ANOVA with VS Side (Left VS vs. Right VS) and Contralateral SNc/VTA Target (SNc vs. VTA) as within-subject variables

2.1.7.7 – Contralateral Connectivity to and from the PFC

Connectivity density of the SNc and VTA to and from the contralateral PFC was used as the dependent measure in a 2 x 6 x 2 repeated-measures ANOVA with SNc/VTA Structure (SNc vs. VTA), PFC Subregion (Frontal Pole vs. Superior Frontal Gyrus vs. Middle Frontal Gyrus vs. Paracingulate Gyrus vs. Anterior Cingulate Gyrus vs. Subcallosal Cortex), and Contralateral PFC Side (Left PFC vs. Right PFC) as within-subject variables.

Connectivity density of the Left and Right PFC regions to and from the Contralateral SNc/VTA was used as the dependent measure in a 6 x 2 x 2 repeated-measures ANOVA with PFC Subregion (Frontal Pole vs. Superior Frontal Gyrus vs. Middle Frontal Gyrus vs. Paracingulate Gyrus vs. Anterior Cingulate Gyrus vs. Subcallosal Cortex), PFC Side (Left PFC vs. Right PFC), and SNc/VTA Structure (SNc vs. VTA) as within-subject variables.

2.1.7.8 – Comparisons of Connectivity to and from Ipsilateral DS, VS, and PFC

To compare between contralateral connectivity to and from the DS and VS, connectivity of the SNc to and from the contralateral DS and contralateral VS was used as the dependent measure in a 2 x 2 repeated-measures ANOVA with Contralateral Target (DS vs. VS) and SNc Side (Left SNc vs Right) as within-subject variables.

To allow for comparisons to the PFC regions, we first averaged the connectivity of the left SNc to and from the six right PFC regions (right frontal pole, superior frontal gyrus, middle frontal gyrus, paracingulate gyrus, anterior cingulate gyrus, subcallosal cortex) to generate one left SNc connectivity to contralateral PFC value. We then averaged the connectivity of the right SNc to and from the six left PFC regions right frontal pole, superior frontal gyrus, middle frontal gyrus, paracingulate gyrus, anterior cingulate gyrus, subcallosal cortex) to generate one right SNc connectivity to contralateral PFC value

To compare between SNc contralateral connectivity to and from the DS and PFC, connectivity of the SNc to and from the contralateral DS and contralateral PFC was used as the dependent measure in a 2 x 2 repeated-measures ANOVA with Contralateral Target (DS vs. PFC) and SNc Side (Left SNc vs Right) as within-subject variables.

To compare between SNc contralateral connectivity to and from the DS and PFC, connectivity of the SNc to and from the contralateral VS and contralateral PFC was used as the dependent measure in a 2 x 2 repeated-measures ANOVA with Contralateral Target (VS vs. PFC) and SNc Side (Left SNc vs Right) as within-subject variables.

These analyses will also be performed with VTA contralateral connectivity using the same procedures.

2.1.7.9 – Connectivity to and from Ipsilateral non-PFC Regions

Though not forming part of our main hypotheses, we also examined the connectivity of the SNc and VTA to and from ipsilateral non-PFC targets. First, we noted which non-PFC regions had connectivity above 1%.

To explore the influence of SNc and VTA on these regions, we used connectivity of the SNc and VTA to and from these ipsilateral non-PFC regions as the dependent measure in a 2 x *number of non-PFC regions >1%* x 2 repeated-measures ANOVA with SNc/VTA Structure (SNc vs. VTA), non-PFC Subregion, and Ipsilateral PFC Side (Left PFC vs. Right PFC) as within-subject variables

Connectivity density of Left and Right non-PFC regions to and from the Ipsilateral SNc/VTA was used as the dependent measure in a *number of non-PFC regions >1%* x 2 x 2 repeated-measures ANOVA with non-PFC Subregion, non-PFC Side (Left PFC vs. Right PFC), and SNc/VTA Structure (SNc vs. VTA) as within-subject variables.

2.1.7.10 – Adjustments for Multiple Comparisons

For each set of analyses (i.e, section 2.1.7.1, 2.1.7.2, 2.1.7.3, 2.1.7.4, 2.1.7.5, 2.1.7.6, 2.1.7.7, 2.1.7.8, 2.1.7.9), we adjusted for multiple comparisons by controlling for false discovery rate (FDR) according to the Benjamini-Hochberg procedure (Benjamini & Hochberg, 1995). *P*-values were ordered from lowest to highest. For each *p*-value, an adjusted *p*-value was calculated by multiplying the unadjusted *p*-value by the number of comparisons and dividing it by its rank in the order. An FDR rate was set to 0.05.

2.2 – Experiment 2: PD vs. Healthy Control

2.2.1 – Participants

Twenty-one recently-diagnosed PD patients (i.e. diagnosed within the last five years), 21 healthy, age-matched healthy controls (HCs) participated in the MRI study. PD patients were recruited from a movement disorders database at the London Health Sciences Centre. Elderly control participants consisted of PD participant's spouses, friends, or family who volunteered to participate or individuals who were recruited through paper advertisements in the London, Ontario area. PD patients were previously diagnosed by a licensed neurologist and met the UK Brain Bank criteria for PD diagnosis (Hughes, Daniel, Kilford, & Lees, 1992). PD participants were excluded if they had previous or current neurological illness other than PD, including

dementia, or any major neuropsychiatric disorder. Participants were also excluded if they had a history of overusing alcohol or other prescription or illegal drugs. Those taking cognitive-enhancing medications like methylphenidate, donepezil, rivastigmine, galantine, or memantine were also excluded. HCs had the same exclusions as the PD patient with the added exclusion that they did not have PD and were not treated with DAergic therapy. The Health Sciences Research Ethics Board of the University of Western Ontario approved this study (REB # 18517). All participants provided written informed consent according to the Declaration of Helsinki (World Medical Association, 2013). The age of these PD patients (M = 67.24, SD = 6.34) and HCs (M = 65.00, SD = 6.68) did not differ significantly, $t = -1.038$, $p = 0.306$.

Three PD patients and one control participant were excluded because they scored lower than 25 on the Montreal Cognitive Assessment (MoCA), and one additional PD patient was excluded due to excessive motion inside the MRI machine. Thus, 17 PD patients and 20 healthy elderly control participants were included in our analyses of this study.

The ages of the PD Group after these exclusions (M = 65.00, SEM = 1.494) and the HC Group (M = 67.235, SEM = 1.538), hence those who were included for analyses, did not differ significantly ($t = -1.038$, $p = 0.306$). PD patients had been diagnosed with PD for an average of 2.229 years (SEM = 0.381) years before their testing date and had an average levodopa equivalent dose (LED) of 374.412 mg (SEM = 70.856). LED was calculated according to the following formula: L-dopa dose + L-dopa × 1/3 if on entacapone + bromocriptine (mg) × 67 + ropinerole (mg) × 20 + pergolide (mg) × 100 + apomorphine (mg) × 8. **Table 1** presents a complete outline of PD and HC demographic information.

Table 1: Demographic data for PD patients and controls

	PD	HC
n	17	20
Age	65 (1.494)	67.235 (1.538)
Sex	11M:6F	8M:12F

Education	15.267 (0.658)	15.421 (0.480)
Disease duration	2.222 (0.381)	-
LED	374.412 (70.856)	-
MoCA	27.875 (0.427)	28.706 (0.340)
BAI	8.588 (1.764)	2.158 (0.685)
BDI-II	9.765 (1.482)	3.263 (0.851)
ESS	7.118 (1.057)	5.789 (0.801)
NFOG	3.235 (1.110)	-
SAS	12.765 (1.265)	9.222 (1.589)
Oxford	4.137 (0.148)	5.065 (0.117)
ANART	122.504 (2.388)	123.979 (1.892)
F-Words	13.706 (1.162)	15.632 (1.082)
A-Words	10.235 (0.941)	13.579 (1.033)
S-Words	14.118 (0.992)	15.789 (0.984)
Animals	18.765 (0.893)	20.737 (1.204)
Heart rate	73.313 (2.966)	72.789 (3.250)
Blood pressure (Sys)	129.824 (2.848)	122.526 (3.651)
Blood pressure (Dia)	80.529 (1.717)	76.526 (2.302)

All values are reported as Mean (SEM). Age is reported in years. Education refers to the amount of years in the education system starting at grade 1. LED reported in mg. Heart rate is reported in beats per minutes. Blood pressure millimeters of mercury. The remaining variables are cognitive assessments, with scores reported. A description of these assessments are as follows: MoCA = Montreal Cognitive Assessment, BAI = Beck Anxiety Inventory, BDI-II = Beck Depression Inventory II, ESS = Epworth Sleepiness Scale, NFOG = New Freezing of Gait Questionnaire, SAS = Starkstein Apathy Scale, Oxford = Oxford Happiness Questionnaire, ANART = National Adult Reading Test, F-, A-, S-Words = the number of words beginning with the letter F, A, or S, respectively, produced in 60s, Animals = the number of words of animals produced in 60s.

2.2.2 – MRI Acquisition

Participants were scanned on a Siemens Prisma Fit 3T scanner, in which anatomical MPRAGE and DWI sequences were performed. MPRAGE was obtained with the following parameters: TR = 2300 ms, TE = 2.9 8ms, TI = 900 ms, flip angle = 9º, FOV = 256x256 mm, voxel size = 1 mm x 1mm x 0.9mm, and acquisition time = 5min, 35s. A DWI EPI series was obtained with the following parameters: gradient directions = 95, b-value = 2000 s/mm^2, TR = 3800 ms, TE = 87.60 ms, FOV = 224x224 mm, acquisition matrix = 128x128 pixels, and with one whole brain image consisting of 72 slices with slice thickness = 2mm and with 2 mm x 2 mm x 2mm voxels.

2.2.3 – T1 and DWI Pre-preprocessing

T1w and DWI images were imported and converted into NIFTI volume files using dcm2niix. T1w and DWI images were pre-processed using the prepdwi_dev in-house pipeline (https://github.com/khanlab/prepdwi). T1w pre-processing included skull-stripping (FSL BET), non-uniformity correction (N4), and intensity normalization. DWI pre-processing included linear registration to the b0 image (FSL eddy correct), co-registration to the T1w image (NiftyReg), tensor fitting (FSL drift), and fibre modelling for probabilistic ball and stick tractography (FSL BEDPOSTX). Quality assurance steps were built into the pipeline to check for registration failures, which were corrected by initializing unsuccessful registrations to the registrations of a participant whose pre-processing was successful.

2.2.4 – Mask Segmentation

To analyze the independent connectivity of the SNc/VTA to subregions of a parcellated striatum, we used the CIT168 SNc/VTA atlas, the CIT168 striatum atlas, and the Harvard-Oxford cortical atlas, each of which was lateralized by side (Fischl et al., 2004; Pauli et al., 2018; Rademacher et al., 1992).

2.2.4.1 - Cortical Parcellation

The cortical mask was sub-divided into seven subregions that consider gross functional specialization, according to Tziortzi et al. (Tziortzi et al., 2014). These consisted of the limbic, executive, rostral motor (RM), caudal motor (CM), parietal, occipital, and temporal subregions, which overlap with subregions of the Harvard-Oxford atlas (Appendix A). Briefly, the limbic, executive, RM, and CM subregions overlap with the frontal lobe, and were delineated with respect to meta-data of frontal lobe functioning. The limbic subregion consists of medial and prefrontal cortical regions, including orbitofrontal cortex and anterior cingulate, and correspond to brain regions that involved in emotion and reward-processing. The executive subregions consists of the superior and medial frontal gyri and the dorsal PFC, and it is involved in executive functions like decision-making, planning, and set-switching. Inferior frontal gyrus, caudal portions of the lateral and medial superior gyrus, pre-supplementary motor, and rostral operculum cortex made up the RM subregion, which is largely responsible for planning and controlling movements. The CM subregion contained the primary motor cortex and the caudal portion of the pre-motor cortex, and it is involved in the execution of movements. The parietal, occipital, and temporal subregions correspond to the parietal, occipital, and temporal lobes, respectively. Each subregion was lateralized to the left and right side for a total of 14 subregions.

2.2.4.2 – Atlas Registration

All cortical, striatal, and VTA/SNc labels were registered to each participant using NiftyReg linear and deformable b-spline registration tools. The probabilistic labels of the entire cortex, striatum, and VTA/SNc were then transformed back into MNI space with non-linear transformations. Following atlas registration, each participant's T1w image was overlaid with each brain region segmentation; this was then observed for quality assurance.

2.2.5 – Striatum Parcellation

Maximal probabilistic multi-fibre ball and stick tractography (FSL PROBTRACKX) was used to parcellate the striatum (Behrens et al., 2007; Behrens, Johansen-Berg, et al., 2003; **Figure 4**). 5000 probabilistic streamlines were seeded from each voxel of the striatum. Participant-specific parcellations of the striatum were generated in a winner-take-all approach, such that each voxel was labelled as whichever cortical subregion its seeded streamlines maximally targeted.
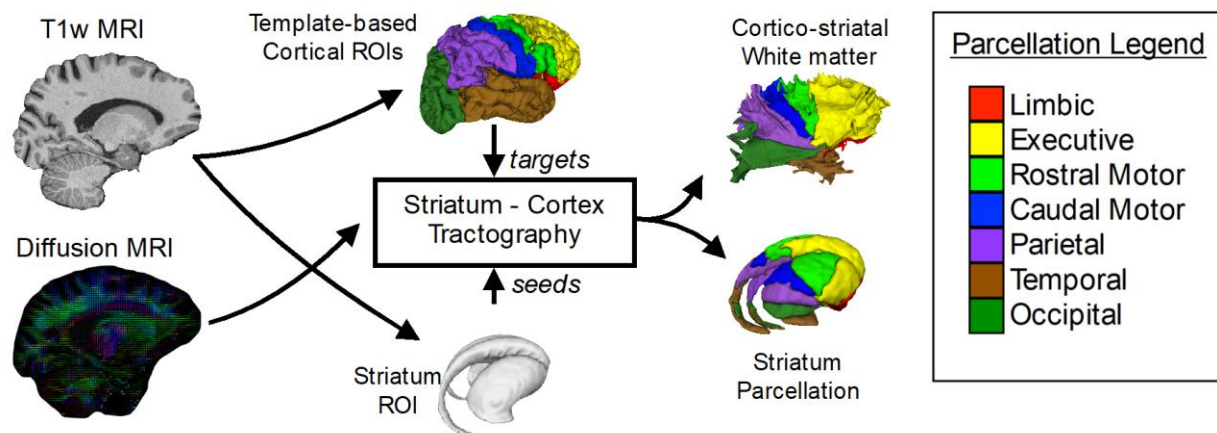
Figure 4: Parcellation scheme for the PD versus HC Comparison. Progressing from left to right, the T1w anatomical and DWI images for each participant were pre-processed. T1w images underwent skull-stripping, non-uniformity correction, and intensity normalization. DWI images underwent linear registration to the b0 image, co-registration to the T1w image, tensor fitting, and FSL BEDPOSTX. Participant cortices were parcellated into seven subregions as described by Tziortzi et al. (2014), which include the limbic (red), executive (yellow), rostral motor (light green), caudal motor (blue), parietal (purple), temporal (brown), and occipital (dark green). Then, FSL PROBTRACKX probabilistic tractography was performed with seeds in the striatum and targeting the cortex following cortico-striatal white matter. The striatum was parcellated in a winner-take-all approach, such that each voxel was labelled as whichever cortical subregion its seeded streamlines maximally targeted.

2.2.6 – SNc/VTA Independent Connectivity

To calculate independent connectivity, we at first used FSL PROBTRACKX to calculate the number of seeded streamlines from each SNc/VTA voxel to the striatum. 5000 streamlines were seeded from each voxel to proximal probability density functions established by FSL BEDPOSTX. Default step length of 0.5mm and curvature of 0.2 (80°) were used. Streamlines that made contact with a striatal parcellation were tallied.

For the measure of independent connectivity, for a given striatal target region, the streamline count map was generated (i.e., all SNc/VTA seed voxels, with intensity as the number of streamlines reaching the target region). The streamline count map was normalized by its largest value such that values are from 0-1 and then averaged across all seed voxels to generate an aggregate connectivity value from 0-1. The aggregate value was multiplied by 100% to generate independent connectivity density.

Notably, independent connectivity measures for parietal, occipital, and temporal striatum targets were not included for similar reasons. In pilot data, connectivity from the SNc/VTA to the parietal, occipital, and temporal striatal subregions were highly variable across different runs and relatively insignificant. We therefore opted to target solely the limbic, executive, RM, and CM striatum.

2.2.7 – Connectivity from the Entire SNc to the Entire Striatum

FSL PROBTRACKX was used to calculate connectivity density from seeds voxels in the SNc. 5000 streamlines were seeded from each seed voxel to proximal probability density functions previously established by FSL BEDPOST. Settings and procedures are the same as described in 2.1.5.1, except the CIT168 striatum was used instead of the striatumstruc atlas. Targets included the CPu and the NAcc.

To acquire an aggregate value for the connectivity from the entire SNc to the entire Striatum, we averaged the generated connectivity values across SNc side (Left SNc and Right SNc) and striatum target region (Caudate nucleus, putamen, and NAcc).

2.2.7– Statistical Procedures

To understand the impact of PD on independent connectivity, we performed two planned *a priori* independent-sample between-subject *t*-tests, one for each hemisphere, with Group (PD vs. HC) as the between-subject factor and independent connectivity from the SNc/VTA to the CM

striatum as the dependent measure, expecting independent connectivity to the CM striatum to be reduced in PD.

To examine the difference of the CM striatum in the context of all other striatum subregions, we performed 8 independent-sample between-subject *t*-tests, one for each striatum subregion in each hemisphere, with Group (PD vs. HC) as the between-subject factor and Independent connectivity from the SNc/VTA to each striatum target (i.e., limbic, executive, RM, CM) as the dependent measures. We adjusted for multiple comparisons by controlling for false discovery rate (FDR) according to the Benjamini-Hochberg procedure, as described above (Benjamini & Hochberg, 1995).

Finally, to test whether connectivity from the whole SNc to the whole striatum was diminished in the PD patients, we performed an independent-sample between-subject *t*-test with Group (PD vs. HC) as the between-subject factor and Average Connectivity from the SNc to the Striatum as the dependent measure.

Chapter 3: Results

3.1 – Experiment 1: HCP Anatomical Connectivity

dMRI probabilistic tractography allowed us to construct connectivity profiles of the SNc and VTA to and from the DS, VS, and cortex. Connectograms of the connectivity profile of the SNc (**Figure 5**) and VTA (**Figure 6**) are shown for visualization.

Average connectivity densities of the SNc and VTA to and from the ipsilateral DS, VS, and PFC are shown in **Table 2.**

Average ipsilateral connectivity densities of the DS, VS, and PFC to and from the ipsilateral SNc and VTA are shown in **Table 3.**

Average connectivity densities of the SNc and VTA to and from the ipsilateral DS, VS, and PFC are shown in **Table 4 .**

Average ipsilateral connectivity densities of the DS, VS, and PFC to and from the ipsilateral SNc and VTA are shown in **Table 5.**
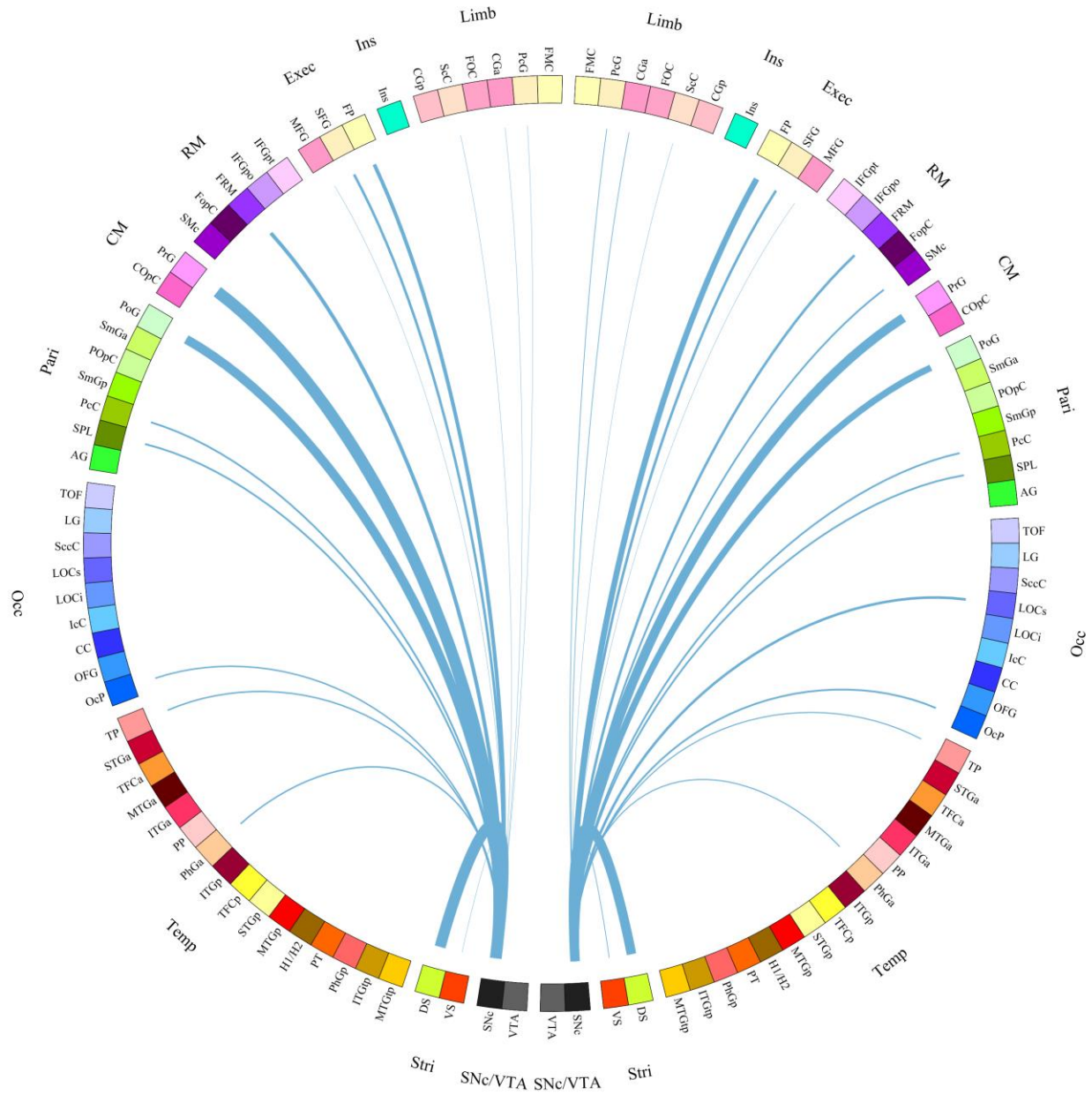
Figure 5: Connectogram showing connectivity density profile of the SNc to and from the striatal and cortical subregions. Connectivity densities were weighted against an arbitrary link width of 50 pixels. Connections between the SNc to the DS, VS, and PFC are shown. Only SNc connections with non-PFC regions with connectivity densities >1% are shown. (Limb = Limbic, Ins = Insula, Exec = Executive, RM = Rostral Motor, CM = Caudal Motor, Pari = Parietal, Occ = Occipital, Temp = Temporal, Stri = Striatum, SNc/VTA = Substantia nigra pars compacta/ventral tegmental area) (Please see Appendix A for subregion abbreviations)
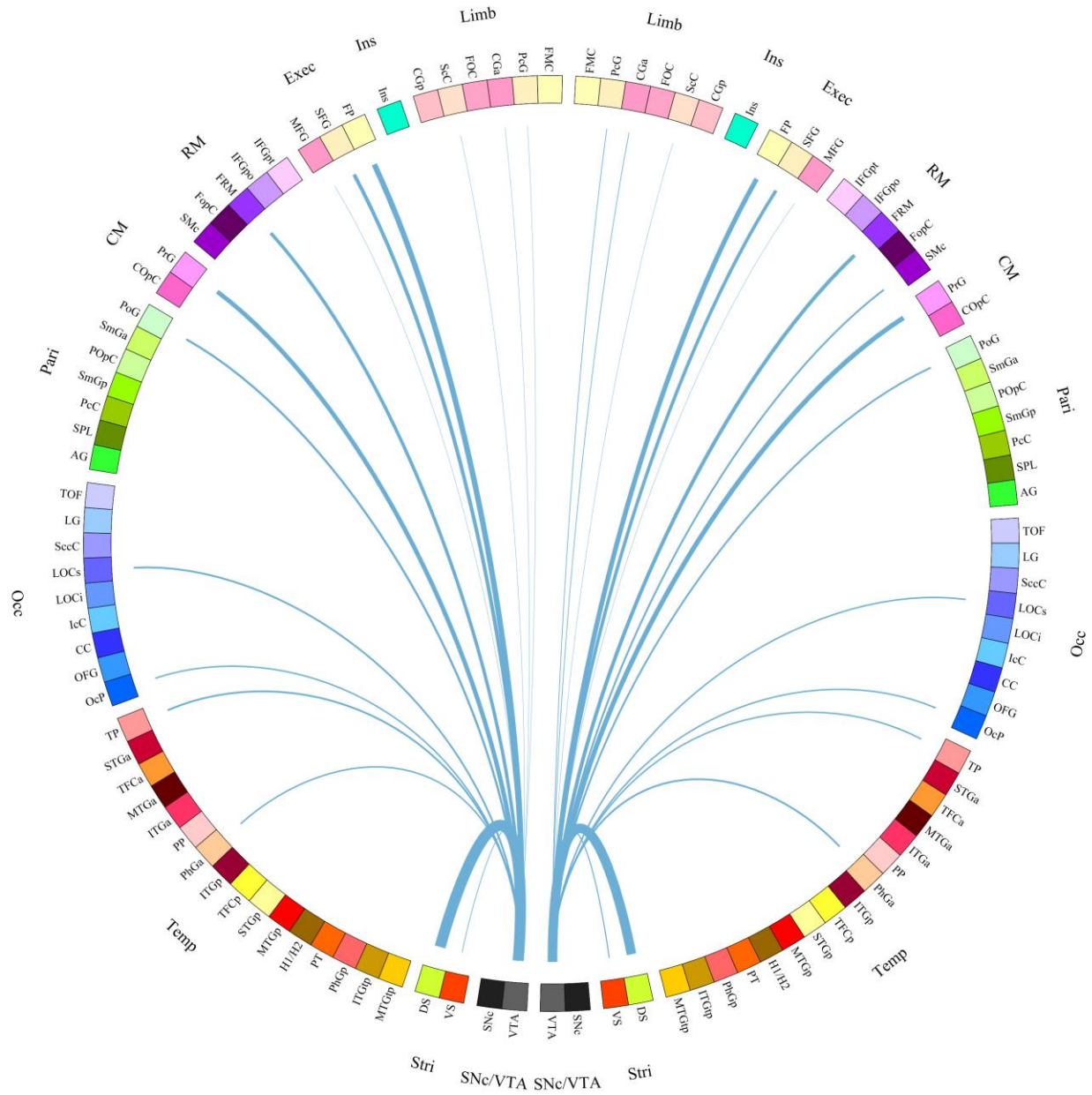
Figure 6: Connectogram showing connectivity density profile of the VTA to and from the striatal and cortical subregions. densities were weighted against an arbitrary link width of 50 pixels. Connections between the SNc to the DS, VS, and PFC are shown. Only SNc connections with non-PFC regions with connectivity densities >1% are shown. (Limb = Limbic, Ins = Insula, Exec = Executive, RM = Rostral Motor, CM = Caudal Motor, Pari = Parietal, Occ = Occipital, Temp = Temporal, Stri = Striatum, SNc/VTA = Substantia nigra pars compacta/ventral tegmental area) (See Appendix A for subregion abbreviations)

3.1.1 – Ipsilateral Connectivity to and from the DS

Connectivity density of the SNc and VTA to and from the ipsilateral DS was used as the dependent measure in a 2 x 2 repeated-measures ANOVA with SNc/VTA Structure (SNc vs. VTA) and Ipsilateral DS Target (Left DS vs. Right DS) as within-subject variables. We found no main effect of SNc vs. VTA Structure, $F(1,98) < 1$. We found a main effect of Ipsilateral DS Target, $F(1,98) = 13.483$, $MSe = 16.232$, $p < 0.001$, whereby ipsilateral connectivity to the Left DS was greater than ipsilateral connectivity to the Right DS overall. There was no SNc/VTA Structure x Ipsilateral DS Target interaction, $F(1,98) < 1$.

Connectivity density of the Left and Right DS to and from the Ipsilateral SNc/VTA was used as the dependent measure in a 2 x 2 repeated-measures ANOVA with DS Side (Left DS vs. Right DS) and Ipsilateral SNc/VTA Target (SNc vs. VTA) as within-subject variables. We found a main effect of SNc versus VTA Target, $F(1,98) = 300.055$, $MSe = 0.039$, $p < 0.001$, whereby connectivity to the SNc was greater than connectivity to the VTA.

3.1.2 – Ipsilateral Connectivity to and from the VS

Connectivity density of the SNc and VTA to and from the ipsilateral VS was used as the dependent measure in a 2 x 2 repeated-measures ANOVA with SNc/VTA Structure (SNc vs. VTA) and Ipsilateral VS Target (Left VS vs. Right VS) as within-subject variables. We found a main effect of SNc vs. VTA Structure, $F(1,98) = 41.583$, $MSe = 0.163$, $p < 0.001$, whereby VTA connectivity to ipsilateral VS was greater SNc connectivity to ipsilateral VS. We found a main effect of Ipsilateral VS Target, $F(1,98) = 29.602$, $MSe = 0.302$, $p < 0.001$, whereby ipsilateral connectivity to the Left VS was greater than ipsilateral connectivity to the Right VS overall. There was no SNc/VTA Structure x Ipsilateral VS Target interaction, $F(1,98) = 1.453$, MSe 0.148, $p = 0.231$. Notably, connectivity density to the VS tended to be <1%.

Connectivity density of the Left and Right VS to and from the Ipsilateral SNc/VTA was used as the dependent measure in a 2 x 2 repeated-measures ANOVA with VS Side (Left VS vs. Right VS) and Ipsilateral SNc/VTA Target (SNc vs. VTA) as within-subject variables. We found a

main effect of SNc versus VTA Target, $F(1,98) = 78.850$, $MSe = 0.004$, $p < 0.001$, whereby connectivity to the SNc was greater than connectivity to the VTA.

3.1.3 – Ipsilateral Connectivity to and from the PFC

Connectivity density of the SNc and VTA to and from the ipsilateral PFC was used as the dependent measure in a 2 x 6 x 2 repeated-measures ANOVA with SNc/VTA Structure (SNc vs. VTA), PFC Subregion (Frontal Pole vs. Superior Frontal Gyrus vs. Middle Frontal Gyrus vs. Paracingulate Gyrus vs. Anterior Cingulate Gyrus vs. Subcallosal Cortex), and Ipsilateral PFC Side (Left PFC vs. Right PFC) as within-subject variables. We found a main effect of SNc vs. VTA Structure, $F(1,98) = 16.798$, $MSe = 4.791$, $p < 0.001$, whereby VTA connectivity to ipsilateral PFC regions was greater than SNc connectivity to ipsilateral PFC regions. The PFC Region violated the assumption of sphericity according to Mauchly's Test of Sphericity, $\chi^2(14) = 614.696$, $p < 0.001$. Consequently, degrees of freedom were corrected using Greenhouse-Geisser estimates of sphericity ($\varepsilon = 0.325$). The main effect of PFC region was significant, $F(1.627,159.423) = 470.628$, $MSe = 11.538$, $p < 0.001$. Post-hoc, pairwise comparisons revealed that connectivity to PFC regions decreased according to the following order: frontal pole ($M = 5.298$, $SEM = 0.211$) > superior frontal gyrus ($M = 3.121$, $SEM = 0.128$) > paracingulate gyrus ($M = 0.452$, $SEM = 0.034$) and anterior cingulate gyrus ($M = 0.464$, $SEM = 0.034$) > middle frontal gyrus ($M = 0.225$, $SEM = 0.017$) and subcallosal cortex ($M = 0.248$, $SEM = 0.035$). Finally, the main effect of Ipsilateral PFC Side reached significance, $F(1,98) = 9.883$, $MSe = 3.312$, $p = 0.002$, whereby ipsilateral connectivity to the Right PFC was greater than ipsilateral connectivity to the Left PFC overall. Notably, connectivity to the PFC regions was <1% for all but the frontal pole and middle frontal gyrus.

Connectivity density of Left and Right PFC regions to and from the Ipsilateral SNc/VTA was used as the dependent measure in a 6 x 2 x 2 repeated-measures ANOVA with PFC Subregion (Frontal Pole vs. Superior Frontal Gyrus vs. Middle Frontal Gyrus vs. Paracingulate Gyrus vs. Anterior Cingulate Gyrus vs. Subcallosal Cortex), PFC Side (Left PFC vs. Right PFC), and SNc/VTA Structure (SNc vs. VTA) as within-subject variables. We found a main effect of SNc

versus VTA Structure, $F(1,98) = 142.676$, $MSe = 0.008$, $p < 0.001$, whereby connectivity to the SNc was greater than to the VTA.

Table 2: Average connectivity density values of the SNc and VTA to and from the ipsilateral DS, VS, and PFC

Seed	Connectivity Density	Ipsilateral Target
SNc	11.169 (0.359)	DS
	0.419 (0.025)	VS
	4.929 (0.260)	Frontal pole
	2.506 (0.126)	Superior frontal gyrus
	0.181 (0.012)	Middle frontal gyrus
	0.443 (0.043)	Paracingulate Gyrus
	0.413 (0.032)	Anterior Cingulate Gyrus
	0.232 (0.031)	Subcallosal Cortex
VTA	11.189 (0.342)	DS
	0.681 (0.053)	VS
	5.667 (0.276)	Frontal pole
	3.734 (0.002)	Superior frontal gyrus
	0.268 (0.025)	Middle frontal gyrus
	0.461 (0.039)	Paracingulate Gyrus
	0.515 (0.041)	Anterior Cingulate Gyrus
	0.265 (0.042)	Subcallosal Cortex

All values are measured in % and are reported as Mean (SEM). Seed refers to the seed region during probabilistic tractography, and target refers to the target brain region. Connectivity Density reports the average ipsilateral connectivity of left seed to left target and right seed to right target.

Table 3: Average connectivity density values of the DS, VS, and PFC to and from ipsilateral SNc and VTA

Seed	Connectivity Density	Ipsilateral Target
DS	0.504 (0.024)	SNc
VS	0.120 (0.010)	
Frontal pole	0.148 (0.008)	
Superior frontal gyrus	0.175 (0.010)	
Middle frontal gyrus	0.108 (0.009)	
Paracingulate Gyrus	0.038 (0.003)	
Anterior Cingulate Gyrus	0.039 (0.003)	
Subcallosal Cortex	0.005 (0.000)	
DS	0.158 (0.007)	VTA
VS	0.063 (0.006)	
Frontal pole	0.064 (0.006)	
Superior frontal gyrus	0.103 (0.007)	
Middle frontal gyrus	0.047 (0.004)	
Paracingulate Gyrus	0.022 (0.002)	
Anterior Cingulate Gyrus	0.020 (0.002)	
Subcallosal Cortex	0.002 (0.000)	

All values are measured in % and are reported as Mean (SEM). Seed refers to the seed region during probabilistic tractography, and target refers to the target brain region. Connectivity Density reports the average ipsilateral connectivity of left seed to left target and right seed to right target.

3.1.4 – Comparisons of Connectivity to and from Ipsilateral DS, VS, and PFC

3.1.4.1 – SNc Connectivity to and from Ipsilateral DS, VS, and PFC

Connectivity of the SNc to and from ipsilateral DS and ipsilateral VS was used as the dependent measure in a 2 x 2 repeated-measures ANOVA with Ipsilateral Target (DS vs. VS) and SNc Side (Left SNc vs Right) as within-subject variables. We found a main effect of Ipsilateral Target, $F(1,98) = 970.860$, $MSe = 11.785$, $p < 0.001$, with connectivity to the ipsilateral DS being greater than to the ipsilateral VS.

Connectivity of the SNc to and from ipsilateral DS and ipsilateral PFC was used as the dependent measure in a 2 x 2 repeated-measures ANOVA with Ipsilateral Target (DS vs. PFC) and SNc Side (Left SNc vs Right) as within-subject variables. We found a main effect of Ipsilateral Target, $F(1,98) = 932.049$, $MSe = 10.032$, $p < 0.001$, with connectivity to the ipsilateral DS being greater than to the ipsilateral PFC.

Connectivity of the SNc to and from ipsilateral VS and ipsilateral PFC was used as the dependent measure in a 2 x 2 repeated-measures ANOVA with Ipsilateral Target (VS vs. PFC) and SNc Side (Left SNc vs Right) as within-subject variables. We found a main effect of Ipsilateral Target, $F(1,98) = 287.117$, $MSe = 0.367$, $p < 0.001$, with connectivity to the ipsilateral PFC being greater than to the ipsilateral VS.

3.1.4.2 – VTA Connectivity to and from Ipsilateral DS, VS, and PFC

Connectivity of the VTA to and from ipsilateral DS and ipsilateral VS was used as the dependent measure in a 2 x 2 repeated-measures ANOVA with Ipsilateral Target (DS vs. VS) and VTA Side (Left VTA vs Right) as within-subject variables. We found a main effect of Ipsilateral

Target, $F(1,98) = 1042.235$, $MSe = 10.998$, $p < 0.001$, with connectivity to the ipsilateral DS being greater than to the ipsilateral VS.

Connectivity of the VTA to and from ipsilateral DS and ipsilateral PFC was used as the dependent measure in a 2 x 2 repeated-measures ANOVA with Ipsilateral Target (DS vs. PFC) and VTA Side (Left VTA vs Right) as within-subject variables. We found a main effect of Ipsilateral Target, $F(1,98) = 1056.997$, $MSe = 8.223$, $p < 0.001$, with connectivity to the ipsilateral DS being greater than to the ipsilateral PFC.

Connectivity of the VTA to and from ipsilateral VS and ipsilateral PFC was used as the dependent measure in a 2 x 2 repeated-measures ANOVA with Ipsilateral Target (VS vs. PFC) and VTA Side (Left VTA vs Right) as within-subject variables. We found a main effect of Ipsilateral Target, $F(1,98) = 190.643$, $MSe = 0.673$, $p < 0.001$, with connectivity to the ipsilateral PFC being greater than to the ipsilateral VS.

3.1.5 – Contralateral Connectivity to and from the DS

Connectivity of the SNc and VTA to and from the contralateral DS was used as the dependent measure in a 2 x 2 repeated-measures ANOVA with SNc/VTA Structure (SNc vs. VTA) and Contralateral DS Target (Left DS vs. Right DS) as within-subject variables. We found a main effect of SNc versus VTA Structure, $F(1,98) = 89.036$, $MSe = 0.403$, $p < 0.001$, whereby VTA connectivity to contralateral DS was greater than SNc connectivity to contralateral DS. We found a main effect of Contralateral DS Target, $F(1,98) = 11.583$, $MSe = 0.249$, $p = 0.001$, whereby contralateral connectivity to the Right DS was greater than contralateral connectivity to the Left DS overall. There was no SNc/VTA Structure x Contralateral DS Target interaction, $F(1,98) = 2.755$, $MSe = 0.228$, p = 0.100. Table 1 as above paragraphs.

Connectivity density of the Left and Right DS to and from the Contralateral SNc/VTA was used as the dependent measure in a 2 x 2 repeated-measures ANOVA with DS Side (Left DS vs. Right DS) and Contralateral SNc/VTA Target (SNc vs. VTA) as within-subject variables. We found a main effect of SNc versus VTA Target, $F(1,98) = 46.124$, $MSe = 0.000$, $p < 0.001$, whereby connectivity to the SNc was greater than connectivity to the VTA.

3.1.6 – Contralateral Connectivity to and from the VS

Connectivity of the SNc and VTA to and from the contralateral VS was used as the dependent measure in a 2 x 2 repeated-measures ANOVA with SNc/VTA Structure (SNc vs. VTA) and Contralateral VS Target (Left VS vs. Right VS) as within-subject variables. We found a main effect of SNc versus VTA Structure, $F(1,98) = 21.207$, $MSe = 0.004$, $p < 0.001$, whereby VTA connectivity to contralateral DS was greater SNc connectivity to contralateral DS. We found a main effect of Contralateral DS Target, $F(1,98) = 26.601$, $MSe = 0.003$, $p < 0.001$, whereby contralateral connectivity to the Right VS was greater than contralateral connectivity to the Left VS overall. There was a significant SNc/VTA Structure x Contralateral VS Target interaction, $F(1,98) = 10.754$, $MSe = 0.003$, $p = 0.001$, indicating that there was a significant difference in the SNc compared to VTA projections on the right but not the left side.

Connectivity density of the Left and Right VS to and from the Contralateral SNc/VTA was used as the dependent measure in a 2 x 2 repeated-measures ANOVA with VS Side (Left VS vs. Right VS) and Contralateral SNc/VTA Target (SNc vs. VTA) as within-subject variables. We found a main effect of SNc versus VTA Target, $F(1,98) = 4.642$, $MSe = 0.000$, $p = 0.034$, whereby connectivity to the SNc was greater than connectivity to the VTA.

3.1.7 – Contralateral Connectivity to and from the PFC

Connectivity of the SNc and VTA to and from the contralateral PFC was used as the dependent measure in a 2 x 6 x 2 repeated-measures ANOVA with SNc/VTA Structure (SNc vs. VTA), PFC Subregion (Frontal Pole vs. Superior Frontal Gyrus vs. Middle Frontal Gyrus vs. Paracingulate Gyrus vs. Anterior Cingulate Gyrus vs. Subcallosal Cortex), and Contralateral PFC Side (Left PFC vs. Right PFC) as within-subject variables. We found a main effect of SNc versus. VTA Structure, $F(1,98) = 79.235$, $MSe = 0.214$, $p < 0.001$, whereby VTA connectivity to contralateral PFC regions was greater than SNc connectivity to contralateral PFC regions. The PFC Region violated the assumption of sphericity according to Mauchly's Test of Sphericity, $\chi^2(14) = 236.064$, $p < 0.001$; therefore, degrees of freedom were corrected using Greenhouse-

Geisser estimates of sphericity ($\varepsilon = 0.569$). The main effect of PFC region was significant, $F(2.844, 278.666) = 230.431$, $MSe = 0.257$, $p < 0.001$. Post-hoc, pairwise comparisons revealed that connectivity to PFC regions decreased according to the following order: frontal pole ($M = 0.764$, $SEM = 0.032$) > superior frontal gyrus ($M = 0.668$, $SEM = 0.028$) > anterior cingulate gyrus ($M = 0.337$, $SEM = 0.026$) > middle frontal gyrus ($M = 0.152$, $SEM = 0.009$), paracingulate gyrus ($M = 0.111$, $SEM = 0.006$), and subcallosal cortex ($M = 0.111$, $SEM = 0.020$). Finally, the main effect of Ipsilateral PFC Side reached significance, $F(1,98) = 18.722$, $MSe = 0.171$, $p < 0.001$, whereby contralateral connectivity to the Right PFC was greater than contralateral connectivity to the Left PFC overall.

Connectivity density of the Left and Right PFC regions to and from the Contralateral SNc/VTA was used as the dependent measure in a 6 x 2 x 2 repeated-measures ANOVA with PFC Subregion (Frontal Pole vs. Superior Frontal Gyrus vs. Middle Frontal Gyrus vs. Paracingulate Gyrus vs. Anterior Cingulate Gyrus vs. Subcallosal Cortex), PFC Side (Left PFC vs. Right PFC), and SNc/VTA Structure (SNc vs. VTA) as within-subject variables. We found a main effect of SNc versus VTA Structure, $F(1,98) = 61.839$, $MSe = 0.002$ $p < 0.001$, whereby connectivity to the SNc was greater than to the VTA.

Table 4: Average connectivity density values of the SNc and VTA to and from the contralateral DS, VS, and PFC

Seed	Connectivity Density	Contralateral Target
SNc	0.329 (0.017)	DS
	0.026 (0.002)	VS
	0.567 (0.022)	Frontal pole
	0.478 (0.023)	Superior frontal gyrus
	0.088 (0.006)	Middle frontal gyrus
	0.116 (0.007)	Paracingulate Gyrus
	0.285 (0.023)	Anterior Cingulate Gyrus
	0.099 (0.016)	Subcallosal Cortex
VTA	0.931 (0.065)	DS
	0.054 (0.006)	VS
	0.958 (0.052)	Frontal pole
	0.857 (0.045)	Superior frontal gyrus
	0.134 (0.009)	Middle frontal gyrus
	0.187 (0.013)	Paracingulate Gyrus
	0.388 (0.031)	Anterior Cingulate Gyrus
	0.012 (0.024)	Subcallosal Cortex

All values are measured in % and are reported as Mean (SEM). Seed refers to the seed region during probabilistic tractography, and target refers to the target brain region. Connectivity Density reports the average contralateral connectivity of left seed to right target and right seed to left target.

Table 5: Average connectivity density values of the DS, VS, and PFC to and from contralateral SNc and VTA

Seed	Connectivity Density	Ipsilateral Target
DS	0.033 (0.003)	SNc
VS	0.013 (0.002)	
Frontal pole	0.020 (0.001)	
Superior frontal gyrus	0.063 (0.005)	
Middle frontal gyrus	0.035 (0.003)	
Paracingulate Gyrus	0.059 (0.005)	
Anterior Cingulate Gyrus	0.047 (0.004)	
Subcallosal Cortex	0.003 (0.000)	
DS	0.019 (0.001)	VTA
VS	0.008 (0.001)	
Frontal pole	0.013 (0.001)	
Superior frontal gyrus	0.038 (0.002)	
Middle frontal gyrus	0.021 (0.002)	
Paracingulate Gyrus	0.035 (0.003)	
Anterior Cingulate Gyrus	0.023 (0.002)	
Subcallosal Cortex	0.001 (0.000)	

All values are measured in % and are reported as Mean (SEM). Seed refers to the seed region during probabilistic tractography, and target refers to the target brain region. Connectivity Density reports the average contralateral connectivity of left seed to right target and right seed to left target.

3.1.8 – Comparisons of Connectivity to and from Contralateral DS, VS, and PFC

3.1.8.1 – SNc Connectivity to and from Contralateral DS, VS, and PFC

Connectivity of the SNc to and from the Contralateral DS and Contralateral VS was used as the dependent measure in a 2 x 2 repeated-measures ANOVA with Contralateral Target (DS vs. VS) and SNc Side (Left SNc vs Right) as within-subject variables. We found a main effect of Contralateral Target, $F(1,98) = 383.821$, $MSe = 0.024$, $p < 0.001$, with connectivity to the Contralateral DS being greater than to the Contralateral VS.

Connectivity of the SNc to and from the Contralateral DS and Contralateral PFC was used as the dependent measure in a 2 x 2 repeated-measures ANOVA with Contralateral Target (DS vs. PFC) and SNc Side (Left SNc vs Right) as within-subject variables. We found a main effect of Contralateral Target, $F(1,98) = 16.271$, $MSe = 0.020$, $p < 0.001$, with connectivity to the Contralateral DS being greater than to the Contralateral PFC.

Connectivity of the SNc to and from the Contralateral VS and Contralateral PFC was used as the dependent measure in a 2 x 2 repeated-measures ANOVA with Contralateral Target (VS vs. PFC) and SNc Side (Left SNc vs Right) as within-subject variables. We found a main effect of Contralateral Target, $F(1,98) = 578.296$, $MSe = 0.010$, $p < 0.001$, with connectivity to the Contralateral PFC being greater than to the Contralateral VS.

3.1.8.2 – VTA Connectivity to and from Contralateral DS, VS, and PFC

Connectivity of the VTA to and from the Contralateral DS and Contralateral VS was used as the dependent measure in a 2 x 2 repeated-measures ANOVA with Contralateral Target (DS vs. VS) and VTA Side (Left VTA vs Right) as within-subject variables. We found a main effect of

Contralateral Target, $F(1,98) = 206.795$, $MSe = 0.368$, $p < 0.001$, with connectivity to the Contralateral DS being greater than to the Contralateral VS.

Connectivity of the VTA to and from the Contralateral DS and Contralateral PFC was used as the dependent measure in a 2 x 2 repeated-measures ANOVA with Contralateral Target (DS vs. PFC) and VTA Side (Left VTA vs Right) as within-subject variables. We found a main effect of Contralateral Target, $F(1,98) = 74.343$, $MSe = 0.320$, $p < 0.001$, with connectivity to the Contralateral DS being greater than to the Contralateral PFC.

Connectivity of the VTA to and from the Contralateral VS and Contralateral PFC was used as the dependent measure in a 2 x 2 repeated-measures ANOVA with Contralateral Target (VS vs. PFC) and VTA Side (Left VTA vs Right) as within-subject variables. We found a main effect of Contralateral Target, $F(1,98) = 370.576$, $MSe = 0.040$, $p < 0.001$, with connectivity to the Contralateral PFC being greater than to the Contralateral VS.

3.1.9 – Connectivity to and from non-PFC Regions

Though not forming part of our main hypotheses, connectivity of the SNc and VTA to and from several ipsilateral non-PFC cortical regions >1% were also noted. Specifically, ipsilateral connections of the SNc and VTA to and from the precentral gyrus, temporal pole, postcentral gyrus, superior division of the lateral occipital cortex, anterior parahippocampal gyrus, occipital pole, and frontal rostral motor regions were >1% (**Table 6).**

Table 6: Average connectivity density values of the SNc and VTA to and from ipsilateral non-PFC regions

Seed	Connectivity Density	Ipsilateral Target
SNc	11.526 (0.413)	Precentral gyrus
	1.155 (0.081)	Temporal pole
	8.630 (0.309)	Postcentral gyrus
	2.752 (0.108)	Superior division of the lateral occipital cortex
	1.294 (0.121)	Anterior parahippocampal gyrus
	1.592 (0.078)	Occipital pole
	3.315 (0.174)	Frontal rostral motor region
VTA	4.859 (0.255)	Precentral gyrus
	1.579 (0.108)	Temporal pole
	2.066 (0.144)	Postcentral gyrus
	1.596 (0.064)	Superior division of the lateral occipital cortex
	1.706 (0.192)	Anterior parahippocampal gyrus
	1.422 (0.069)	Occipital pole
	3.724 (0.185)	Frontal rostral motor region

All values are measured in % and are reported as Mean (SEM). Seed refers to the seed region during probabilistic tractography, and target refers to the target brain region. Connectivity Density reports the average ipsilateral connectivity of left seed to left target and right seed to right target. Only ipsilateral connectivity densities >1% are shown here.

To explore the influence of SNc and VTA on these regions, we used connectivity of the SNc and VTA to and from these ipsilateral non-PFC regions as the dependent measure in a 2 x 7 x 2 repeated-measures ANOVA with SNc/VTA Structure (SNc vs. VTA), non-PFC Subregion (Precentral Gyrus vs. Temporal Pole vs. Postcentral Gyrus vs. Superior Division of the Lateral Occipital Cortex vs. Anterior Parahippocampal Gyrus vs. Occipital Pole vs. Frontal Rostral Motor Region), and Ipsilateral PFC Side (Left PFC vs. Right PFC) as within-subject variables. We found a main effect of SNc vs. VTA Structure, $F(1,98) = 423.348$, MSe 5.920, $p < 0.001$,

whereby SNc connectivity was greater than VTA connectivity to ipsilateral non-PFC regions that received greater than 1% projections from these DAergic regions.

Connectivity density of Left and Right non-PFC regions to and from the Ipsilateral SNc/VTA was used as the dependent measure in a 7 x 2 x 2 repeated-measures ANOVA with nonPFC Subregion ((Precentral Gyrus vs. Temporal Pole vs. Postcentral Gyrus vs. Superior Division of the Lateral Occipital Cortex vs. Anterior Parahippocampal Gyrus vs. Occipital Pole vs. Frontal Rostral Motor Region), non-PFC Side (Left PFC vs. Right PFC), and SNc/VTA Structure (SNc vs. VTA) as within-subject variables. We found a main effect of SNc versus VTA Structure, $F(1,98) = 476.348$, $MSe = 0.072$, $p < 0.001$, whereby connectivity to the SNc was greater than to the VTA.

.

3.2 – Experiment 2: PD versus Healthy Control

3.2.1 – SNc/VTA Independent Connectivity

To understand the impact of PD on independent connectivity, we performed eight *a priori* independent-sample between-subject *t*-tests, one for each striatum subregion in each hemisphere, with Group (PD vs. HC) as the between-subject factor and independent connectivity from the SNc/VTA to each striatum target (i.e., limbic, executive, RM, CM) as the dependent measures, expecting connectivity in the CM SNc to be reduced in PD. Indeed, independent connectivity to the right CM striatum was significantly lower in PD patients compared to HC, $t = 2.711$, $p = 0.010$ (**Figure 7).**

If adjusting for multiple comparisons across the eight target subregions using Benjamini-Hochberg procedure, of all striatal targets, only independent connectivity to the right CM striatum was marginally significant, $t = 2.711$, $p = 0.083$. Adjusted *p*-values to all other striatum subregions were above 0.60.
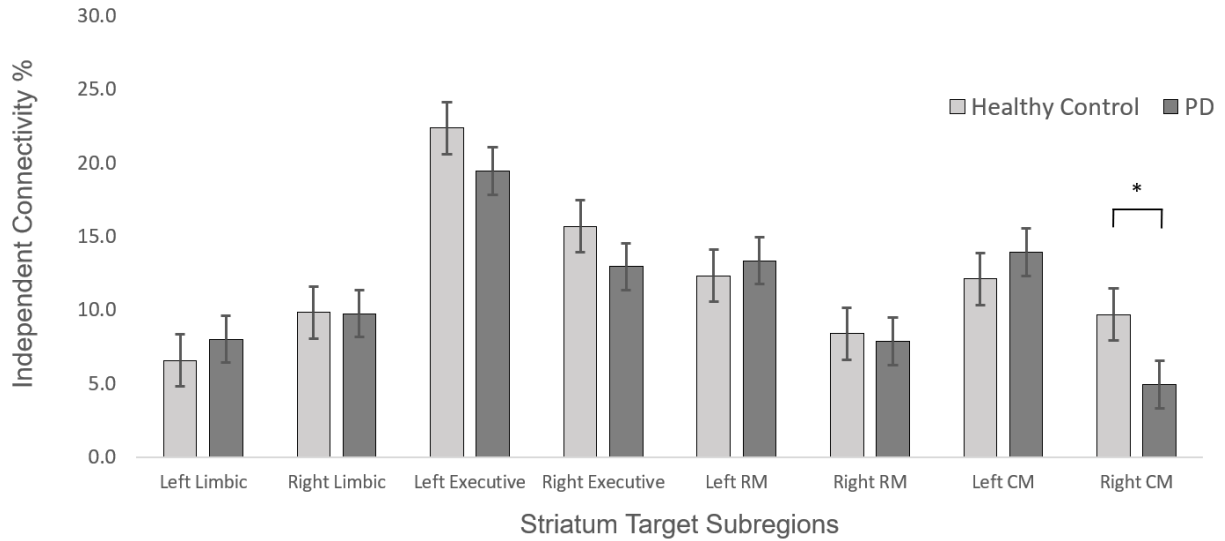
Figure 7: Independent connectivity values to each striatum subregion, divided into left and right sides. For each striatal target region, a streamline count map was generated. The streamline count map was normalized by its largest value such that values are from 0-1 and then averaged across all seed voxels to generate an aggregate connectivity value from 0-1. The aggregate value was multiplied by 100% to generate independent connectivity density for each of the bilateral striatum subregions. Light gray bars represent healthy, elderly controls whereas dark gray represent PD patients. Error bars represent SEM. Only Right CM SNc independent connectivity was reduced for PD relative to age-matched controls, as predicted. *RM = Rostral motor, CM = Caudal motor

3.2.2 – Connectivity from the Entire SNc to the Entire Striatum

An independent-sample between-subject *t*-test with Group (PD vs. HC) as the between-subject factor and Average Connectivity from the SNc to the Striatum as the dependent measure showed that there was no significant difference between Group, $t = 0.175$, $p = 0.862$.

Chapter 4: Discussion

4.1 – Experiment 1: HCP Anatomical Connectivity

4.1.1 – Summary of Findings

In Experiment 1, we used dMRI probabilistic tractography to assess the connectivity of the SNc and the VTA to and from the striatum and the cortex in healthy young humans *in vivo*, constituting one of the first attempts at this kind of analysis. We measured connectivity using an anatomical definition of midbrain SNc and VTA to assess the validity of the conventional pathway heuristic of the DAergic system. This was performed with data from the HCP and with SNc and VTA masks that were derived from the HCP data as well.

Using standard anatomical definitions, we examined the connectivity of SNc versus VTA to and from the DS, VS, and PFC to directly test predictions regarding connectivity based on conventional pathway heuristic of DA circuits. To measure the extent to which the SNc and VTA differentially connect to and from the DS, VS, and PFC with respect to all SNc/VTA connections, we placed seeds in the SNc and VTA and targeted the DS, VS, and PFC, measured the connectivity density from these regions to the targets, then compared the connectivity density between SNc and VTA for each target. To measure the extent of DS, VS, and PFC projections that are accounted by the SNc and the VTA, we placed seeds in the DS, VS, and PFC and targeted the SNc and the VTA. We then measured the connectivity density of these regions to and from the SNc and VTA and compared the connectivity density between SNc and VTA for each seed.

With respect to ipsilateral connectivity, we found that the SNc ($M = 11.169\%$, $SEM = 0.359$) and the VTA ($M = 11.189\%$, $SEM = 0.342$) had equal connectivity densities to and from the ipsilateral DS, that the SNc ($M = 0.419$, $SEM = 0.025$) had lower connectivity density to and from the ipsilateral DS than the VTA ($M = 0.681$, $SEM = 0.053$), and that the SNc ($M = 1.451$, $SEM = 0.064$) had lower connectivity density to and from the ipsilateral PFC than the VTA ($M = 1.819$, $SEM = 0.076$). In general, connectivity was greatest to and from the DS, then to and from the PFC, then to the VS.

Conversely, we found that the DS had a greater connectivity density to and from the ipsilateral SNc ($M = 0.504$, *SEM* $= 0.024$) than to and from the ipsilateral VTA ($M = 0.158$, *SEM* $= 0.007$), that the VS had a greater connectivity density to and from the ipsilateral SNc ($M = 0.120$, *SEM* $= 0.010$) than to and from the ipsilateral VTA ($M = 0.063$, *SEM* $= 0.006$), and that the PFC had a greater overall connectivity density to and from the ipsilateral SNc ($M = 0.086$, *SEM* $= 0.005$) than to and from the ipsilateral VTA ($M = 0.043$, *SEM* $= 0.003$).

With respect to contralateral projections, these patterns were largely the same. The only difference was that unlike the equal connectivity density of the SNc and the VTA to and from ipsilateral DS targets, we found that the SNc ($M = 0.329$, *SEM* $= 0.017$) had lower connectivity density to and from the contralateral DS than the VTA ($M = 0.931$, *SEM* $= 0.065$). Like the ipsilateral connectivity, the SNc ($M = 0.026$, *SEM* $= 0.002$) had lower connectivity density to and from the contralateral DS than the VTA ($M = 0.054$, *SEM* $= 0.006$), and the SNc ($M = 0.273$, *SEM* $= 0.011$) had lower connectivity density to and from the contralateral PFC than the VTA ($M = 0.441$, *SEM* $= 0.021$). Like the ipsilateral connectivity, connectivity was greatest to and from the DS, then to and from the PFC, then to and from the VS.

Connectivity of the DS, VS, and PFC to and from contralateral SNc and VTA followed the same patterns as ipsilateral projections. We found that the DS had a greater connectivity density to and from the contralateral SNc ($M = 0.033$, *SEM* $= 0.003$) than to and from the contralateral VTA ($M = 0.019$, *SEM* $= 0.001$), that the VS had a greater connectivity density to and from the contralateral SNc ($M = 0.013$, *SEM* $= 0.002$) than to and from the contralateral VTA ($M = 0.008$, *SEM* 0.001), and that the PFC had a greater overall connectivity density to and from the contralateral SNc ($M = 0.038$, *SEM* $= 0.003$) than to and from the contralateral VTA ($M = 0.022$, *SEM* $= 0.001$).

In addition, we also examined SNc and VTA connectivity to and from non-PFC cortical regions with a connectivity of >1%. We found that this was the case for connections of the SNc and VTA to and from the precentral gyrus, temporal pole, postcentral gyrus, superior division of the lateral occipital cortex, anterior parahippocampal gyrus, occipital pole, and the frontal rostral motor region. We found that the SNc ($M = 4.323$, *SEM* $= 0.101$) had greater connectivity to and from these regions than the VTA *($M = 2.422$, *SEM* $= 0.078$)*. Conversely, we found that these

regions had greater connectivity to and from the SNc ($M = 0.279$, $SEM = 0.011$) than to and from the VTA ($M = 0.057$, $SEM = 0.002$).

4.1.2 – Findings in the Context of the Conventional Pathway Heuristic

Our results are somewhat at odds with the conventional pathway heuristic of DA projections of the SNc and VTA to and from the DS, VS, and PFC (**Figure 8).** Given that we found much higher connectivity among ipsilateral connections, the discussion will focus primarily on the ipsilateral connectivity.

With seeds in the SNc and VTA, we found that the SNc and VTA had substantial connectivity to and from DS, and, at odds with the conventional DA pathway heuristic, SNc versus VTA did not differ significantly in the percentage of total connections of these regions projecting to and from DS. This suggests that neurons in the SNc and the VTA might be equally likely to project to the DS. Conversely, with a seed in the DS, we found that DS projected significantly greater to and from the SNc than to the VTA, potentially suggesting that the DS is more innervated by the SNc. This seemingly paradoxical finding could be explained by the SNc's greater size but also by immunohistochemistry studies of non-human primates that suggest that the SNc has a greater concentration of DA neurons overall than the VTA (François, Yelnik, Tandé, Agid, & Hirsch, 1999). Indeed, that the SNc and VTA have the same connectivity density to and from the DS does not imply that an equal number of neurons connect there, rather it implies that streamlines of the SNc and VTA have an equal chance of projecting there. Given the findings of François et al. (1999), it could be that while the SNc and VTA have equal chance of projecting to the DS, the DS still receives more DA from the SNc.
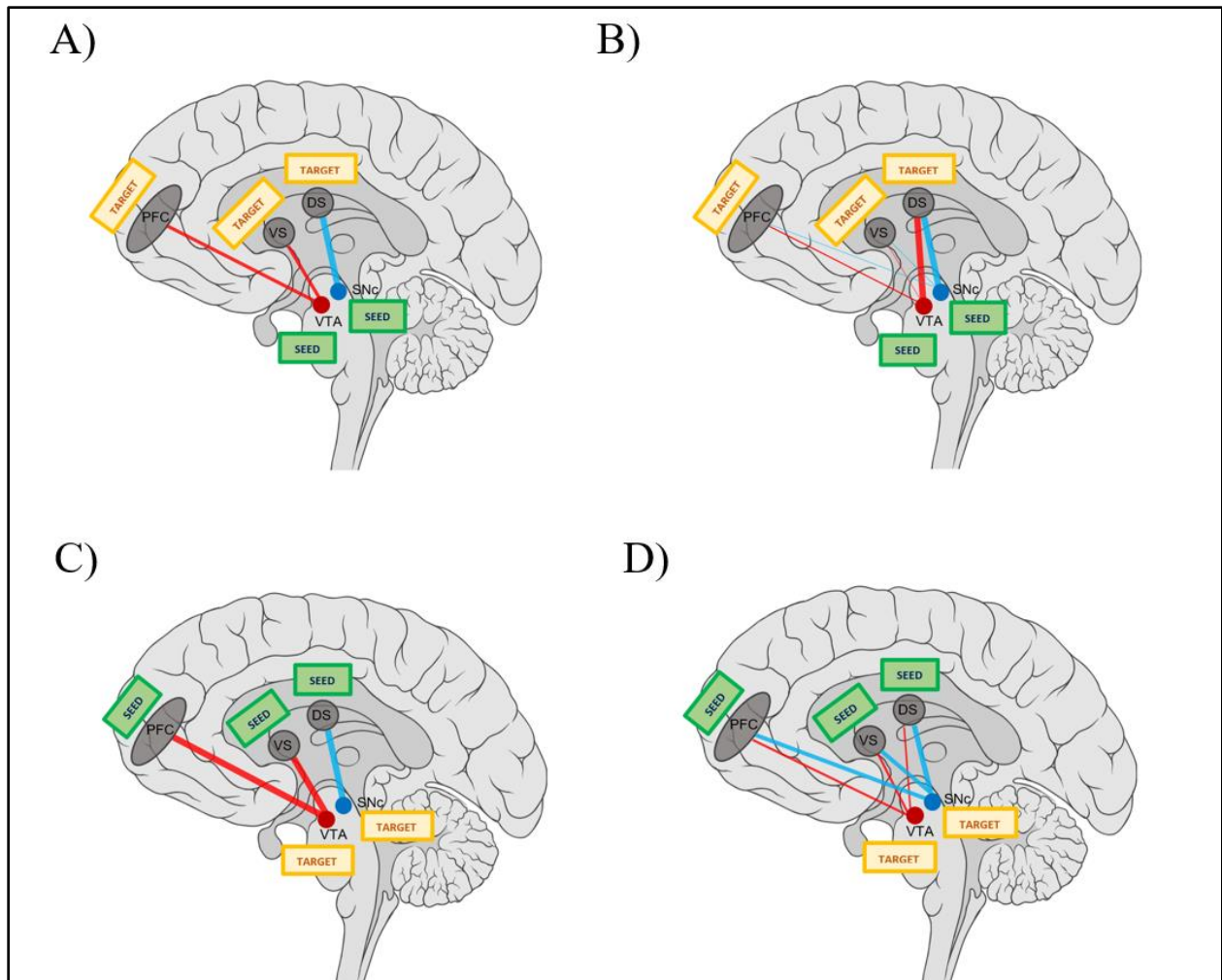
Figure 8: Schematic of the conventional pathway heuristic (8A) and 8C)) versus our findings (8B) and 8D)).
Figure 8A) shows what the connectivity density of the SNc and VTA to and from the DS, VS, and PFC would be if the conventional pathway heuristic were true; Figure 8B) shows the connectivity density of the SNc and VTA to and from the DS, VS, and PFC as measured in the HCP data. Figure 8C) shows the connectivity density of the DS, VS, and PFC to and from the SNc and VTA if the conventional pathway heuristic was assumed to be true; Figure 8D) shows the relative connectivity densities of the DS, VS, and PFC to and from the SNc and VTA as measured in the HCP data. Seed regions are labelled in green; Target regions are labelled in yellow. Connectivity densities to and from the SNc are labelled blue; connectivity densities to and from the VTA are labelled red. The thickness of each blue or red line represents the relative connectivity density revealed by probabilistic tractography. Thickness is only relative within each subsection of the figure; for example, line thicknesses found in 8B) are not relative to line thicknesses in 8D). In the case of 8B) and 8D), the largest connectivity was set to an arbitrary arrow width (3.75), and all others were adjusted to be relative to that width. Marginal means were used to show connectivity to and from the PFC. Only ipsilateral connectivity values are shown. Brain illustrations used with permission from Patrick J. Lynch.

Although we found that less than 1% of both SNc and VTA projections connected to and from the VS, connectivity of the VTA to and from the VS was significantly greater than connectivity

of the SNc to and from the VS. This finding is somewhat in keeping with predictions of conventional DA circuitry theories in which VTA investment to VS is greater than SNc investment to DS. However, conversely, we found that the VS connectivity density to and from the SNc was larger than to and from the VTA. This could suggest that the VS received more SNc neurons than the VTA, which is at odds with the conventional pathway heuristic. Like the innervation of the DS, this could be due to the SNc's greater size and DA concentration (François et al., 1999).

Furthermore, we observed that both the SNc and the VTA had substantial connectivity to and from numerous PFC regions. Connectivity of the VTA to and from the PFC was significantly greater than connectivity of the SNc to and from the PFC. The latter finding is somewhat in keeping with predictions of conventional DA circuitry theories. However, we found that the PFC had greater connectivity to and from the SNc than to and from the VTA, suggesting that the PFC received more SNc neurons than the VTA, at odds with the conventional pathway heuristic.

Finally, we also showed that the SNc and VTA had substantial connectivity to and from a number of non-PFC regions, with the SNc having a greater connectivity to and from these regions than the VTA. Conversely, the non-PFC regions had greater connectivity density to and from the SNc than to and from the VTA.

In summary, we measured the following findings that are at odds with the conventional pathway heuristic: a) that the SNc and VTA have statistically equivalent connectivity to and from the DS, suggesting a VTA to DS pathway, b) that the VS has greater connectivity to and from the SNc than to and from the VTA, suggesting a SNc to VS pathway, c) that the PFC has greater connectivity to and from the SNc than to and from the VTA, suggesting a SNc to PFC pathway, and d) that there was substantial connectivity of the SNc and the VTA to and from multiple non-PFC regions, suggesting a SNc/VTA to non-PFC region pathway.

4.1.3 – VTA Connectivity to DS

A main finding of our study is that, in addition to the predicted SNc connectivity to and from DS, a significant proportion of VTA streamlines targeted the DS. This is one of only a small number of studies that have investigated this issue using neuroimaging and healthy participants. The presence of strong connectivity density between the VTA and the DS, observed here is line with the dMRI study conducted by Chowdhury et al. (2013), in which they were able to parcellate the SNc/VTA into two subregions based upon connectivity to the DS and VS (Chowdhury et al., 2013. They found that both SNc and VTA subregions of the SNc/VTA connected to the VS as well as to the DS, failing to find evidence of the conventional pathway heuristic in which the VTA solely targets the VS.

Interestingly, we did not find a significant difference in terms of the percentage of total SNc streamlines or of total VTA streamlines that terminated in the DS. This was inconsistent with the hypotheses of the conventional DA circuitry. It is also at odds with findings by Kwon and colleagues (2014), who used MRI and probabilistic tractography to measure the connectivity from the SNc and VTA to striatal and cortical targets. They found that SNc had 97.62 % connectivity to the NAcc and that the VTA had 68.25 % to the NAcc. Their definition of connectivity was different to ours, however. They defined connectivity from the SNc/VTA to a target as the percentage of participants' hemispheres in which in which sampled streamlines reached the target region at a threshold of 0.1%. For instance, if 0.1% connectivity occurred from SNc to 90 participant hemispheres out of 100, they would have reported 90%. Thus, their study does not report the nature of the connectivity itself. Further, they defined the DS as the whole CPu and not the bulk of the CPu as we have, potentially explaining their divergent findings from ours. Their study essentially showed in how many participants a certain connectivity density occurred. In our study, we analyzed the connectivity density of the SNc and VTA themselves.

Given that in humans and in non-human primates, the SNc contained approximately five times the amount of DA as the VTA, it would follow, according to these findings, that the DS still receives the bulk of DA from the SNc (Düzel et al., 2009; François et al., 1999) We have added further evidence to these findings, given that a greater percentage of connectivity of the DS went to and from the SNc compared to the VTA.

In all, these findings suggest that while neurons from the SNc and the VTA are both equally likely to project to the DS, the DS is more innervated by the SNc. This configuration is inconsistent with the conventional view that the VTA does not project to the DS.

4.1.4 – SNc/VTA Connectivity to PFC

Contrary to the conventional view that SNc projects exclusively or primarily to DS, we found that there was substantial connectivity density of the SNc as well as the VTA to and from PFC. In line with the conventional theory of DA circuitry, however, we found that the PFC accounted for more of VTA's DA projections than DS's DA projections. However, we also found that a significantly greater proportion of the PFC's connectivity targeted the SNc compared to the VTA. This suggests that the SNc contributes neurons to the PFC, unlike as described in the conventional pathway heuristic.

The finding of an extensive connectivity density between the SNc and the PFC was in line with recent findings of two studies by Cacciola and colleagues (2016, 2017). They used Constrained Spherical Deconvolution, which is another way to model DWI data, on a sample of participants and found that there was substantial connectivity between the PFC and SNc. The authors explained that this was likely due to a glutamatergic tract emerging from the PFC and targeting the SNc (Cacciola et al., 2016, 2017). However, others have demonstrated DAergic efferent connections from the SNc to the PFC in rodents and non-human primates, suggesting that our findings could also be reflective of DA tracts (Gaspar et al., 1992; Loughlin & Fallon, 1984; Williams & Goldman-Rakic, 1998).

4.1.5 – Connectivity to non-PFC Areas

Though not a central question of our study, we also observed substantial connectivity of the SNc and the VTA to and from multiple non-PFC cortical areas. This was consistent with the findings of Cacciola et al., (2016, 2017), who found substantial connectivity density between the SNc and multiple non-PFC cortical areas. Specifically, we found that there was >1% connectivity of the SNc and the VTA to and from the following cortical regions in decreasing order based on

average ipsilateral connectivity density: 1) precentral gyrus, the primary motor cortex, 2) postcentral gyrus, the somatosensory cortex, 3) the frontal rostral motor region, consisting mainly of the frontal eye field and supplementary motor area, 4) lateral occipital subdivision and occipital pole,representing part of the occipital lobe), and 5) the anterior parahippocampal gyrus and temporal pole. This is reflective of the fact that DA projections are found in nearly all regions of the neocortex in non-human primates (Brown, Crane, & Goldman, 1979). In fact, it has been found that cortical DA concentration decreases nearly linearly along the fronto-occipital axis; this seems to be reflected in the connectivity of observed >1% connectivity densities (Brown et al., 1979).

Whether there are direct SNc/VTA DAergic connections to each cortical region remains under investigation. Though a full review of SNc and VTA connections to non-PFC regions of the cortex is beyond the scope of this study, we have focused on evidence of direct connections to the precentral and postcentral gyri, which were the two to have had the greatest connectivity densities in our Experiment 1. With respect to the former, a direct DAergic connection from the VTA to the primary motor cortex has been well-studied, and has been implicated in motor skill learning (Brown et al., 1979; Hosp, Pekanovic, Rioult-Pedotti, & Luft, 2011). A direct SNc connection to the primary motor cortex has also been shown (Gaspar et al., 1992; Luft & Schwarz, 2009) though these studies did not investigate the impact of these connections on function. With respect to the latter, it is possible that DA from the SNc/VTA projects to the somatosensory cortex, though perhaps quite minimally. However, the potential role of these potential connections is unknown (Jacob & Nienborg, 2018; Lewis, Campbell, Foote, Goldstein, & Morrison, 1987).

4.2 – Experiment 2: PD versus Healthy Control

Finally, given our thorough understanding of the pathophysiological changes involving SNc/VTA in PD, particularly in the early stages, testing our *in vivo* approach for SNc/VTA connectivity measurement in recently-diagnosed PD patients relative to HCs provided a means for validation. The CM SNc/VTA is known to degenerate first and most in PD. Consequently,

we predicted that only independent connectivity to the CM striatum would be reduced in our early-staged PD patients relative to HC.

4.3 – Independent Connectivity

Using probabilistic tractography, we were able to measure the independent connectivity of the SNc/VTA to subregions of the striatum. This technique is beneficial because it allows for the measurement of connectivity density even within the context of overlapping subregions. We found that there was a significant difference of independent connectivity to the right CM striatum between PD and HCs. Adjusting for multiple comparisons revealed a marginally significant difference to this region. Whether *a priori* testing is statistically valid is debated in the literature (Frame, 2015; Lindquist & Mejia, 2015). However, we suggest that in this case, there is a real significant difference between PD patients and HCs to the right CM striatum because a) it represents known DAergic loss in PD patients, and b) it matches the finding of volumetric CM striatal decrease in PD patients (Khan et al., 2019).

4.4 – Validation

Numerous studies have been conducted to assess the validity of dMRI to represent the underlying neural tracts, though few have been undertaken to assess the validity of dMRI to measure tracts from the midbrain (Berman, Berger, Chung, Nagarajan, & Henry, 2007). In one study that compared dMRI measurement of SNc tracts, it was determined that diffusion measures such as MD were found to correlate to nigral DA neurons and striatal fiber density in non-human primates (Shimony et al., 2018). To our knowledge, no study has validated the use of probabilistic tractography from the SNc/VTA against a non-human primate gold standard. However, studies that have parcellated the SNc/VTA based on connectivity to the striatum have reported parcellation schemes that match the known bounds of cytoarchitecture differences in the SNc/VTA, suggesting that the connectivity from the SNc/VTA to the striatum reflects the DAergic neural tracts (Chowdhury et al., 2013; Menke et al., 2010; Yu Zhang et al., 2017). In

our experiment 2, that independent connectivity to the right CM striatum was decreased in PD patients as compared to HCs serves to help validate this method. Given the known neuropathology of PD patients, in which the degeneration of SNc and VTA DAergic neurons underlie the motor and non-motor symptoms, and given that we found a reduction of connectivity density to the region that is responsible for motor movements, we suspect that use of dMRI tractography to measure neural tracts is at least sensitive enough to make inferences, but not conclusions, about the structural connections that emerge from the SNc/VTA.

4.5 – Limitations

While dMRI can offer unique insights into the structural connectivity of the human brain *in vivo*, it is prone to numerous limitations that prevent the conclusive determination of connective tracts (Jbabdi & Johansen-Berg, 2011; Jbabdi, Sotiropoulos, Haber, Van Essen, & Behrens, 2015; Jones, Knösche, & Turner, 2013; Thomas et al., 2014). Importantly, dMRI cannot determine the direction of neural propagation. Though we have described the connections as being from the SNc/VTA to the striatum/cortex, this is a reflection of the propagation of seeded streamlines from the seed (SNc/VTA) to the target (striatum/cortex), not neuron direction. We have interpreted our findings as being efferent in the case of SNc/VTA to DS, VS, and PFC and afferent in the case of DS, VS, and PFC to SNc/VTA based on known neuroanatomy and based on our validation, but we cannot conclude this conclusively. Further, dMRI cannot make any determination about the neurotransmitter of a measured tract. We have interpreted the majority of measured connections as DAergic based off our validation, but the BG system is influenced heavily by other neurotransmitters like glutamate and GABA. Further, dMRI cannot perfectly resolve crossing fibers within a voxel; for instance, limiting the inference of bending or crossing neurons. We attempted to somewhat resolve this issue by using BEDPOSTX, but even still, it does not perfectly resolve the issue (Behrens et al., 2007). Further, as a matter of mathematical construction, dMRI is known to be prone to false positives and negatives and to favour shorter connections. We have employed ultra-high resolution data to reduce the effects of these limitations; however, future studies of human connectivity could utilize more optimal diffusion modelling techniques such as High angular resolution diffusion imaging (HARDI) (Berman, Lanza, Blaskey, Edgar, & Roberts, 2013; Glasser et al., 2013; Sotiropoulos et al., 2013).

Furthermore, though the Pauli atlas has a multitude of benefits that are advantageous to this analysis, there are limitations in the boundaries between the SNc and VTA with respect to other brain regions (Pauli et al., 2018). Even though the boundary between SNc and VTA was well-defined in the CIT168 atlas, it is possible that the two regions succumbed to partial volume effects, whereby voxels between the SNc and VTA contain information of both tissues but are only labelled as one or the other. However, this problem is, in effect, also the case for the anatomical definitions of the SNc and VTA, which are posited as separate structures despite known overlapping areas between them (Haber & Knutson, 2010). Thus, we suspect that partial volume effects might be reflective of the limitations of conventional anatomical boundaries. Second, the boundary between the SNc and the SNr was reported not to be a poorly defined boundary, as they were difficult to differentiate on the T1w/T2w pairs. Thus, it is possible that a small portion of the voxels within the SNc segmentations are comprised of the SNr.

With respect to the validation step, it is possible, given that the CIT168 atlas was defined in a sample of healthy adults rather than PD patients, that some of the variability between groups could be explained by the atlas being more similar to the HC group than the PD group. This issue could have potentially been avoided by using a subcortical atlas developed using data from PD patients, but to our knowledge, no such atlas exists.

Finally, though we did find a significant difference in the caudal motor independent connectivity between PD and HC group before adjustments for multiple comparison, we did not after the adjustment. We suspect that this is likely due to a low sample size.

4.6 – Conclusion

We have performed one of the first studies measuring the connectivity of the SNc and the VTA to the striatum and cortex, in which we implemented ultra-high resolution data and anatomical masks. We have found evidence to suggest that the SNc potentially connects with the VS, that the VTA potentially connects with the DS, and that the SNc connects with the PFC. This counters the conventional pathway heuristic and adds to a growing body of evidence to suggest that it is an oversimplification of DAergic connectivity We have also measured the connectivity to other regions of the cortex that seem to reflect known anatomical connections.

We extended the use of dMRI to assess if it could be used to measure differences between population groups. We found that in PD patients, the independent connectivity to the right CM region of the striatum was significantly reduced, as hypothesized. Understanding dMRI connectivity patterns within healthy controls and within PD patients could help understand the influence of DA on other diseases like schizophrenia, SUD, and OCD.

References

Adcock, R. A., Thangavel, A., Whitfield-Gabrieli, S., Knutson, B., & Gabrieli, J. D. E. (2006). Reward-Motivated Learning: Mesolimbic Activation Precedes Memory Formation. *Neuron*, *50*(3), 507–517.

Alcaro, A., Huber, R., & Panksepp, J. (2007). Behavioral functions of the mesolimbic dopaminergic system: an affective neuroethological perspective. *Brain Research Reviews*, *56*(2), 283–321.

Alexander, A. L., Lee, J. E., Lazar, M., & Field, A. S. (2007). Diffusion Tensor Imaging of the Brain. *Neurotherapeutics*, *4*(3),

Alexander, G. E. (2004). Biology of Parkinson's disease: pathogenesis and pathophysiology of a multisystem neurodegenerative disorder. *Dialogues in Clinical Neuroscience*, *6*(3), 259–280.

Andén, N. -E., Dahlström, A., Fuxe, K., Larsson, K., Olson, L., & Ungerstedt, U. (1966). Ascending Monoamine Neurons to the Telencephalon and Diencephalon. *Acta Physiologica Scandinavica*, *67*(3–4), 313–326. https://doi.org/10.1111/j.1748-1716.1966.tb03318.x

Andén, N. -E, Dahlström, A., Fuxe, K., & Larsson, K. (1966). Functional Role of the Nigro-Neostriatal Dopamine Neurons*). *Acta Pharmacologica et Toxicologica*, *24*(2–3), 263–274.

Andersson, J. L. R., Jenkinson, M., Smith, S., Jenkinson, M., SMITH, S., Andersson, J. L. R., … Smith, S. W. (2007). Non-Linear Registration aka Spatial Normalisation FMRIB Technial Report TR07JA2.

Andersson, J. L. R., Skare, S., & Ashburner, J. (2003). How to correct susceptibility distortions in spin-echo echo-planar images: application to diffusion tensor imaging. *NeuroImage*, *20*(2), 870–888.

Andersson, J. L. R., & Sotiropoulos, S. N. (2015). Non-parametric representation and prediction of single- and multi-shell diffusion-weighted MRI data using Gaussian processes. *NeuroImage*, *122*, 166–176.

Andersson, J. L. R., & Sotiropoulos, S. N. (2016). An integrated approach to correction for off-

resonance effects and subject movement in diffusion MR imaging. *NeuroImage*, *125*, 1063–1078.

Aransay, A., Rodríguez-López, C., García-Amado, M., Clascá, F., & Prensa, L. (2015). Long-range projection neurons of the mouse ventral tegmental area: a single-cell axon tracing analysis. *Frontiers in Neuroanatomy*, *9*, 59.

Arias-Carrión, O., Stamelou, M., Murillo-Rodríguez, E., Menéndez-González, M., & Pöppel, E. (2010). Dopaminergic reward system: a short integrative review. *International Archives of Medicine*, *3*, 24.

Ashok, A. H., Mizuno, Y., Volkow, N. D., & Howes, O. D. (2017). Association of Stimulant Use With Dopaminergic Alterations in Users of Cocaine, Amphetamine, or Methamphetamine. *JAMA Psychiatry*, *74*(5), 511.

Atkinson-Clement, C., Pinto, S., Eusebio, A., & Coulon, O. (2017). Diffusion tensor imaging in Parkinson's disease: Review and meta-analysis. *NeuroImage. Clinical*, *16*, 98–110.

Attwell, D., Buchan, A. M., Charpak, S., Lauritzen, M., Macvicar, B. A., & Newman, E. A. (2010). Glial and neuronal control of brain blood flow. *Nature*, *468*(7321), 232–243.

Attwell, D., & Laughlin, S. B. (2001). An Energy Budget for Signaling in the Grey Matter of the Brain. *Journal of Cerebral Blood Flow & Metabolism*, *21*(10), 1133–1145.

Bammer, R. (2003). Basic principles of diffusion-weighted imaging. *European Journal of Radiology*, *45*(3), 169–184.

Bär, K., De, F., Schumann, A., Koehler, S., Sauer, H., Critchley, H., & Wagner, G. (2016). NeuroImage Functional connectivity and network analysis of midbrain and brainstem nuclei. *NeuroImage*, *134*, 53–63.

Baser, P. J. (1995). Inferring Microstructural Features and the Physiological State of Tissues from Diffusion-Weighted Images. *NMR n Biomeidicine*, *8*(8-8), 333-344.

Basser, P. J., & Jones, D. K. (2002). Diffusion-tensor MRI: theory, experimental design and data analysis - a technical review. *NMR in Biomedicine*, *15*(7–8), 456–467.

Basser, P. J., Pajevic, S., Pierpaoli, C., Duda, J., & Aldroubi, A. (2000). In vivo fiber

tractography using DT-MRI data. *Magnetic Resonance in Medicine*, *44*(4), 625–632.

Baumeister, A. A. (2013). The chlorpromazine enigma. *Journal of the History of the Neurosciences*, *22*(1), 14–29.

Beaulieu, J.-M., & Gainetdinov, R. R. (2011). The Physiology, Signaling, and Pharmacology of Dopamine Receptors. *Pharmacological Reviews*, *63*(1), 182–217.

Beckstead, R. M., Domesick, V. B., & Nauta, W. J. H. (1979). Efferent connections of the substantia nigra and ventral tegmental area in the rat. *Brain Research*, *175*(2), 191–217.

Behrens, T. E. J., Berg, H. J., Jbabdi, S., Rushworth, M. F. S., & Woolrich, M. W. (2007). Probabilistic diffusion tractography with multiple fibre orientations: What can we gain? *NeuroImage*, *34*(1), 144–155.

Behrens, T. E. J., Johansen-Berg, H., Woolrich, M. W., Smith, S. M., Wheeler-Kingshott, C. A. M., Boulby, P. A., … Matthews, P. M. (2003). Non-invasive mapping of connections between human thalamus and cortex using diffusion imaging. *Nature Neuroscience*, *6*(7), 750–757.

Behrens, T. E. J., Woolrich, M. W., Jenkinson, M., Johansen-Berg, H., Nunes, R. G., Clare, S., … Smith, S. M. (2003). Characterization and propagation of uncertainty in diffusion-weighted MR imaging. *Magnetic Resonance in Medicine*, *50*(5), 1077–1088.

Beier, K. T., Gao, X. J., Xie, S., DeLoach, K. E., Malenka, R. C., & Luo, L. (2019). Topological Organization of Ventral Tegmental Area Connectivity Revealed by Viral-Genetic Dissection of Input-Output Relations. *Cell Reports*, *26*(1), 159–167.e6.

Benjamini, Y., & Hochberg, Y. (1995). Controlling the False Discovery Rate: A Practical and Powerful Approach to Multiple Testing. *Journal of the Royal Statistical Society. Series B (Methodological)*. WileyRoyal Statistical Society.

Berman, J. I., Berger, M. S., Chung, S., Nagarajan, S. S., & Henry, R. G. (2007). Accuracy of diffusion tensor magnetic resonance imaging tractography assessed using intraoperative subcortical stimulation mapping and magnetic source imaging. *Journal of Neurosurgery*, *107*(3), 488–494.

Berman, J. I., Lanza, M. R., Blaskey, L., Edgar, J. C., & Roberts, T. P. L. (2013). High angular resolution diffusion imaging probabilistic tractography of the auditory radiation. *AJNR. American Journal of Neuroradiology*, *34*(8), 1573–1578.

Berridge, K. C. (2007). The debate over dopamine's role in reward: the case for incentive salience. *Psychopharmacology*, *191*(3), 391–431.

Berridge, K. C., & Robinson, T. E. (2016). Liking, wanting, and the incentive-sensitization theory of addiction. *The American Psychologist*, *71*(8), 670–679.

Bissonette, G. B., & Roesch, M. R. (2016). Development and function of the midbrain dopamine system: what we know and what we need to. *Genes, Brain, and Behavior*, *15*(1), 62–73.

Björklund, A., & Dunnett, S. B. (2007). Dopamine neuron systems in the brain: an update. *Trends in Neurosciences*, *30*(5), 194–202.

Bonilha, L., Gleichgerrcht, E., Fridriksson, J., Rorden, C., Breedlove, J. L., Nesland, T., … Focke, N. K. (2015). Reproducibility of the Structural Brain Connectome Derived from Diffusion Tensor Imaging. *PLOS ONE*, *10*(9), e0135247.

Bressan, R. A., & Crippa, J. A. (2005). The role of dopamine in reward and pleasure behaviour - review of data from preclinical research. *Acta Psychiatrica Scandinavica*, *111*(s427), 14–21.

Brisch, R., Saniotis, A., Wolf, R., Bielau, H., Bernstein, H.-G., Steiner, J., … Gos, T. (2014). The role of dopamine in schizophrenia from a neurobiological and evolutionary perspective: old fashioned, but still in vogue. *Frontiers in Psychiatry*, *5*, 47.

Brischoux, F., Chakraborty, S., Brierley, D. I., & Ungless, M. A. (2009). Phasic excitation of dopamine neurons in ventral VTA by noxious stimuli. *Proceedings of the National Academy of Sciences*, *106*(12), 4894–4899.

Brog, J. S., Salyapongse, A., Deutch, A. Y., & Zahm, D. S. (1993). The patterns of afferent innervation of the core and shell in the "accumbens" part of the rat ventral striatum: Immunohistochemical detection of retrogradely transported fluoro-gold. *The Journal of Comparative Neurology*, *338*(2), 255–278.

Bromberg-Martin, E. S., Matsumoto, M., & Hikosaka, O. (2010). Dopamine in motivational control: rewarding, aversive, and alerting. *Neuron*, *68*(5), 815–834.

Brown, R. M., Crane, A. M., & Goldman, P. S. (1979). Regional distribution of monoamines in the cerebral cortex and subcortical structures of the rhesus monkey: concentrations and in vivo synthesis rates. *Brain Research*, *168*(1), 133–150.

Bucholz, K. K., Cadoret, R., Cloninger, C. R., Dinwiddie, S. H., Hesselbrock, V. M., Nurnberger, J. I., … Schuckit, M. A. (1994). A new, semi-structured psychiatric interview for use in genetic linkage studies: a report on the reliability of the SSAGA. *Journal of Studies on Alcohol*, *55*(2), 149–158.

Burns, R. S., Chiueh, C. C., Markey, S. P., Ebert, M. H., Jacobowitz, D. M., & Kopin, I. J. (1983). A primate model of parkinsonism: selective destruction of dopaminergic neurons in the pars compacta of the substantia nigra by N-methyl-4-phenyl-1,2,3,6-tetrahydropyridine. *Proceedings of the National Academy of Sciences of the United States of America*, *80*(14), 4546–4550.

Cacciola, A., Calamuneri, A., Milardi, D., Mormina, E., Chillemi, G., Marino, S., … Quartarone, A. (2017). A Connectomic Analysis of the Human Basal Ganglia Network. *Frontiers in Neuroanatomy*, *11*, 85.

Cacciola, A., Milardi, D., Anastasi, G. P., Basile, G. A., Ciolli, P., Irrera, M., … Quartarone, A. (2016). A Direct Cortico-Nigral Pathway as Revealed by Constrained Spherical Deconvolution Tractography in Humans. *Frontiers in Human Neuroscience*, *10*, 374.

Calabresi, P., Picconi, B., Tozzi, A., Ghiglieri, V., & Di Filippo, M. (2014). Direct and indirect pathways of basal ganglia: a critical reappraisal. *Nature Neuroscience*, *17*(8), 1022–1030.

Caminiti, S. P., Presotto, L., Baroncini, D., Garibotto, V., Moresco, R. M., Gianolli, L., … Perani, D. (2017). Axonal damage and loss of connectivity in nigrostriatal and mesolimbic dopamine pathways in early Parkinson's disease. *NeuroImage. Clinical*, *14*, 734–740.

Carlsson, A., & Lindqvist, M. (1963). Effect of Chlorpromazine or Haloperidol on Formation of 3-Methoxytyramine and Normetanephrine in Mouse Brain. *Acta Pharmacologica et Toxicologica*, *20*(2), 140–144.

Chowdhury, R., Lambert, C., Dolan, R. J., & Düzel, E. (2013). Parcellation of the human substantia nigra based on anatomical connectivity to the striatum. *NeuroImage*, *81*, 191–198.

Chung, M. K., Hanson, J. L., Adluru, N., Alexander, A. L., Davidson, R. J., & Pollak, S. D. (2017). Integrative Structural Brain Network Analysis in Diffusion Tensor Imaging. *Brain Connectivity*, *7*(6), 331–346.

Cohen, J. Y., Haesler, S., Vong, L., Lowell, B. B., & Uchida, N. (2012). Neuron-type-specific signals for reward and punishment in the ventral tegmental area. *Nature*, *482*(7383), 85–88.

Cools, R., Ivry, R. B., & D'Esposito, M. (2006). The Human Striatum is Necessary for Responding to Changes in Stimulus Relevance. *Journal of Cognitive Neuroscience*, *18*(12), 1973–1983.

Da Cunha, C., Angelucci, M. E. M., Canteras, N. S., Wonnacott, S., & Takahashi, R. N. (2002). The Lesion of the Rat Substantia Nigra pars compacta Dopaminergic Neurons as a Model for Parkinson's Disease Memory Disabilities. *Cellular and Molecular Neurobiology*, *22*(3), 227–237.

Damoiseaux, J. S., Rombouts, S. A. R. B., Barkhof, F., Scheltens, P., Stam, C. J., Smith, S. M., & Beckmann, C. F. (2006). Consistent resting-state networks across healthy subjects. *Proceedings of the National Academy of Sciences of the United States of America*, *103*(37), 13848–13853.

Del Casale, A., Kotzalidis, G. D., Rapinesi, C., Serata, D., Ambrosi, E., Simonetti, A., … Girardi, P. (2011). Functional Neuroimaging in Obsessive-Compulsive Disorder. *Neuropsychobiology*, *64*(2), 61–85.

Deng, X.-Y., Wang, L., Yang, T.-T., Li, R., & Yu, G. (2018). A meta-analysis of diffusion tensor imaging of substantia nigra in patients with Parkinson's disease. *Scientific Reports*, *8*(1), 2941.

Deperrois, N., & Gutkin, B. (2018). Nicotinic and Cholinergic Modulation of Reward Prediction Error Computations in the Ventral Tegmental Area: a Minimal Circuit Model. *BioRxiv*, 423806.

Di Martino, A., Scheres, A., Margulies, D. S., Kelly, A. M. C., Uddin, L. Q., Shehzad, Z., … Milham, M. P. (2008). Functional Connectivity of Human Striatum: A Resting State fMRI Study. *Cerebral Cortex*, *18*(12), 2735–2747.

Düzel, E., Bunzeck, N., Guitart-Masip, M., Wittmann, B., Schott, B. H., & Tobler, P. N. (2009). Functional imaging of the human dopaminergic midbrain. *Trends in Neurosciences*, *32*(6), 321–328.

Ehringer, H., & Hornykiewicz, O. (1960). Verteilung Von Noradrenalin Und Dopamin (3-Hydroxytyramin) Im Gehirn Des Menschen Und Ihr Verhalten Bei Erkrankungen Des Extrapyramidalen Systems. *Klinische Wochenschrift*, *38*(24), 1236–1239.

Eickhoff, S. B., Thirion, B., Varoquaux, G., & Bzdok, D. (2015). Connectivity-based parcellation: Critique and implications. *Human Brain Mapping*, *36*(12), 4771–4792.

Fallon, J. H. (1988). Topographic Organization of Ascending Dopaminergic Projections. *Annals of the New York Academy of Sciences*, *537*(1 The Mesocorti), 1–9.

Fallon, J. H., & Moore, R. Y. (1978). Catecholamine innervation of the basal forebrain IV. Topography of the dopamine projection to the basal forebrain and neostriatum. *The Journal of Comparative Neurology*, *180*(3), 545–579.

Faure, A., Haberland, U., Condé, F., & El Massioui, N. (2005). Lesion to the Nigrostriatal Dopamine System Disrupts Stimulus-Response Habit Formation. *Journal of Neuroscience*, *25*(11), 2771–2780.

Fearnley, J. M., & Lees, A. J. (1991). Ageing and Parkinson's Disease: Susbtantia Nigra Regional Selectivity. *Brain*, *114*(5), 2283–2301.

Figee, M., Vink, M., de Geus, F., Vulink, N., Veltman, D. J., Westenberg, H., & Denys, D. (2011). Dysfunctional Reward Circuitry in Obsessive-Compulsive Disorder. *Biological Psychiatry*, *69*(9), 867–874.

Fischl, B. (2012). FreeSurfer. *NeuroImage*, *62*(2), 774–781.

Fischl, B., van der Kouwe, A., Destrieux, C., Halgren, E., Ségonne, F., Salat, D. H., … Dale, A. M. (2004). Automatically Parcellating the Human Cerebral Cortex. *Cerebral Cortex*, *14*(1),

11-22.

Frame, A. V. (2015). Planned Hypothesis Tests Are Not Necessarily Exempt From Multiplicity Adjustment. *Journal of Research Practice*, *11*(1).

Frank, M. J., & Surmeier, D. J. (2009). Do Substantia Nigra Dopaminergic Neurons Differentiate Between Reward and Punishment? *Journal of Molecular Cell Biology*, *1*(1), 15–16.

François, C., Yelnik, J., Tandé, D., Agid, Y., & Hirsch, E. C. (1999). Dopaminergic cell group A8 in the monkey: Anatomical organization and projections to the striatum. *The Journal of Comparative Neurology*, *414*(3), 334–347.

Ganepola, T., Nagy, Z., Ghosh, A., Papadopoulo, T., & Sereno, M. I. (2018). Using diffusion MRI to discriminate areas of cortical grey matter. *NeuroImage*, *182*, 456–468.

Gao, Y., Schilling, K. G., Stepniewska, I., Plassard, A. J., Choe, A. S., Li, X., … Anderson, A. W. (2018). Tests of cortical parcellation based on white matter connectivity using diffusion tensor imaging. *NeuroImage*, *170*, 321–331.

Gaspar, P., Stepniewska, I., & Kaas, J. H. (1992). Topography and collateralization of the dopaminergic projections to motor and lateral prefrontal cortex in owl monkeys. *The Journal of Comparative Neurology*, *325*(1), 1–21.

Glasser, M. F., Sotiropoulos, S. N., Wilson, J. A., Coalson, T. S., Fischl, B., Andersson, J. L., … Jenkinson, M. (2013). The minimal preprocessing pipelines for the Human Connectome Project. *NeuroImage*, *80*, 105–124.

Goense, J., Bohraus, Y., & Logothetis, N. K. (2016). fMRI at High Spatial Resolution: Implications for BOLD-Models. *Frontiers in Computational Neuroscience*, *10*, 66.

Goldman, J. G., Vernaleo, B. A., Camicioli, R., Dahodwala, N., Dobkin, R. D., Ellis, T., … Simmonds, D. (2018). Cognitive impairment in Parkinson's disease: a report from a multidisciplinary symposium on unmet needs and future directions to maintain cognitive health. *Npj Parkinson's Disease*, *4*(1), 19.

Gong, G., He, Y., Concha, L., Lebel, C., Gross, D. W., Evans, A. C., & Beaulieu, C. (2009). Mapping Anatomical Connectivity Patterns of Human Cerebral Cortex Using In Vivo

Diffusion Tensor Imaging Tractography. *Cerebral Cortex*, *19*(3), 524–536.

Gotham, A. M., Brown, R. G., & Marsden, C. D. (1986). Levodopa treatment may benefit or impair "frontal" function in Parkinson's disease. *Lancet*, *2*(8513), 970–971.

Haber, S., & Fudge JL. (1997). The primate substantia nigra and VTA: integrative circuitry and function. *Crit Rev Neurobiol*, *11*(4), 323–342. Retrieved from

Haber, S. N., Fudge, J. L., & McFarland, N. R. (2000). Striatonigrostriatal pathways in primates form an ascending spiral from the shell to the dorsolateral striatum. *The Journal of Neuroscience*, *20*(6), 2369–2382.

Haber, S. N., & Knutson, B. (2010). The Reward Circuit: Linking Primate Anatomy and Human Imaging. *Neuropsychopharmacology*, *35*(1), 4–26.

Hawrylycz, M. J., Lein, E. S., Guillozet-Bongaarts, A. L., Shen, E. H., Ng, L., Miller, J. A., … Jones, A. R. (2012). An anatomically comprehensive atlas of the adult human brain transcriptome. *Nature*, *489*(7416), 391–399.

Hodge, M. R., Horton, W., Brown, T., Herrick, R., Olsen, T., Hileman, M. E., … Marcus, D. S. (2016). ConnectomeDB--Sharing human brain connectivity data. *NeuroImage*, *124*(Pt B), 1102–1107.

Honey, C. J., Sporns, O., Cammoun, L., Gigandet, X., Thiran, J. P., Meuli, R., & Hagmann, P. (2009). Predicting human resting-state functional connectivity from structural connectivity. *Proceedings of the National Academy of Sciences of the United States of America*, *106*(6), 2035–2040.

Hosp, J. A., Pekanovic, A., Rioult-Pedotti, M. S., & Luft, A. R. (2011). Dopaminergic projections from midbrain to primary motor cortex mediate motor skill learning. *The Journal of Neuroscience : The Official Journal of the Society for Neuroscience*, *31*(7), 2481–2487.

Howes, O. D., & Kapur, S. (2009). The Dopamine Hypothesis of Schizophrenia: Version III--The Final Common Pathway. *Schizophrenia Bulletin*, *35*(3), 549–562.

Howes, O. D., Williams, M., Ibrahim, K., Leung, G., Egerton, A., McGuire, P. K., &

Turkheimer, F. (2013). Midbrain dopamine function in schizophrenia and depression: a post-mortem and positron emission tomographic imaging study. *Brain*, *136*(Pt 11), 3242–3251.

Howes, O., McCutcheon, R., & Stone, J. (2015). Glutamate and dopamine in schizophrenia: An update for the 21st century. *Journal of Psychopharmacology*, *29*(2), 97–115.

Huang, H., & Ding, M. (2016). Linking Functional Connectivity and Structural Connectivity Quantitatively: A Comparison of Methods. *Brain Connectivity*, *6*(2), 99.

Huang, S. Y., Nummenmaa, A., Witzel, T., Duval, T., Cohen-Adad, J., Wald, L. L., & McNab, J. A. (2015). The impact of gradient strength on in vivo diffusion MRI estimates of axon diameter. *NeuroImage*, *106*, 464–472.

Huettel, S. A., Song, A. W., & McCarthy, G. (2008). *Functional magnetic resonance imaging*. Sinauer Associates.

Hughes, A. J., Daniel, S. E., Kilford, L., & Lees, A. J. (1992). Accuracy of clinical diagnosis of idiopathic Parkinson's disease: a clinico-pathological study of 100 cases. *Journal of Neurology, Neurosurgery & Psychiatry*, *55*(3), 181–184.

Humphries, M. D., & Prescott, T. J. (2010). The ventral basal ganglia, a selection mechanism at the crossroads of space, strategy, and reward. *Progress in Neurobiology*, *90*(4), 385–417.

Irimia, A., Chambers, M. C., Torgerson, C. M., & Van Horn, J. D. (2012). Circular representation of human cortical networks for subject and population-level connectomic visualization. *NeuroImage*, *60*(2), 1340–1351.

Iversen, S. D., & Iversen, L. L. (2007). Dopamine: 50 years in perspective. *Trends in Neurosciences*, *30*(5), 188–193.

Jacob, S. N., & Nienborg, H. (2018). Monoaminergic Neuromodulation of Sensory Processing. *Frontiers in Neural Circuits*, *12*, 51.

Jasinska, A. J., Stein, E. A., Kaiser, J., Naumer, M. J., & Yalachkov, Y. (2014). Factors modulating neural reactivity to drug cues in addiction: A survey of human neuroimaging studies. *Neuroscience & Biobehavioral Reviews*, *38*, 1–16.

Jbabdi, S., & Johansen-Berg, H. (2011). Tractography: Where Do We Go from Here? *Brain Connectivity*, *1*(3), 169–183.

Jbabdi, S., Sotiropoulos, S. N., Haber, S. N., Van Essen, D. C., & Behrens, T. E. (2015). Measuring macroscopic brain connections in vivo. *Nature Neuroscience*, *18*(11), 1546–1555.

Jenkinson, M., Bannister, P., Brady, M., & Smith, S. (2002). Improved Optimization for the Robust and Accurate Linear Registration and Motion Correction of Brain Images. *NeuroImage*, *17*(2), 825–841.

Jenkinson, M., Beckmann, C. F., Behrens, T. E. J., Woolrich, M. W., & Smith, S. M. (2012). FSL. *NeuroImage*, *62*(2), 782–790.

Joel, D., & Weiner, I. (2000). The connections of the dopaminergic system with the striatum in rats and primates: an analysis with respect to the functional and compartmental organization of the striatum. *Neuroscience*, *96*(3), 451–474.

Johansen-Berg, H., Behrens, T. E. J., Sillery, E., Ciccarelli, O., Thompson, A. J., Smith, S. M., & Matthews, P. M. (2005). Functional–Anatomical Validation and Individual Variation of Diffusion Tractography-based Segmentation of the Human Thalamus. *Cerebral Cortex*, *15*(1), 31–39.

Jones, D. K., Knösche, T. R., & Turner, R. (2013). White matter integrity, fiber count, and other fallacies: The do's and don'ts of diffusion MRI. *NeuroImage*, *73*, 239–254.

Khan, A. R., Hiebert, N. M., Vo, A., Wang, B. T., Owen, A. M., Seergobin, K. N., & MacDonald, P. A. (2019). Biomarkers of Parkinson's disease: Striatal sub-regional structural morphometry and diffusion MRI. *NeuroImage: Clinical*, *21*, 101597.

Kirilina, E., Lutti, A., Poser, B. A., Blankenburg, F., & Weiskopf, N. (2016). The quest for the best: The impact of different EPI sequences on the sensitivity of random effect fMRI group analyses. *NeuroImage*, *126*, 49–59.

Kish, S. J., Shannak, K., & Hornykiewicz, O. (1988). Uneven Pattern of Dopamine Loss in the Striatum of Patients with Idiopathic Parkinson's Disease. *New England Journal of Medicine*, *318*(14), 876–880.

Klein, M. O., Battagello, D. S., Cardoso, A. R., Hauser, D. N., Bittencourt, J. C., & Correa, R. G. (2019). Dopamine: Functions, Signaling, and Association with Neurological Diseases. *Cellular and Molecular Neurobiology*, *39*(1), 31–59.

Koslow, S. H., Cattabeni, F., Costa, E., Stinus, L., & Glowinski, J. (1972). Norepinephrine and dopamine: assay by mass fragmentography in the picomole range. *Science, 176*(4031), 177–180.

Krzywinski, M., Schein, J., Birol, I., Connors, J., Gascoyne, R., Horsman, D., … Marra, M. A. (2009). Circos: An information aesthetic for comparative genomics. *Genome Research*, *19*(9), 1639–1645.

Kwon, H. G., & Jang, S. H. (2014). Differences in neural connectivity between the substantia nigra and ventral tegmental area in the human brain. *Frontiers in Human Neuroscience*, *8*, 41.

Ladd, M. E., Bachert, P., Meyerspeer, M., Moser, E., Nagel, A. M., Norris, D. G., … Zaiss, M. (2018). Pros and cons of ultra-high-field MRI/MRS for human application. *Progress in Nuclear Magnetic Resonance Spectroscopy*, *109*, 1–50.

Lambert, C., Zrinzo, L., Nagy, Z., Lutti, A., Hariz, M., Foltynie, T., … Frackowiak, R. (2012). Confirmation of functional zones within the human subthalamic nucleus: patterns of connectivity and sub-parcellation using diffusion weighted imaging. *NeuroImage*, *60*(1), 83–94.

Langley, J., Huddleston, D. E., Merritt, M., Chen, X., McMurray, R., Silver, M., … Hu, X. (2016). Diffusion tensor imaging of the substantia nigra in Parkinson's disease revisited. *Human Brain Mapping*, *37*(7), 2547–2556.

Lee, C. R., & Tepper, J. M. (2009). Basal ganglia control of substantia nigra dopaminergic neurons. *Journal of Neural Transmission. Supplementum*, (73), 71–90. Retrieved from

Lenglet, C., Abosch, A., Yacoub, E., De Martino, F., Sapiro, G., & Harel, N. (2012). Comprehensive in vivo Mapping of the Human Basal Ganglia and Thalamic Connectome in Individuals Using 7T MRI. *PLoS ONE*, *7*(1), e29153.

Lewis, D. A., Campbell, M. J., Foote, S. L., Goldstein, M., & Morrison, J. H. (1987). The

distribution of tyrosine hydroxylase-immunoreactive fibers in primate neocortex is widespread but regionally specific. *The Journal of Neuroscience*, *7*(1), 279–290.

LeWitt, P. A. (2015). Levodopa therapy for Parkinson's disease: Pharmacokinetics and pharmacodynamics. *Movement Disorders*, *30*(1), 64–72.

Lidsky, T. I. (1995). Reevaluation of the Mesolimbic Hypothesis of Antipsychotic Drug Action. *Schizophrenia Bulletin*, *21*(1), 67–74.

Lindquist, M. A., & Mejia, A. (2015). Zen and the art of multiple comparisons. *Psychosomatic Medicine*, *77*(2), 114–125.

Lindvall, O., Björklund, A., Moore, R. Y., & Stenevi, U. (1974). Mesencephalic dopamine neurons projecting to neocortex. *Brain Research*, *81*(2), 325–331.

Liu, H., Qin, W., Li, W., Fan, L., Wang, J., Jiang, T., & Yu, C. (2013). Connectivity-based parcellation of the human frontal pole with diffusion tensor imaging. *The Journal of Neuroscience : The Official Journal of the Society for Neuroscience*, *33*(16), 6782–6790.

Loughlin, S. E., & Fallon, J. H. (1984). Substantia nigra and ventral tegmental area projections to cortex: Topography and collateralization. *Neuroscience*, *11*(2), 425–435.

Luft, A. R., & Schwarz, S. (2009). Dopaminergic signals in primary motor cortex. *International Journal of Developmental Neuroscience*, *27*(5), 415–421.

Lv, J., Guo, L., Hu, X., Zhang, T., Li, K., Zhang, D., … Liu, T. (2010). Fiber-centered analysis of brain connectivities using DTI and resting state FMRI data. *Medical Image Computing and Computer-Assisted Intervention : MICCAI … International Conference on Medical Image Computing and Computer-Assisted Intervention*, *13*(Pt 2), 143–150.

Lynd-Balta, E., & Haber, S. N. (1994). The organization of midbrain projections to the striatum in the primate: sensorimotor-related striatum versus ventral striatum. *Neuroscience*, *59*(3), 625–640.

MacDonald, P. A., & Monchi, O. (2011). Differential Effects of Dopaminergic Therapies on Dorsal and Ventral Striatum in Parkinson's Disease: Implications for Cognitive Function. *Parkinson's Disease*, 1–18.

Manitt, C., Mimee, A., Eng, C., Pokinko, M., Stroh, T., Cooper, H. M., … Flores, C. (2011). The Netrin Receptor DCC Is Required in the Pubertal Organization of Mesocortical Dopamine Circuitry. *Journal of Neuroscience*, *31*(23), 8381–8394.

Matsuda, W., Furuta, T., Nakamura, K. C., Hioki, H., Fujiyama, F., Arai, R., & Kaneko, T. (2009). Single Nigrostriatal Dopaminergic Neurons Form Widely Spread and Highly Dense Axonal Arborizations in the Neostriatum. *The Journal of Neuroscience*, *29*(2), 444–453.

Matsumoto, M., & Hikosaka, O. (2009). Two types of dopamine neuron distinctly convey positive and negative motivational signals. *Nature*, *459*(7248), 837–841.

Menke, R. A., Jbabdi, S., Miller, K. L., Matthews, P. M., & Zarei, M. (2010). Connectivity-based segmentation of the substantia nigra in human and its implications in Parkinson's disease. *NeuroImage*, *52*(4), 1175–1180.

Meola, A., Yeh, F.-C., Fellows-Mayle, W., Weed, J., & Fernandez-Miranda, J. C. (2016). Human Connectome-Based Tractographic Atlas of the Brainstem Connections and Surgical Approaches. *Neurosurgery*, *79*(3), 437–455.

Meyer, J. S., & Quenzer, L. F. (2012). Psychopharmacology: Drugs, the brain, and behavior, 2nd ed. - PsycNET.

Moore, R. Y., & Bloom, F. E. (1978). Central Catecholamine Neuron Systems: Anatomy and Physiology of the Dopamine Systems. *Annual Review of Neuroscience*, *1*(1), 129–169.

Morales, M., & Margolis, E. B. (2017). Ventral tegmental area: cellular heterogeneity, connectivity and behaviour. *Nature Reviews Neuroscience*, *18*(2), 73–85.

Murty, V. P., Shermohammed, M., Smith, D. V, Carter, R. M., Huettel, S. A., & Adcock, R. A. (2014). NeuroImage Resting state networks distinguish human ventral tegmental area from substantia nigra. *NeuroImage*, *100*, 580–589.

Nauta, W. J. H., Smith, G. P., Faull, R. L. M., & Domesick, V. B. (1978). Efferent connections and nigral afferents of the nucleus accumbens septi in the rat. *Neuroscience*, *3*(4–5), 385–401.

Ogawa, S., Lee, T. M., Kay, A. R., & Tank, D. W. (1990). Brain magnetic resonance imaging

with contrast dependent on blood oxygenation. *Proceedings of the National Academy of Sciences*, *87*(24), 9868–9872.

Oliva, I., & Wanat, M. J. (2016). Ventral Tegmental Area Afferents and Drug-Dependent Behaviors. *Frontiers in Psychiatry*, *7*, 30.

Ott, T., & Nieder, A. (2019). Dopamine and Cognitive Control in Prefrontal Cortex. *Trends in Cognitive Sciences*, *23*(3), 213–234.

Owen, M. J., Sawa, A., & Mortensen, P. B. (2016). Schizophrenia. *The Lancet*, *388*(10039), 86–97.

Pan, W. X., Mao, T., & Dudman, J. T. (2010). Inputs to the Dorsal Striatum of the Mouse Reflect the Parallel Circuit Architecture of the Forebrain. *Frontiers in Neuroanatomy*, *4*, 147.

Parent, A., Mackey, A., & De Bellefeuille, L. (1983). The subcortical afferents to caudate nucleus and putamen in primate: A fluorescence retrograde double labeling study. *Neuroscience*, *10*(4), 1137–1150.

Parker, G. J. M., & Alexander, D. C. (2003). Probabilistic Monte Carlo Based Mapping of Cerebral Connections Utilising Whole-Brain Crossing Fibre Information (pp. 684–695). Springer, Berlin, Heidelberg.

Pauli, W. M., Nili, A. N., & Tyszka, J. M. (2018). A high-resolution probabilistic in vivo atlas of human subcortical brain nuclei. *Scientific Data*, *5*, 180063.

Peterson, A. C., Zhang, S., Hu, S., Chao, H. H., & Li, C. R. (2017). The Effects of Age, from Young to Middle Adulthood, and Gender on Resting State Functional Connectivity of the Dopaminergic Midbrain. *Frontiers in Human Neuroscience*, *11*, 52.

Pfeiffer, R. F. (2016). Non-motor symptoms in Parkinson's disease. *Parkinsonism & Related Disorders*, *22*, S119–S122.

Prensa, L., & Parent, A. (2001). The nigrostriatal pathway in the rat: A single-axon study of the relationship between dorsal and ventral tier nigral neurons and the striosome/matrix striatal compartments. *The Journal of Neuroscience, 21*(18), 7247–7260.

Rademacher, J., Galaburda, A. M., Kennedy, D. N., Filipek, P. A., & Caviness, V. S. (1992). Human Cerebral Cortex: Localization, Parcellation, and Morphometry with Magnetic Resonance Imaging. *Journal of Cognitive Neuroscience*, *4*(4), 352–374.

Rice, M. W., Roberts, R. C., Melendez-Ferro, M., & Perez-Costas, E. (2016). Mapping dopaminergic deficiencies in the substantia nigra/ventral tegmental area in schizophrenia. *Brain Structure and Function*, *221*(1), 185–201.

Rodríguez-López, C., Clascá, F., & Prensa, L. (2017). The Mesoaccumbens Pathway: A Retrograde Labeling and Single-Cell Axon Tracing Analysis in the Mouse. *Frontiers in Neuroanatomy*, *11*.

Rogers, B. P., Morgan, V. L., Newton, A. T., & Gore, J. C. (2007). Assessing functional connectivity in the human brain by fMRI. *Magnetic Resonance Imaging*, *25*(10), 1347–1357.

Santos, J. P., Seixas, D., Brandão, S., & Moutinho, L. (2011). Investigating the role of the ventromedial prefrontal cortex in the assessment of brands. *Frontiers in Neuroscience*, *5*, 77.

Schiffler, P., Tenberge, J.-G., Wiendl, H., & Meuth, S. G. (2017). Cortex Parcellation Associated Whole White Matter Parcellation in Individual Subjects. *Frontiers in Human Neuroscience*, *11*, 352.

Schultz, W., Dayan, P., & Montague, P. R. (1997). A neural substrate of prediction and reward. *Science, 275*(5306), 1593–1599.

Setsompop, K., Kimmlingen, R., Eberlein, E., Witzel, T., Cohen-Adad, J., McNab, J. A., … Wald, L. L. (2013). Pushing the limits of in vivo diffusion MRI for the Human Connectome Project. *NeuroImage*, *80*, 220–233.

Shi, Y., & Toga, A. W. (2017). Connectome imaging for mapping human brain pathways. *Molecular Psychiatry*, *22*(9), 1230–1240.

Shimony, J. S., Rutlin, J., Karimi, M., Tian, L., Snyder, A. Z., Loftin, S. K., … Perlmutter, J. S. (2018). Validation of diffusion tensor imaging measures of nigrostriatal neurons in macaques. *PLOS ONE*, *13*(9), e0202201.

Skudlarski, P., Jagannathan, K., Calhoun, V. D., Hampson, M., Skudlarska, B. A., & Pearlson, G. (2008). Measuring brain connectivity: diffusion tensor imaging validates resting state temporal correlations. *NeuroImage*, *43*(3), 554–561.

Soares, J. M., Marques, P., Alves, V., & Sousa, N. (2013). A hitchhiker's guide to diffusion tensor imaging. *Frontiers in Neuroscience*, *7*, 31.

Sotiropoulos, S. N., Jbabdi, S., Xu, J., Andersson, J. L., Moeller, S., Auerbach, E. J., … Behrens, T. E. J. (2013). Advances in diffusion MRI acquisition and processing in the Human Connectome Project. *NeuroImage*, *80*, 125–143.

Stern G. (1966). The Effects of Lesions in the Substantia Nigra. *Brain*, *89*(3), 449–478.

Stevens, J. R. (1973). An Anatomy of Schizophrenia? *Archives of General Psychiatry*, *29*(2), 177.

Szabo, J. (1980). Organization of the ascending striatal afferents in monkeys. *The Journal of Comparative Neurology*, *189*(2), 307–321.

Takahashi, Y. K., Roesch, M. R., Stalnaker, T. A., Haney, R. Z., Calu, D. J., Taylor, A. R., … Schoenbaum, G. (2009). The Orbitofrontal Cortex and Ventral Tegmental Area Are Necessary for Learning from Unexpected Outcomes. *Neuron*, *62*(2), 269–280.

Theisen, F., Leda, R., Pozorski, V., Oh, J. M., Adluru, N., Wong, R., … Gallagher, C. L. (2017). Evaluation of striatonigral connectivity using probabilistic tractography in Parkinson's disease. *NeuroImage: Clinical*, *16*, 557–563.

Thibault, D., Giguère, N., Loustalot, F., Bourque, M.-J., Ducrot, C., El Mestikawy, S., & Trudeau, L.-É. (2016). Homeostatic regulation of excitatory synapses on striatal medium spiny neurons expressing the D2 dopamine receptor. *Brain Structure and Function*, *221*(4), 2093–2107.

Thomas, C., Ye, F. Q., Irfanoglu, M. O., Modi, P., Saleem, K. S., Leopold, D. A., & Pierpaoli, C. (2014). Anatomical accuracy of brain connections derived from diffusion MRI tractography is inherently limited. *Proceedings of the National Academy of Sciences*, *111*(46), 16574–16579.

Tomasi, D., & Volkow, N. D. (2014). Functional connectivity of substantia nigra and ventral tegmental area: maturation during adolescence and effects of ADHD. *Cerebral Cortex*, *24*(4), 935–944.

Tsang, A., Lebel, C. A., Bray, S. L., Goodyear, B. G., Hafeez, M., Sotero, R. C., … Frayne, R. (2017). White Matter Structural Connectivity Is Not Correlated to Cortical Resting-State Functional Connectivity over the Healthy Adult Lifespan. *Frontiers in Aging Neuroscience*, *9*, 144.

Tziortzi, A. C., Haber, S. N., Searle, G. E., Tsoumpas, C., Long, C. J., Shotbolt, P., … Gunn, R. N. (2014). Connectivity-based functional analysis of dopamine release in the striatum using diffusion-weighted MRI and positron emission tomography. *Cerebral Cortex*, *24*(5), 1165–1177.

Tziortzi, A. C., Searle, G. E., Tzimopoulou, S., Salinas, C., Beaver, J. D., Jenkinson, M., … Gunn, R. N. (2011). Imaging dopamine receptors in humans with [11C]-(+)-PHNO: Dissection of D3 signal and anatomy. *NeuroImage*, *54*(1), 264–277.

Uğurbil, K., Xu, J., Auerbach, E. J., Moeller, S., Vu, A. T., Duarte-Carvajalino, J. M., … Yacoub, E. (2013). Pushing spatial and temporal resolution for functional and diffusion MRI in the Human Connectome Project. *NeuroImage*, *80*, 80–104.

Ungerstedt, U. (1971). Stereotaxic Mapping of the Monoamine Pathways in the Rat Brain*. *Acta Physiologica Scandinavica*, *82*(S367), 1–48.

Vaillancourt, D. E., Schonfeld, D., Kwak, Y., Bohnen, N. I., & Seidler, R. (2013). Dopamine overdose hypothesis: evidence and clinical implications. *Movement Disorders, 28*(14), 1920–1929.

Van Essen, D. C., Smith, S. M., Barch, D. M., Behrens, T. E. J., Yacoub, E., Ugurbil, K., & WU-Minn HCP Consortium, for the W.-M. H. (2013). The WU-Minn Human Connectome Project: an overview. *NeuroImage*, *80*, 62–79.

Van Essen, D. C., Ugurbil, K., Auerbach, E., Barch, D., Behrens, T. E. J., Bucholz, R., … WU-Minn HCP Consortium. (2012). The Human Connectome Project: A data acquisition perspective. *NeuroImage*, *62*(4), 2222–2231.

Van Wijk, B. C. M., Stam, C. J., & Daffertshofer, A. (2010). Comparing Brain Networks of Different Size and Connectivity Density Using Graph Theory. *PLoS ONE*, *5*(10), e13701.

Viallet, F., Trouche, E., Beaubaton, D., Nieoullon, A., & Legallet, E. (1981). Bradykinesia following unilateral lesions restricted to the substantia nigra in the baboon. *Neuroscience Letters*, *24*(1), 97–102.

Volkow, N. D., & Morales, M. (2015). The Brain on Drugs: From Reward to Addiction. *Cell*, *162*(4), 712–725.

Voorn, P., Vanderschuren, L. J. M. ., Groenewegen, H. J., Robbins, T. W., & Pennartz, C. M. . (2004). Putting a spin on the dorsal–ventral divide of the striatum. *Trends in Neurosciences*, *27*(8), 468–474.

Vosberg, D. E., Zhang, Y., Menegaux, A., Chalupa, A., Manitt, C., Zehntner, S., … Leyton, M. (2018). Mesocorticolimbic Connectivity and Volumetric Alterations in DCC Mutation Carriers. *The Journal of Neuroscience, 38*(20), 4655–4665.

Weickenmeier, J., Kurt, M., Ozkaya, E., de Rooij, R., Ovaert, T. C., Ehman, R. L., … Kuhl, E. (2018). Brain stiffens post mortem. *Journal of the Mechanical Behavior of Biomedical Materials*, *84*, 88–98.

Wickens, J. R., Budd, C. S., Hyland, B. I., & Arbuthnott, G. W. (2007). Striatal Contributions to Reward and Decision Making: Making Sense of Regional Variations in a Reiterated Processing Matrix. *Annals of the New York Academy of Sciences*, *1104*(1), 192–212.

Wiegell, M. R., Tuch, D. S., Larsson, H. B. ., & Wedeen, V. J. (2003). Automatic segmentation of thalamic nuclei from diffusion tensor magnetic resonance imaging. *NeuroImage*, *19*(2), 391–401.

Williams, S., & Goldman-Rakic, P. S. (1998). Widespread origin of the primate mesofrontal dopamine system. *Cerebral Cortex*, *8*(4), 321–345.

Wise, R. A. (2009). Roles for nigrostriatal--not just mesocorticolimbic--dopamine in reward and addiction. *Trends in Neurosciences*, *32*(10), 517–524.

Wood, J., & Ahmari, S. E. (2015). A Framework for Understanding the Emerging Role of

Corticolimbic-Ventral Striatal Networks in OCD-Associated Repetitive Behaviors. *Frontiers in Systems Neuroscience*, *9*, 171.

World Medical Association. (2013). World Medical Association Declaration of Helsinki. *JAMA*, *310*(20), 2191.

Yetnikoff, L., Lavezzi, H. N., Reichard, R. A., & Zahm, D. S. (2014). An update on the connections of the ventral mesencephalic dopaminergic complex. *Neuroscience*, *282*, 23–48.

Zaghloul, K. A., Blanco, J. A., Weidemann, C. T., McGill, K., Jaggi, J. L., Baltuch, G. H., & Kahana, M. J. (2009). Human substantia nigra neurons encode unexpected financial rewards. *Science (New York, N.Y.)*, *323*(5920), 1496–1499.

Zhang, Y., Fan, L., Zhang, Y., Wang, J., Zhu, M., Zhang, Y., … Jiang, T. (2014). Connectivity-Based Parcellation of the Human Posteromedial Cortex. *Cerebral Cortex*, *24*(3), 719–727.

Zhang, Y., Larcher, K. M.-H., Misic, B., & Dagher, A. (2017). Anatomical and functional organization of the human substantia nigra and its connections. *ELife*, *6*.

Appendices

Appendix A: Cortical Subregions, abbreviations, and indication of Tziortzi et al. (2014) subregion

* Not included in the Tziortzi et al. (2014) parcellation

† Used as PFC subregion

RM = Rostral Motor, CM = Caudal Motor, Pari = Parietal, Occi = Occipital, Temp = Temporal

Cortical Region	Abbreviation	Tziortzi subregion
Frontal Medial Cortex	FMC	Limbic
Paracingulate Gyrus* †	PcG	Limbic
Cingulate Gyrus Ant*†	Cga	Limbic
Frontal Orbital Cortex	FOC	Limbic
Subcallosal Cortex*†	ScC	Limbic
Cingulate Gyrus Post*	CGp	Limbic
Insular Cortex	Ins	Insula
Frontal Pole†	FP	Executive
Superior Frontal Gyrus †	SFG	Executive
Middle Frontal Gyrus†	MFG	Executive
Inf. Frontal Gyrus (Pars Tri)	IFGpt	RM
Inf. Frontal Gyrus (Pars Oper)	IFGpo	RM
Frontal Rostral Motor	FRM	RM
Frontal Operculum Cortex	FopC	RM
Juxtapositional Lobule Cortex	SMC	RM
Precentral Gyrus	PrG	CM
Central Opercular Cortex	COpC	CM
Postcentral Gyrus	PoG	Pari

Supramarginal Gyrus Ant Division	SmGa	Pari
Parietal Operculum Cortex	POpC	Pari
Supramarginal Gyrus Post Division	SmGp	Pari
Precuneous Cortex	PcC	Pari
Superior Parietal Lobule	SPL	Pari
Angular Gyrus	AG	Pari
Temporal Occipiral Fusiform Cortex	TOF	Occi
Lingual Gyrus	LG	Occi
Supracalcarine Sulcus	SccC	Occi
Lateral Occipital Cortex Sup Division	LOCs	Occi
Lateral Occipital Cortex Inf Division	LOCi	Occi
Intracalcarine Cortex	IcC	Occi
Cuneal Cortex	CC	Occi
Occipiral Fusiform Gyrus	OFG	Occi
Occipiral Pole	OcP	Occi
Temporal Pole	TP	Temp
Superior Temporal Gyrus Ant.	STGa	Temp
Temporal Fusiform Cortex Ant.	TFCa	Temp
Mid. Temporal Gyrus Ant.	MTGa	Temp
Inf. Temporal Gyrus Ant.	ITGa	Temp
Planum Polare	PP	Temp
Parahippocampal Gyrus Ant.	PhGa	Temp
Inf. Temporal Gyrus Post.	ITGp	Temp
Temporal Fusiform Cortex Post.	TFCp	Temp
Superior Temporal Gyrus Post.	STGp	Temp
Mid. Temporal Gyrus Post.	MTGp	Temp
Hershel's Gyrus (H1&H2)	H1/H2	Temp
Planum Temporale	PT	Temp

Parahippocampal Gyrus Post.	PhGp	Temp
Inf. Temporal Gyrus Temporooccipital	ITGtp	Temp
Mid. Temporal Gyrus Temporooccipital	MTGtp	Temp

Appendix B. Ethics approval notice

Western Research

Western University Health Science Research Ethics Board
HSREB Amendment Approval Notice

Principal Investigator: Dr. Penny MacDonald
Department & Institution: Schulich School of Medicine and Dentistry\Clinical Neurological Sciences,London Health Sciences Centre

Review Type: Full Board
HSREB File Number: 102018
Study Title: Distinguishing the roles of ventral and dorsal striatum in cognition (REB #18517)
Sponsor: Canadian Excellence Research Chair

HSREB Amendment Approval Date: December 18, 2015
HSREB Expiry Date: November 29, 2016

Documents Approved and/or Received for Information:

Document Name	Comments	Version Date
Amendment	List of changes to ethics protocol and consent form	2015/11/19
Revised Western University Protocol	Marked version of updated ethics protocol	2015/11/19
Instruments	UPPS-P Impulsive Behavior Scale	2015/11/19
Instruments	Domain Specific Risk Taking Scale DOSPERT	2015/11/19
Instruments	Behavioral Inhibition/Approach Scale BIS/BAS Scale	2015/11/19
Revised Letter of Information & Consent		2015/11/19
Revised Western University Protocol		2015/11/19

The Western University Health Science Research Ethics Board (HSREB) has reviewed and approved the amendment to the above named study, as of the HSREB Initial Approval Date noted above.

HSREB approval for this study remains valid until the HSREB Expiry Date noted above, conditional to timely submission and acceptance of HSREB Continuing Ethics Review.

The Western University HSREB operates in compliance with the Tri-Council Policy Statement Ethical Conduct for Research Involving Humans (TCPS2), the International Conference on Harmonization of Technical Requirements for Registration of Pharmaceuticals for Human Use Guideline for Good Clinical Practice Practices (ICH E6 R1), the Ontario Personal Health Information Protection Act (PHIPA, 2004), Part 4 of the Natural Health Product Regulations, Health Canada Medical Device Regulations and Part C, Division 5, of the Food and Drug Regulations of Health Canada.

Members of the HSREB who are named as Investigators in research studies do not participate in discussions related to, nor vote on such studies when they are presented to the REB.

The HSREB is registered with the U.S. Department of Health & Human Services under the IRB registration number IRB 00000940.

Appendix C. Approval to use sagittal brain figure

Patrick Lynch
to me ▾

Nicholas,

You are welcome to use any of the illustrations that I placed on Wikimedia. There are no restrictions on their use (commercial, non-commercial, whatever).

Good luck with your thesis,

Pat Lynch

...

Appendix D. Montreal Cognitive Assessment (MoCA)

MONTREAL COGNITIVE ASSESSMENT (MOCA)
Version 7.1 Original Version

VISUOSPATIAL / EXECUTIVE		POINTS

Copy cube

Draw CLOCK (Ten past eleven) (3 points)

[ ]   [ ]   [ ] Contour   [ ] Numbers   [ ] Hands   ___/5

NAMING

[ ]   [ ]   [ ]   ___/3

MEMORY

Read list of words, subject must repeat them. Do 2 trials, even if 1st trial is successful. Do a recall after 5 minutes.

	FACE	VELVET	CHURCH	DAISY	RED	No points
1st trial						
2nd trial						

ATTENTION

Read list of digits (1 digit/ sec.).

Subject has to repeat them in the forward order   [ ] 2 1 8 5 4
Subject has to repeat them in the backward order [ ] 7 4 2   ___/2

Read list of letters. The subject must tap with his hand at each letter A. No points if ≥ 2 errors

[ ] F B A C M N A A J K L B A F A K D E A A A J A M O F A A B   ___/1

Serial 7 subtraction starting at 100   [ ] 93   [ ] 86   [ ] 79   [ ] 72   [ ] 65

4 or 5 correct subtractions: **3 pts**, 2 or 3 correct: **2 pts**, 1 correct: **1 pt**, 0 correct: **0 pt**   ___/3

LANGUAGE

Repeat : I only know that John is the one to help today. [ ]
The cat always hid under the couch when dogs were in the room. [ ]   ___/2

Fluency / Name maximum number of words in one minute that begin with the letter F   [ ] _____ (N ≥ 11 words)   ___/1

ABSTRACTION

Similarity between e.g. banana - orange = fruit   [ ] train – bicycle   [ ] watch - ruler   ___/2

DELAYED RECALL

Has to recall words WITH NO CUE	FACE [ ]	VELVET [ ]	CHURCH [ ]	DAISY [ ]	RED [ ]	Points for UNCUED recall only	___/5
Optional Category cue							
Multiple choice cue							

ORIENTATION   [ ] Date   [ ] Month   [ ] Year   [ ] Day   [ ] Place   [ ] City   ___/6

© Z.Nasreddine MD   www.mocatest.org   Normal ≥ 26 / 30   TOTAL   ___/30

Administered by: _____   Add 1 point if ≤ 12 yr edu

96

Appendix E. Epworth Sleepiness Scale

How likely are you to doze off or fall asleep in the situations described below, in contrast to feeling just tired?

This refers to your usual way of life in recent times.

Even if you haven't done some of these things recently try to work out how they would have affected you.

Use the following scale to choose the most appropriate number for each situation:-

0 = would never doze
1 = Slight chance of dozing
2 = Moderate chance of dozing
3 = High chance of dozing

Situation	Chance of dozing
Sitting and reading	
Watching TV	
Sitting, inactive in a public place (e.g. a theatre or a meeting)	
As a passenger in a car for an hour without a break	
Lying down to rest in the afternoon when circumstances permit	
Sitting and talking to someone	
Sitting quietly after a lunch without alcohol	
In a car, while stopped for a few minutes in the traffic	
Total	

Score:

0-10   Normal range
10-12   Borderline
12-24   Abnormal

Appendix F. New Freezing of Gait Questionnaire

For administrator's use only	Date (dd/mm/yy):	
	Subject #:	Session #:
Score:	Medication:	Time:

New Freezing of Gait Questionnaire

Part I – Distinction Freezer – non-Freezer, over the past month

1. Did you experience "freezing episodes" over the past month?
 	
Without video
 	
Freezing is the feeling that your feet are transiently glued to the floor while trying to initiate walking, making a turn or when walking through narrow spaces or in crowded places? Sometimes it can be accompanied with trembling of the legs and small shuffling steps.
 	
Additional instructions with video
We will watch a short video together to see the many ways in which freezing can occur. Also, look carefully for how long these episodes last, as you can expect some questions on this later. (tester points out the clock on video clip)
 	
    0. I have not experienced such a feeling or episode over the past month
    1. I have experienced such a feeling or episode over the past month
 	
If the answer is 1 (patient is a freezer) complete part II and III. The sum of part II and III is the final NFOG score.

Part II – Freezing severity

2.   How frequently do you experience freezing episodes?
 	
    0. Less than once a week
    1. Not often, about once a week
    2. Often, about once a day
    3. Very often, more than once a day

3.   How frequently do you experience freezing episodes during turning?
 	
    0. Never
    1. Rarely, about one a month
    2. Not often, about once a week
    3. Often, about once a day
    4. Very often, more than once a day
 	
If the answer is 1 or more go to question #4. If the answer is 0, go directly to #5.

4.   How long is your longest freezing episode during turning?
 	
    1. Very short, 1 sec
    2.   Short, 2 - 5 s.
    3. Long, between 5 and 30 s.
    4. Very long, unable to walk for more than 30 s.

5. How frequently do you experience episodes of freezing when initiating the first step?

    0. Never

    1. Rarely, about once a month

    2. Not often, about once a week

    3. Often, about once a day

    4. Very often, more than once a day

If the answer 1 or more go to question #6. If the answer is 0, go directly to #7.

6. How long is your longest freezing episode when initiating the first step?

    1.   Very short, 1 s.

    2.   Short, 2-5 s.

    3.   Long, between 5 and 30 s.

    4.   Very long, unable to walk for more than 30 s.

Part III – Freezing impact on daily life

7. How disturbing are the freezing episodes for your daily walking?

    0. Not at all

    1. Very little

    2. Moderately

    3. Significantly

8. Do the freezing episodes cause feelings of insecurity and fear of falling?

    0. Not at all

    1. Very little

    2. Moderately

    3. Significantly

9. Are your freezing episodes affecting your daily activities?

(Rate the impact of freezing on daily activities only. Not the impact of the disease in general)

    0. Not at all, I continue doing things as normal

    1. Mildly, I avoid only few daily activities

    2. Moderately, I avoid a significant amount (about half) of daily activities

    3. Severely, I am very restricted in carrying out most daily activities

Appendix G. Starkstein Apathy Scale

Starkstein Apathy Scale

Instructions: For each question, indicate as "Not at all", "Slightly", "Some", or "A lot" with an 'X' while leaving the other spaces blank.

Questions	Not at all	Slightly	Some	A lot
1. Are you interested in learning new things?				
2. Does anything interest you?				
3. Are you concerned about your condition?				
4. Do you put much effort into things?				
5. Are you always looking for something to do?				
6. Do you have plans and goals for the future?				
7. Do you have motivation?				
8. Do you have the energy for daily activities?				
9. Does someone have to tell you what to do each day?				
10. Are you indifferent to things?				
11. Are you unconcerned with many things?				
12. Do you need a push to get started on things?				
13. Are you neither happy nor sad, just in between?				
14. Would you consider yourself apathetic?				

Appendix H. Oxford Happiness Questionnaire

For administrator's use only	Date (dd/mm/yy):	Session #:
	Subject #:	Time:
Score:	Medication:	

Oxford Happiness Questionnaire

The Oxford Happiness Questionnaire was developed by psychologists Michael Argyle and Peter Hills at Oxford University.

Instructions

Below are a number of statements about happiness. Please indicate how much you agree or disagree with each by entering a number in the blank after each statement, according to the following scale:

1 = strongly disagree
2 = moderately disagree
3 = slightly disagree
4 = slightly agree
5 = moderately agree
6 = strongly agree

Please read the statements carefully, some of the questions are phrased positively and others negatively. Don't take too long over individual questions; there are no "right" or "wrong" answers (and no trick questions). The first answer that comes into your head is probably the right one for you. If you find some of the questions difficult, please give the answer that is true for you in general or for most of the time.

The Questionnaire

1. I don't feel particularly pleased with the way I am. (R) _____
2. I am intensely interested in other people. _____
3. I feel that life is very rewarding. _____
4. I have very warm feelings towards almost everyone. _____
5. I rarely wake up feeling rested. (R) _____
6. I am not particularly optimistic about the future. (R) _____
7. I find most things amusing. _____
8. I am always committed and involved. _____
9. Life is good. _____
10. I do not think that the world is a good place. (R) _____
11. I laugh a lot. _____
12. I am well satisfied about everything in my life. _____
13. I don't think I look attractive. (R) _____
14. There is a gap between what I would like to do and what I have done. (R) _____
15. I am very happy. _____

16. I find beauty in some things. _____

17. I always have a cheerful effect on others. _____

18. I can fit in (find time for) everything I want to. _____

19. I feel that I am not especially in control of my life. (R) _____

20. I feel able to take anything on. _____

21. I feel fully mentally alert. _____

22. I often experience joy and elation. _____

23. I don't find it easy to make decisions. (R) _____

24. I don't have a particular sense of meaning and purpose in my life. (R) _____

25. I feel I have a great deal of energy. _____

26. I usually have a good influence on events. _____

27. I don't have fun with other people. (R) _____

28. I don't feel particularly healthy. (R) _____

29. I don't have particularly happy memories of the past. (R) _____

1 = Strongly Disagree
2 = Moderately Disagree
3 = Slightly Disagree
4 = Slightly Agree
5 = Moderately Agree
6 = Strongly Agree

Calculate your score

Step 1. Items marked (R) should be scored in reverse:

For example, if you gave yourself a "1," cross it out and change it to a "6."
Change "2" to a "5"
Change "3" to a "4"
Change "4" to a "3"
Change "5" to a "2"
Change "6" to a "1"

Step 2. Add the numbers for all 29 questions. (Use the converted numbers for the 12 items that are reverse scored.)

Step 3. Divide by 29. So your happiness score = the total (from step 2) divided by 29.

Your Happiness Score: _____

Reference:
http://www.meaningandhappiness.com/oxford-happiness-questionnaire/214/

Appendix I. American National Adult Reading Test (ANART)

ANART Score Sheet

1. ache	_____	(eyk)	26. simile	_____	(**sim**-uh-lee)
2. debt	_____	(det)	27. blatant	_____	(**bleyt**-nt)
3. pint	_____	(pahynt)	28. cellist	_____	(**chel**-ist)
4. depot	_____	(**dee**-poh)	29. zealot	_____	(**zel**-uht)
5. chord	_____	(kawrd)	30. abstemious	_____	(ab-**stee**-mee-uhs)
6. bouquet	_____	(boh-**kay**)	31. meringue	_____	(muh-**rang**)
7. deny	_____	(dih-**nahy**)	32. placebo	_____	(pluh-**see**-boh)
8. capon	_____	(**kay**-pon)	33. façade	_____	(fuh-**sahd**)
9. heir	_____	(air)	34. pugilist	_____	(**pyoo**-juh-list)
10. aisle	_____	(ahyl)	35. virulent	_____	(**vir**-yuh-luhnt)
11. subtle	_____	(**suht**-l)	36. worsted	_____	(**woos**-tid, **wur**-stid)
12. nausea	_____	(**naw**-zee-uh)	37. détente	_____	(dey-**tahnt**)
13. gauge	_____	(geyj)	38. anise	_____	(**an**-is)
14. naïve	_____	(nah-**eev**)	39. sieve	_____	(siv)
15. thyme	_____	(time)	40. chassis	_____	(**chas**-ee)
16. courteous	_____	(**kur**-tee-uhs)	41. beatify	_____	(bee-**at**-uh-fahy)
17. algae	_____	(**al**-jee)	42. scion	_____	(**sahy**-uhn)
18. fetal	_____	(**feet**-l)	43. cabal	_____	(kuh-**bal**)
19. quadruped	_____	(**kwod**-roo-ped)	44. apropos	_____	(ap-ruh-**poh**)
20. epitome	_____	(ih-**pit**-uh-mee)	45. caprice	_____	(kuh-**prees**)
21. superfluous	_____	(soo-**pur**-floo-uhs)	46. demesne	_____	(dih-**meyn**)
22. chamois	_____	(**sham**-ee, sha-**mwah**)	47. imbroglio	_____	(im-**brohl**-yoh)
23. papyrus	_____	(puh-**pahy**-ruhs)	48. hyperbole	_____	(hahy-**pur**-buh-lee)
24. asthma	_____	(**az**-muh)	49. syncope	_____	(**sing**-kuh-pee)
25. hiatus	_____	(hahy-**ey**-tuhs)	50. prelate	_____	(**prel**-it)

Appendix J. Verbal Category Fluency

Verbal Category Fluency

F	A	S
Total:	Total:	Total:
Category		
Total:		

Curriculum Vitae

Nicholas Handfield-Jones

Education

2017-Present:

University of Western Ontario, London, Ontario | Brain and Mind Institute

MSc of Neuroscience

Supervisors: Dr. Penny MacDonald (PI), Dr. Ali Khan, Dr. Adrian Owen

Thesis: Clarifying Dopaminergic Projections of the Ventral Tegmental Area and Substantia Nigra in Humans using Structural Magnetic Resonance Imaging (Pending)

2013-2016:

Amsterdam University College, Amsterdam, The Netherlands | Amsterdam University & Vrije Universiteit

Bachelor's of Liberal Arts & Science – Honours – Graduated *Cum Laude*

Supervisor: Dr. Pieter Voorn

Honour's Thesis: Impulse Control Disorder, a Common Complication of Parkinson's Disease Treatment: Dopamine Receptor Theories and Possible Treatments

Research Contributions

Manuscripts Submitted to a Refereed Journal

Handfield-Jones N, Prenger M, MacDonald PA. 2019. Montreal Cognitive Assessment Scores are lower in Parkinson's disease patients without mild cognitive impairment. *Mov Disord: Clin Pract*. (In Review)

Other Publications

Handfield-Jones N. 2016. Stressful Sickness: An Examination and Evaluation of Two Neurobiological Theories of Somatic Symptom Disorder. Science of the Human Body. 1: 19-23.

Conference Platform Presentations

Handfield-Jones N, Alushaj E, Hiebert NM, Owen AM, Khan AR, MacDonald PA, The Use of Diffusion Weighted MRI to Distinguish Parkinson's Disease Patients from Healthy Controls, 2019 May, Clinical Neurological Science Day 2019, London, Ontario, Canada.

Handfield-Jones N, Alushaj E, Hiebert NM, Owen AM, Khan AR, MacDonald PA, Clarifying Dopaminergic Projections of the Ventral Tegmental Area and Substantia Nigra using Structural Magnetic Resonance Imaging, 2019 April, London Health Research Day 2019, London, Ontario, Canada.

Handfield-Jones N, Alushaj E, Hiebert NM, Owen AM, Khan AR, MacDonald PA, Clarifying Dopaminergic Projections of the Ventral Tegmental Area and Substantia Nigra using Structural Magnetic Resonance Imaging, 2018 April, Clinical Neurological Science Research Day 2018, London, Ontario, Canada.

Handfield-Jones N, Alushaj E, Hiebert NM, Owen AM, Khan AR, MacDonald PA, Clarifying Dopaminergic Projections of the Ventral Tegmental Area and Substantia Nigra in Human using Structural Magnetic Resonance Imaging, 2018 March, Western Research Forum, London, Ontario, Canada.

Conference Poster Presentations

Handfield-Jones N, Alushaj E, Hiebert NM, Owen AM, Khan AR, MacDonald PA, Clarifying Dopaminergic Projections of the Ventral Tegmental Area and Substantia Nigra in Humans using Structural Magnetic Resonance Imaging, 2019 June, Robarts Research Retreat 2019, London, On, Canada. (Declined)

Handfield-Jones N, Alushaj E, Hiebert NM, Owen AM, Khan AR, MacDonald PA, Clarifying Dopaminergic Projections of the Ventral Tegmental Area and Substantia Nigra in Humans using Structural Magnetic Resonance Imaging, 2019 May, Canadian Association for Neuroscience (CAN) Conference 2019, Toronto, Ontario, Canada.

Handfield-Jones N*, Alushaj E, Hiebert NM, Owen AM, Khan AR, MacDonald PA, Clarifying Dopaminergic Projections of the Ventral Tegmental Area and Substantia Nigra in Humans using Structural Magnetic Resonance Imaging, 2018 June, Robarts Research Retreat 2018, London, On, Canada, Co-Author. ***Poster Presentation Winner**

Handfield-Jones N, Alushaj E, Hiebert NM, Owen AM, Khan AR, MacDonald PA, Clarifying Dopaminergic Projections of the Ventral Tegmental Area and Substantia Nigra in Humans using Structural Magnetic Resonance Imaging, 2018 May, SONA Annual Meeting 2018, Guelph, Ontario, Canada.